www.jresm.org

Research on Engineering Structures & Materials

Volume 5 Issue 4 December 2019 P-ISSN: 2148-9807 E-ISSN: 2149-4088

Special Focus on:

Computational modeling applied to ocean engineering structures

Edited by:

Liércio André Isoldi

Hayri Baytan Özmen

Research Group

The International Journal of **Research on Engineering Structures and Materials (RESM**) is a peer-reviewed open access journal (p-ISSN: 2148-9807; o-ISSN: 2149-4088) published by MIM Research Group. It is published in February, June, September, and December.

The main objective of RESM is to provide an International academic platform for researchers to share scientific results related to all aspects of mechanical, civil and material engineering areas.

RESM aims the publication of original research articles, reviews, short communications technical reports, and letters to the editor on the latest developments in the related fields.

All expenditures for the publication of the manuscripts are most kindly reimbursed by *MIM Research Group*. Thus, authors do not need to pay for publishing their studies in the journal.

The scope of the journal covers (but not limited to) behavior of structures, machines and mechanical systems, vibration, impact loadings and structural dynamics, mechanics of materials (elasticity, plasticity, fracture mechanics), material science (structure and properties of concrete, metals, ceramics, composites, plastics, wood, etc.,), nano-materials performances of new and existing buildings and other structural systems, design of buildings and other structural systems, seismic behavior of buildings and other structural systems, repair and strengthening of structural systems, case studies and failure of structural systems, safety and reliability in structural and material engineering, use of new and innovative materials and techniques in energy systems and mechanical aspects of biological systems (biomechanics and biomimetics).

The topics covered in RESM include:

- Structural Engineering
- Mechanical Engineering
- Material Engineering
- Earthquake Engineering
- Nano-technology
- Energy Systems
- Biomechanics and Biomimetics

Abstracting and Indexing
Please visit http://www.jresm.org for more information.

Graphics and Design

H Ersen Balcıoğlu ersen.balcioglu@usak.edu.tr

Yunus Demirtaş yunus.demirtas@usak.edu.tr

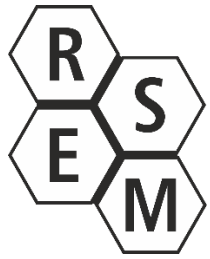

RESEARCH on ENGINEERING STRUCTURES & MATERIALS

Published by MIM Research Group

RESEARCH on ENGINEERING STRUCTURES & MATERIALS

Editors

Editor in Chief		
Hayri Baytan Özmen	Usak University	Turkey
Guest Editor		
Liércio André Isoldi	Universidade Federal do Rio Grande	Brazil

Editorial Office

Publishing Manager & Copyeditor		
H. Ersen Balcıoğlu	Usak University	Turkey
Publishing Assistant		
Yunus Demritaş	Usak University	Turkey

Editorial Board Members

Farid Abed-Meraim	Arts et Metiers ParisTech	France
P. Anbazhagan	Indian Institute of Science	India
Raffaele Barretta	University of Naples Federico II	Italy
R.S. Beniwal	Council of Scientific and Industrial Research	India
Antonio Caggiano	University of Buenos Aires	Argentina
Noel Challamel	University of South Brittany	France
Abdulkadir Çevik	Gaziantep University	Turkey
J. Paulo Davim	University of Aveiro	Portugal
Hom Nath Dhakal	University of Portsmouth	UK
Ali Faghidian	Islamic Azad University	Iran
S. Amir M. Ghannadpour	Shahid Beheshti University	Iran
Ali Goodarzi	Harvard University	USA
Jian Jiang	National Institute of Standards and Technology	USA
Ramazan Karakuzu	Dokuz Eylül University	Turkey
Arkadiusz Kwiecien	Cracow University of Technology	Poland
Stefano Lenci	Universita Politecnica delle Marche	Italy
Yuan Meini	North University of China	China
Stergios A. Mitoulis	University of Surrey	UK
Mohammad Mehdi Rashidi	University of Tongji	China
Pier Paolo Rossi	University of Catania	Italy
Neritan Shkodrani	Polythecnic University of Tirana	Albania
Faris Tarlochan	Qatar University	Qatar
Y.B. Yang	National Taiwan University	Taiwan

Advisory Board Members

Yaser Acikbas	Usak University	Turkey
Yasin Alemdag	Karadeniz Technical University	Turkey
Samim Ali	National Institute of Standards and Technology	USA
Duygu Alparslan	Yuzuncu Yıl University	Turkey
Irekti Amar	University M'Hamed Bougara of Boumerdes	Algeria
Carla Tatiana Mota Anflor	University of Brasilia	Brazil
Faezeh Atri	Tehran University of Medical Sciences	Iran
Massimiliano Avalle	Università degli Studi di Genova	Italy
Ozgur Avsar	Eskisehir Technical University	Turkey
Ayse Aytac	Kocaeli University	Turkey
Huseyin Ersen Balcıoglu	Usak University	Turkey
Raffaele Barretta	University of Naples Federico II	Italy
Kleber Bianchi	Universidade Federal de Goias	Brazil
Antonio Caggiano	University of Buenos Aires	Brazil
Sanjay Kumar Chak	Netaji Subhas Institute of Technology	India
Leda Coltro	Instituto de Tecnologia de Alimentos	Brazil
Sérgio Correia	Pólo II da Univ. de Coimbra	Portugal
Eduardo Costa Couto	Federal University of Pelotas	Brazil
Thiago da Silveira	Universidade Federal do Pampa	Brazil
Preeta Datta	North Carolina State University	USA
Hasan Demir	Osmaniye Korkut Ata University	Turkey
Ayse Pınar Demir	Usak University	Turkey
Umit Bilge Demirci	French National Centre for Scientific Research	France
Leonid Director	Russian Academy of Science	Russia
Halil Enginsoy	Usak University	Turkey

Advisory Board Members

Yavuz Ergun	Usak University	Turkey
Tuba Ersen Dudu	Yuzuncu Yıl University	Turkey
Saeed Farahani	Clemson University	USA
Carlos Eduardo Marcos Guilherme	Universidade Federal do Rio Grande	Brazil
Alper Gurarslan	Comftech Co.	Italy
Ahmet Gural	Gazi University	Turkey
Dulce Franco Henriques	Instituto Politécnico de Lisboa	Portugal
Saddam Hossain	Bangladesh University of Engineering and Technology	Bangladesh
Liércio André Isoldi	Universidade Federal do Rio Grande	Brazil
Berrin Ikizler	Ege University	Turkey
Zeynep İlbay	Usak University	Turkey
Ali Karaipekli	Cankırı Karatekin University	Turkey
Alp Karakoc	Aalto University	Finland
Jibran Khaliq	Northumbria University	UK
Mehdi Khorasanian	Shahid Chamran university of Ahvaz	Iran
João Paulo Silva Lima	Universidade Federal de Goias	Brazil
Gabriela Lujan Brollo	University of Campinas	Brazil
Ahmed Maamoun	McMaster University	Canada
Avik Mahata	Missouri University of Science and Technology	USA
K. K. Mahato	National Institute of Technology	India
Upendra K. Mallela	L&L Technology Services	India
Najoua Mekaddem	National Engineering School of Gabes	Tunisia
Suha Orcun Mert	Yuzuncu Yıl University	Turkey
Masoomeh Mirrashid	Semnan University	Iran
Mohsin Talib Mohammed	Kufa University	Iran

Advisory Board Members

Márcio Wrague Moura	Universidade Federal do Rio Grande	Brazil
Muhammad Muddassir	Institute for Composite Materials	Germany
Khurram Munir	RMIT University	Australia
Andrea Mura	Politecnico di Torino	Italy
Engin Nacaroglu	Pamukkale University	Turkey
Susmita Naskar	Johns Hopkins University	USA
Mu Naushad	King Saud University	Saudi Arabia
Olga Netskina	Boreskov Institute of Catalysis	Russia
Hayri B. Ozmen	Usak University	Turkey
Fehime Ozkan	Izmir Intitute of Technology	Turkey
Charlei Marcelo Paliga	Federal University of Pelotas	Brazil
Krishna Murari Pandey	National Institute of Technology	India
Ramon Peña-Garcia	Universidade Federal de Pernambuco	Brazil
Matheus Poletto	University of Caxias do Sul	Brazil
K. Venkatesh Raja	K.S.R. College of Engineering	India
Mauro de Vasconcellos Real	Federal University of Rio Grande	Brazil
Raif Sakin	Balıkesir University	Turkey
Kamyar Shirvani Moghaddam	Deakin University	Australia
Brijesh Singh	National Council for Cement and Building Materials	India
Bheemappa Suresha	The National Institute of Engineering	India
Gulsah Susurluk	Beykent University	Turkey
Selin Sahin Sevgili	İstanbul Cerrahpaşa University	Turkey
Hossein Taghipoor	Semnan University	Iran
Paulo Teixeira	Universidade de Lisboa	Portugal
Tugce Tezel	Akdeniz University	Turkey
Canan Uraz	Ege University	Turkey

Advisory Board Members

Abid Ustaoglu	Bartın University	Turkey
Kursat Oguz Yaykasli	Kahramanmaras Sutcu Imam University	Turkey
Ferhat Yildirim	Dumlupınar University	Turkey
Seyda Zorer Celebi	Yuzuncu Yıl University	Turkey
Aldobenedetto Zotti	Institute for Polymers, Composites and Biomaterials	Italy

In This Issue

Free access to tables of content, abstracts and full text of papers for web visitors.

Copyrigth © 2019

Research on Engineering Structures & Materials
MIM Reseach Group Publications
ISSN 2148-9807
http://www.jresm.org

In This Issue

Free access to tables of content, abstracts and full text of papers for web visitors.

Copyrigth © 2019

Research on Engineering Structures & Materials
MIM Reseach Group Publications
ISSN 2148-9807
http://www.jresm.org

ABSTRACTING / INDEXING

The international journal of Research on Engineering Structures and Materials (RESM) is currently Absracted/Indexed by CrossRef, Google Scholar, Universal Impact Factor, Scientific Indexing Service, Research Bible, CiteFactor, Electronic Journal Library, Open Academic Journals Index, Global Impact Factor, Directory of Research Journals Indexing, Materials Science & Engineering Database (ProQuest) Engineering Journals (ProQuest), ULAKBİM TR Index (Tubitak) and under evaluation by many other respected indexes.

Check web site for current indexing info.

Research on Engineering Structures & Materials
journal homepage: http://jresm.org
Research Group

Research Article

A simplified method for analysis of reinforced concrete beams exposed to fire situation

Marcelo Mesquita do Amaral*[1,a], Matheus Wanglon Ferreira[2,b], Mauro de Vasconcellos Real[1,c]

[1]*Engineering School, Federal University of Rio Grande, Brazil*
[2]*Department of Civil Engineering, Federal University of Rio Grande do Sul, Brazil*

Article Info

Article history:
Received 01 Feb 2019
Revised 16 April 2019
Accepted 15 May 2019

Keywords:

Flexure design;

Beam;

Reinforced concrete;

Harbor structures;

Fire scenario

Abstract

The reinforced concrete structural design consists in determining the structural members dimensions, steel ratio and location of steel rebars so that a limit state is not reached. Currently, when considering fire effects, commercial design software, in general, are limited to do the verifications only based on the tabular method, according to ABNT NBR 15200, without considering internal and external forces, so the designer needs to change the dimensions of the concrete section. This fact does not stimulate the use of the Brazilian standard codes since they do not present economic solutions. This paper aims to propose a simplified method to design reinforced concrete beams, of harbor structures, in a fire situation, which allows the implementation in commercial design software. Such proposed simplified method intends to involve structural safety, improves design facilities and economy in construction. Then, through a numerical example, the practical application of the tabular and simplified method was demonstrated. The results obtained by the simplified method were more economical than the tabular method. The calculation models validation was done through a comparative study with values found in the literature, as well as those calculated by the 500 °C isotherm method, and with the software ANSYS results. At the end of this work, it was concluded that the proposed simplified method, besides this being a method that allows an easy application, presents results, in general, in favor of safety; and, withal, allows more economics results when compared with the tabular method.

© 2019 MIM Research Group. All rights reserved.

1. Introduction

The reinforced concrete structural design consists in determining the structures members dimensions, steel ratio and the location of the steel bars so that a limit state is not reached. The structure must not reach the ultimate limit state, which could correspond to failure or collapse; neither a serviceability limit state that would make the structure unsuitable for its intended use [1].

Currently, when considering fire effects, design commercial software, in general, are limited to do structural verifications only based on the tabular method, according to [2], without considering internal and external forces, so the designer engineer needs to change the dimensions of the concrete section. This fact does not stimulate the use of the Brazilian Standards since they do not present economic solutions. In this way, the aim of this paper is proposing a simplified method to design reinforced concrete beams, of harbor

*Corresponding author: mesquita.amaral@gmail.com
[a] orcid.org/0000-0002-2769-5397; [b] orcid.org/0000-0001-6908-1177; [c] orcid.org/0000-0003-4916-9133
DOI: http://dx.doi.org/10.17515/resm2019.110ms0201

structures, in a fire situation that allows the implementation in commercial design software.

2. Methodology

As pointed out by [2], under usual conditions, the structures are designed at room temperature and, depending on their characteristics and their purpose of use must be verified in a fire situation. There are many methods to do this verification and, Brazilian Standard accepts the following methods: tabular method; simplified calculation method; advanced calculation method and experimental method.

Albuquerque [3] argues that the tabular method is the unique detailed in Brazilian Standard because it is a quite simple and practical method. For the others, the regulation presents only their guidelines for application, since they require specific computer programs or laboratory tests.

However, in this paper will be proposed a simplified method. This model allows beams design in a fire scenario, with manual calculations, in a relatively simple way, without the aid of graphs, abacus, or sophisticated computational programs.

2.1. Tabular method

In order to guarantee the structural safety in fire situation, by the tabular method, it is enough that the beams comply with the minimum dimensions tabulated, as function to the required time of fire resistance (TRRF), determined in accordance with [4], or by the Equivalent Time Method, according to [2]. Such minimum dimensions are presented in Tables 1 and 2.

Table 1 Minimum dimensions for simply supported beams [2]

TRRF (minutes)	Combinations of b_{min}/c_1 (mm/mm)				b_{wmin} (mm)
	1	2	3	4	
30	80/25	120/20	160/15	190/15	80
60	120/40	160/35	190/30	300/25	100
90	140/60	190/45	300/40	400/35	100
120	190/68	240/60	300/55	500/50	120
180	240/80	300/70	400/65	600/60	140

Table 2 Minimum dimensions for continuously supported beams or beams of frames [2]

TRRF (minutes)	Combinations of b_{min}/c_1 (mm/mm)				b_{wmin} (mm)
	1	2	3	4	
30	80/15	160/12	-	-	80
60	120/25	190/12	-	-	100
90	140/37	250/25	-	-	100
120	190/45	300/35	450/35	500/30	120
180	240/60	400/50	550/50	600/40	140

where, b_{min}: minimum width of the cross-section; b_{wmin}: minimum width of the cross-section web of variable width beam; c_1: distance between the longitudinal steel axis (CG) and the concrete surface exposed to fire.

The Brazilian standard NBR 15200 [2], establishes some important prescriptions for the Tabular Method applications; among them, it stands out the case of arranging steel bars just in one layer.

Furthermore, in beams with only one reinforcement layer and width no greater than b_{min} indicated in Table 1 and Table 2, according to the TRRF, the c_{1l} distance (Figure 1) of the beams should be 10 mm larger than the c_1 given by Table 1. This adjustment is necessary due to the fact that there is a temperature concentration along the edges located in the underside of the beam.

As an alternative, to keep the concrete cover both about the underside and to the side of the beam, the following considerations must be applied: for reinforced concrete, to specify corner bars with a diameter immediately greater than the calculated; for prestressed concrete, to consider designing effects, a prestress force equal to 0.7 of the indicated.

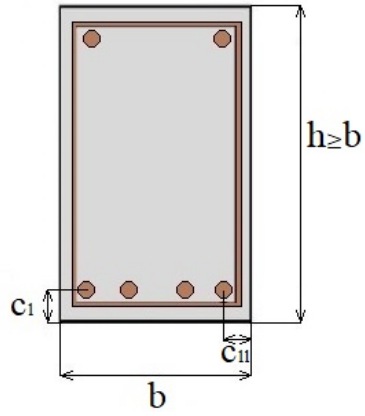

Fig. 1 c_1 and c_{1l} distances, adapted from [2]

2.2. Simplified method

Unlike the Tabular Method, which consists of verification, for a given TRRF, of the minimum beams dimensions, the simplified methods evaluate the fire resistance, by analyzing both the internal and external forces for a given TRRF.

Thus, the fire action usually corresponds to only the reduction of the strength of the material and the structural elements capacity. The ordinary verification of structural safety in a fire situation is guaranteed when the Eq. (1) is satisfied:

$$S_{d,fi} \leq R_{d,fi} \quad (1)$$

where, $S_{d,fi}$: design value of the external force or moment in a fire situation; $R_{d,fi}$: design value of the internal force or moment in a fire situation.

2.2.1 External Bending Moment in Fire Situation

To calculate the external bending moment, considering a fire situation, one can use the Eq. (2).

$$M_{Sd,fi} = \left(1.2M_{gk} + 0.7\psi_2 M_{qk}\right) \quad (2)$$

where, $M_{Sd,fi}$: design value of the external bending moment, in fire situation [kNm]; M_{gk}: characteristic value of the bending moment relative to the permanent action, at room temperature [kNm]; ψ_2: quasi-permanent combination factor for serviceability limit state [5] [dimensionless]; M_{qk}: characteristic value of the bending moment relative to the variable action, at room temperature [kNm].

Alternatively, for simplification, Eq. (3) can be used. It is important to emphasize that such equations are independent of the fire type or time of fire exposure.

$$M_{Sd,fi} = 0.7M_{Sd} \quad (3)$$

where, M_{Sd}: design value of the external bending moment, at room temperature [kNm].

2.2.2 Proposed Internal Bending Moment in Fire Situation

To calculate the internal moment in a fire situation, $M_{Rd,fi}$, by proposed method, the Eq. (4) can be used.

$$M_{Rd,fi} = f_{yk}k_{s,m}A_s\left(d - \frac{f_{yk}A_s}{2f_{ck}b}\right) \quad (4)$$

where, f_{yk}: characteristic value of yield strength of reinforcing steel, at room temperature[kN/cm^2]; $k_{s,m}$: average reduction factor of steel resistance [dimensionless]; A_s: cross sectional area of longitudinal steel bars [cm^2]; f_{ck}: is characteristic value of concrete compressive strength, at room temperature [kN/cm^2]; b: reinforced concrete beam cross-section width [cm].

All the variables of Eq. (4) are obtained from the design at room temperature, except $k_{s,m}$. Then, the main concern of the equation is $k_{s,m}$, whose value is directly related to each steel bar temperature.

These temperatures, in its turn, can be calculated, with a reasonable simplification, from the method proposed by [6] as a function only of fire exposure time, and of each steel bar depth with coordinates x_i e y_i, as expressed by Eq. (5):

$$\theta_{c,xy} = \left[n_w\left(n_x + n_y - 2n_x n_y\right) + n_x n_y\right]\theta_g \quad (5)$$

where n_w, n_x, n_y, e θ_g, are given by the Eqs. (6)-(9):

$$n_w = 1 - 0.0616t^{-0.88} \quad (6)$$

$$n_x = 0.18ln\left({}^{t}/_{x_i^2}\right) - 0.81 \quad (7)$$

$$n_y = 0.18ln\left({}^{t}/_{y_i^2}\right) - 0.81 \quad (8)$$

$$\theta_g = 345log_{10}(480t + 1) + \theta_0 \quad (9)$$

where, t: time [hours]; x_i: horizontal Cartesian coordinate of the steel bar *i* [m]; y_i: vertical Cartesian coordinate of the steel bar *i* [m]; θ_g: gas temperature in the fire compartment [°C]; θ_0: gas temperature at the instant t=0, usually adopted 20°C.

Knowing the temperature of each steel bar, it is possible to determinate the average reduction factor of steel resistance $k_{s,m}$, by the weighted average of the $k_{s,\theta i}$ as a function of the steel area of each steel bar i, according to Eq. (10).

$$k_{s,m} = \frac{\sum k_{s,\theta i} A_{s,i}}{\sum A_{s,i}} \quad (10)$$

where, $A_{s,i}$: cross-sectional area of bar i of the longitudinal reinforcement [cm^2]; $k_{s,\theta i}$: reduction factor of the yielding strength, at the temperature θ, of the steel bar i, which can be calculated according to Eq. (11).

$$\begin{aligned}
k_{s,\theta i} &= 1 && \text{for } 20^{o}C \leq \theta_s \leq 400^{o}C \\
k_{s,\theta i} &= 1 - 0.0022(\theta_s - 400) && \text{for } 400^{o}C < \theta_s \leq 500^{o}C \\
k_{s,\theta i} &= 0.78 - 0.0031(\theta_s - 500) && \text{for } 500^{o}C < \theta_s \leq 600^{o}C \\
k_{s,\theta i} &= 0.47 - 0.0024(\theta_s - 600) && \text{for } 600^{o}C < \theta_s \leq 700^{o}C \\
k_{s,\theta i} &= 0.23 - 0.0012(\theta_s - 700) && \text{for } 700^{o}C < \theta_s \leq 800^{o}C \\
k_{s,\theta i} &= 0.11 - 0.0005(\theta_s - 800) && \text{for } 800^{o}C < \theta_s \leq 900^{o}C \\
k_{s,\theta i} &= 0.06 - 0.0002(\theta_s - 900) && \text{for } 900^{o}C < \theta_s \leq 1000^{o}C \\
k_{s,\theta i} &= 0.04 - 0.0002(\theta_s - 1000) && \text{for } 1000^{o}C < \theta_s \leq 1100^{o}C \\
k_{s,\theta i} &= 0.02 - 0.0002(\theta_s - 1100) && \text{for } 1100^{o}C < \theta_s \leq 1200^{o}C \\
k_{s,\theta i} &= 0 && \text{for } \theta_s > 1200^{o}C
\end{aligned} \quad (11)$$

As well as in the Tabular Method, in this proposed simplified method the eventual effects of spalling or thermal deformation restrictions are not considered. Besides that simplification, since in the most critical situations (high steel bars temperature), the average yielding strength of steel decreases more than the average compressive strength of concrete, that is, $k_{s,m} < k_{c,m}$ (average reduction factor of concrete compressive strength), consequently $\left(\frac{k_{s,m}}{k_{c,m}}\right) < 1$; therefore, since $k_{c,m}$ is difficult to determine, in order to simplify the determination of the internal bending moment in fire situation, in safety favor, it was considered $\left(\frac{k_{s,m}}{k_{c,m}}\right) = 1$.

3. Proposed method verification

The validation of the procedure for calculating the internal bending moment in fire situation by the proposed simplified method was done through comparison between results found in the literature, with 500°C isotherm method, and with the values determined by the ANSYS software.

Six beams sections, subjected to different times of fire exposure, were analyzed as shown in Figure 2. The comparison of the internal moment calculated in a fire situation can be observed in Table 3.

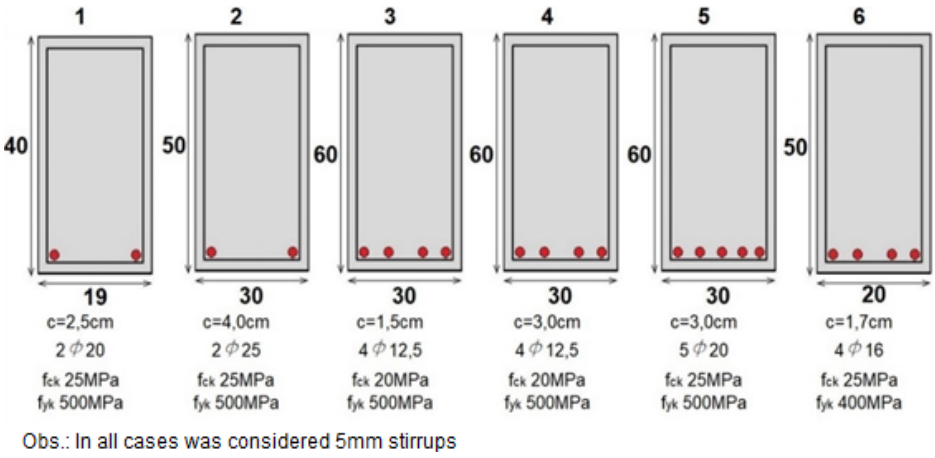

Fig. 2 Representation, without a scale, of analyzed sections, dimensions in centimeters

Through this comparative, the following observations can be made:

- The simplified method proposed presents results very similar to those obtained by 500°C isotherm method, which is an internationally recognizes method;
- The results obtained by the simplified method, compared to those found in the literature, are quite closed in values.
- As illustrated in Table 3, evaluating the proposed simplified method, only one of the results (highlighted in gray) presented a higher value than the ANSYS method, which makes a more rigorous and representative analysis of the reality (since the difference, in this case, was less than 1.0 kNm, that is, negligible); in all other results, lower bending moments than ANSYS were achieved, showing that the proposed simplified method, in general, presents values in favor of the safety.

4. Application example

In this section, it will be demonstrated, through a numerical example, how to apply the tabular and simplified method. The parameters have been defined considering an office building, located in the port area, with TRRF equal to 90 minutes and, from the beam design, taking efforts at room temperature [5] as exposed in Figure 3.

Table 3 Comparison of internal moment calculated in a fire situation

Beam/ Section (Figure 2)	Standard fire time [min]	Comparative Source	Internal moment calculated in a fire situation ($M_{Rd,fi}$)[kNm]			
			Reference value of the comparative source	Steel Temp. ANSYS	Steel temperature Wickström's equation	
				ANSYS Method	500°C Isotherm Method	Simplified Method Proposed
1	90	[3] Albuquerque, 2012	45.3	46.0	38.2	36.4
2	120	[3] Albuquerque, 2012	138.3	137.0	109.4	107.0
3	30	[7] Soares, 2003	127.6	128.4	125.5	125.5
3	60	[7] Soares, 2003	79.7	82.0	81.8	81.0
3	90	[7] Soares, 2003	31.1	47.9	44.7	43.7
3	120	[7] Soares, 2003	21.3	28.7	24.1	23.5
4	30	[7] Soares, 2003	132.1	131.7	131.7	132.1
4	60	[7] Soares, 2003	115.3	120.9	116.4	116.6
4	90	[7] Soares, 2003	78.2	92.7	88.7	88.2
4	120	[7] Soares, 2003	60.8	64.6	60.5	59.6
5	60	[8] Sousa e Silva, 2015	378.4	381.7	367.5	371.8
6	30	[9] Gonçalves, 2007	139.0	139.6	136.8	137.9
6	60	[9] Gonçalves, 2007	94.0	110.6	89.8	88.7
6	90	[9] Gonçalves, 2007	43.0	62.0	47.1	45.3
6	120	[9] Gonçalves, 2007	22.0	32.9	24.8	23.6

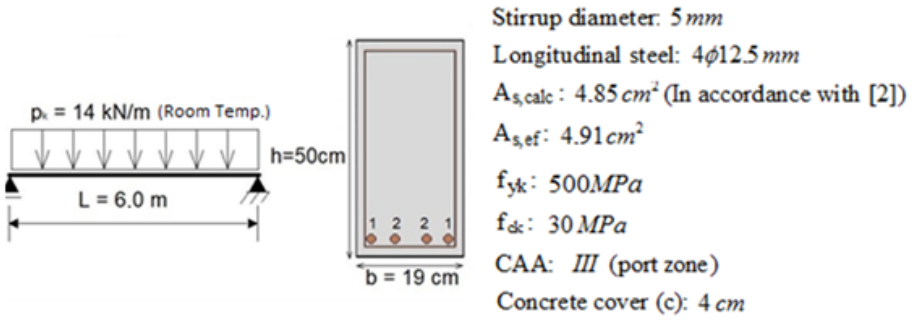

Fig. 3 Reinforced concrete beam parameters

4.1. Tabular method

The first step is to determine the distance between the longitudinal reinforcement axis and the concrete face exposed to fire (c_1). In this case, the calculation can be made as follows:

$$c_1 = c + \emptyset_t + \frac{\emptyset}{2} = 40 + 5 + \frac{12.5}{2} \therefore c_1 = 51.25 \text{ mm}$$

Then, the c_{1min} is determined consulting Table 1, for a TRRF equal to 90 minutes. So, through a simple reading of the table, c_{1min}=45 mm.

Although the tabular method is quite expeditious, there are some alternatives and cares to be taken that may not be so immediate. As previously mentioned in Item 2.1, in sections with only one reinforcement layer and width not greater, in accordance with the TRRF, than b_{min} indicated in column 3 of Table 1, some design changes must be made. This is the case of the analyzed cross-section, where 4 bars with 12.5 mm are arranged in only one layer and the beam width of 190 mm is not greater than 300 mm, as column 3 of Table 1 for TRRF to 90 minutes. This verification with column 3 of Table 1 is suggested by [2]

Therefore, the distance between the longitudinal corner steel axis and the concrete lateral surface exposed to fire (c_{1l}) should be 10 mm higher than c_{1min} found by the tabular method. That is, to ensure structural safety, $c_1$must be greater than c_{1l}=c_{1min}+10mm. In this case, c_{1l}=45+10=55 mm. So, it is not in the safety range, since:

$$c_1 = 51.25 \text{ mm} < c_{1l} = 55 \text{ mm}$$

If no alternative is taken, the time of fire resistance (TRF) must be calculated, considering, in safety favor, c_1 reduced by 10 millimeters. For this example:

$$c_1 = 51.25 - 10 = 41.25 \text{ mm}$$

To calculate the piece TRF, by the linear interpolation of the values given in Table 1, it is recommended to proceed as follows:

If for b_{min}= 190 mm and c_{1min} = 30 mm, the TRF is 60 min;

And for b_{min} = 190 mm and c_{1min} = 45 mm, the TRF is 90 min;

So, for b = 190 mm and c_1= 41.25 mm, the TRF, by interpolation, is equal to 83 minutes;

As a result, in this case the TRF is not safe, because:

$$TRF = 83 \text{ min.} < TRRF = 90 \text{ min.}$$

Therefore, in short, the beam of this example, with same characteristics of the design at room temperature, does not present structural safety in a fire situation, in accordance with the normative tabular method. Based on this, some alternatives were pointed out for the correct design in a fire scenario by the tabular method, as following:

I. Replace the two corner bars for only one with the diameter immediately greater, substituting 4Ø12.5 for 2Ø16 in the corners and 2Ø12.5 in the center (TRF=101 min);

II. Increase beam height, from 50cm to 60cm, considering the possibility of c_1 reduction (TRF=92 min);

III. Increase concrete cover, from 4.0 cm for 4.5cm (TRF=92 min);

IV. Arrange the reinforcement in two layers of 2Ø12.5 each one (TRF=99 min);

V. Considering Δc_1, that is, reduced value of c_1 (TRF=84 min).

The alternatives III and IV, although they satisfy the safety condition, for a fire situation, according to the Tabular Method, they are not valid for the beam design at room temperature. Besides that, the alternative V, in its turn, is not enough to achieve a safety condition.

4.2. Proposed Simplified method

First, it is necessary to calculate the characteristic external bending moment at room temperature. Considering the study refers to a simply supported beam, it can be calculated as follows:

$$M_{Sk} = \frac{p_k L^2}{8} = \frac{14 \times 6^2}{8} \therefore M_{Sk} = 63.0 \text{ kNm}$$

Also, only for possible comparisons, the calculated external bending moment at room temperature can be determined as follows:

$$M_{Sd} = 1.4 \times M_{Sk} \therefore M_{Sd} = 88.2 \text{ kNm}$$

In this example, considering $M_{Sd,fi}=0.7M_{Sd}$, the calculated external moment in a fire situation can be determined as follows:

$$M_{Sd,fi} = 0.7(88.2) \therefore M_{Sd,fi} = 61.74 \text{ kNm}$$

After determining the external bending moment, the internal bending moment is defined. For this, steel bars temperatures are calculated, considering a standard time of fire exposure equal to the TRRF of 90 minutes. By the Wickström's equation, as presented in Eq. (5), the corner bars temperature will be:

$$\theta_{c,xy1} = [0.957(0.333 + 0.333 - 2 \times 0.333 \times 0.333) + 0.333 \times 0.333]1006 =$$

$$\therefore \theta_{s1} = \theta_{c,xy1} = 539^{o}\text{C}$$

The center bars temperature will be:

$$\theta_{c,xy2} = [0.957(0.170 + 0.333 - 2 \times 0.170 \times 0.333) + 0.170 \times 0.333]1006 =$$

$$\therefore \theta_{s2} = \theta_{c,xy2} = 432^{o}\text{C}$$

From bars temperatures is possible to calculate the reduction strength factor of steel, $k_{s,\theta i}$, as presented in Eq. (11), For θ_{s1} and θ_{s2} respectively

$$k_{s,\theta 1} = 0.78 - 0.0031(539 - 500) = 0.6591$$

$$k_{s,\theta 2} = 1 - 0.0022(432 - 400) = 0.9296$$

As such, the average steel reduction strength factor $k_{s,m}$, can be defined, by considering the area of each bar (A_{si}=A_{s1}=A_{s2}=1.2272 cm^2), according to Eq. (10):

$$k_{s,m} = \frac{2 \times 0.6591 \times 1.2272 + 2 \times 0.9296 \times 1.2272}{4 \times 1.2272} = 0.7944$$

Finally, applying the Eq. (4), the calculated internal bending moment, in a fire situation, by the proposed simplified method, is determined:

$$M_{Rd,fi} = 50 \times 0.7944 \times (4 \times 1.2272) \left[44.875 - \frac{50 \times (4 \times 1.2272)}{2 \times 3 \times 19}\right] = 8329 \text{ kNcm}$$

$$M_{Rd,fi} = 83{,}29 \text{ kNm}$$

To verify if the safety condition ($M_{Sd,fi} \leq M_{Rd,fi}$) is satisfied, Eq. (1) is used. In this case, the safety is guaranteed, since:

$$M_{Rd,fi} = 83.29 \text{ kNm} > M_{Sd,fi} = 61.74 \text{ kNm}$$

4.3. Comparative results

The simplest comparison to do is about the structural safety condition, as in Table 3.

Table 3 Comparative of the structural safety condition (TRRF 90 min)

Structural safety condition	
Tabular Method	Proposed Simplified Method
No satisfied	Satisfied
TRF < TRRF	$M_{Rd,fi} > M_{Sd,fi}$

As shown in Table 3, in this example, the proposed simplified method presents more economical results than the Tabular Method. Another comparison that can be made, according to Table 4, is the beam TRF determined by Tabular Method, by 500°C Isotherm Method, and by the Proposed Simplified Method, considering the mentioned alternatives in Item 4.1 of this paper.

As can be seen in all hypotheses of this example, the proposed method is more economical than Tabular. Also, results similarity is observed between 500°C Isotherm Method and the proposed method one. It is important to note that the TRF values determined with the simplified method were obtained by iteration, changing the fire exposure time until reaching the limiting condition: $M_{Sd,fi} = M_{Rd,fi}$.

5. Conclusions

Through a numerical example, it was demonstrated a practical application of the tabular and simplified methods, analyzing some possible alternatives in the reinforced concrete beams design. From that, a comparison between tabular and proposed simplified method has been made, and the results obtained by the proposed method were more economical than those obtained from the tabular method.

Table 4 Comparative of the beam TRF, determined by Tabular Method, by 500°C Isotherm Method, and by the Proposed Simplified Method

Beam data	Time of fire resistance (min)		
	Tabular	500°C Isotherm	Simplified Method
Initial condition: room temperature 19x50 cm; c = 4.0 cm; 4 Ø 12.5 – one layer	83	113	113
According alternative I: increasing corner bars 19x50 cm; c = 4.0 cm; 2 Ø 16 +2 Ø 12.5 – one layer	101	130	129
According alternative II: increasing beam height 19x60 cm; c = 4.0 cm; 4 Ø 12.5 – one layer	92	125*	125*
According alternative III: increasing concrete cover 19x50 cm; c = 4.5 cm; 4 Ø 12.5 – one layer	92	125	125
According alternative IV: Arrange the reinforcement in two layers 19x50 cm; c = 4.0 cm; 4 Ø 12.5 – two layers	99	113	112
According alternative V: considering Δc_1 19x50 cm; c = 4.0 cm; 4 Ø 12.5 – one layer	84	113	113

* Considering the $M_{Sd,fi}$= 63.95 kNm due to the height of 60 cm; for the other cases $M_{Sd,fi}$ =61.74 kNm (height of 50 cm);

Additionally, the results by the 500°C isotherm method and the proposed simplified one are convergent and very close; however, the proposed method showed advantage when the ease of calculation in the procedure is considered, because, through some simplifications, is not necessary to determine the cross-section reduced width, as a function of the 500°C isotherm.

Then, is also important to emphasize that, in almost all examples, through proposed simplified method were obtained lesser internal bending moments than the ANSYS method, which makes a more rigorous and representative analysis of the problem. This is an evidence that, in general, the proposed method values are in safety favor.

Moreover, the most important advantage of the proposed simplified method is that calculation can be done manually, in a relatively simple way (easier than the 500°C isotherm method or using ANSYS), without using graphics, abacus or sophisticated computational programs. However, even so, it is possible to design reinforced concrete beams, with safety in fire situations, and in some cases, it could be more economical than the normative tabular method.

The validation of calculation models of both temperatures and bending moments in fire situation was done through a comparative study with values found in the literature, as well as those calculated by the 500°C isotherm method and those obtained with the aid of ANSYS software.

Therefore, it is believed that the proposed simplified method, if implemented, could allow development or improvement in some commercial design software. Since, currently in the marketplace, such tools are limited to do the verifications only based on the tabular method, without considering the external and internal forces. In this scenario, the designer often has the need of changing the dimensions of the concrete cross-section. This fact does not present economic advantages and, probably because of that, the use of the Brazilian Standards is not stimulated, as [10] argues that only a small portion of the professionals in this area uses NBR 15200 [2].

Finally, the proposed simplified method, besides being an easy method to apply, presents results usually in safety favor; and, even so, allows more economical results than the tabular method. In cases where the structural design at room temperature does not satisfy the TRRF determined by the tabular method, rather than in the first moment increase the dimensions of the structure, it is recommended to verify by the proposed simplified method. So, the designers will be stimulated to use NBR 15200 [2] in their projects, guaranteeing, in a more economical way, structural safety in a fire situation.

Acknowledgement

The authors would like to thank CAPES, CNPq and FAPERGS for financial support during the development of this project. The authors would also like to thank the Federal University of Rio Grande for the structure offered for conducting this research.

References

[1] Araújo JM. Curso de Concreto Armado - 4 Vols. Rio Grande: Editora Dunas, 2014.
[2] ABNT NBR 15200, de 26 de abril de 2012. Projeto de estruturas de concreto em situação de incêndio. Rio de Janeiro: Brazilian Association of Thecnical Rules.
[3] Albuquerque GB de ML de. Dimensionamento de vigas de concreto armado em situação de incêndio (Master Thesis). University of São Paulo, São Paulo, 2012.
[4] ABNT NBR 14432, de 30 de novembro de 2001. Exigências de resistência ao fogo de elementos construtivos de edificações - Procedimento. Rio de Janeiro: Brazilian Association of Thecnical Rules.
[5] ABNT NBR 6118, de 29 de abril de 2014. Projeto de estruturas de concreto. Rio de Janeiro: Brazilian Association of Thecnical Rules.
[6] Wickstrom U. A very simple method for estimating temperature in fire exposed concrete structures (SP Rapport), 1986.
[7] Soares EMP. Verificação de peças usuais de concreto armado em situação de incêndio (Dissertação de mestrado). Engineering School of the Federal University of Minas Gerais, Belo Horizonte, MG, 2003.
[8] Sousa DA de, Silva GP. Estruturas de concreto em situação de incêndio (Trabalho de conclusão de curso). Federal University of Goiás, Goiânia, GO, 2015.
[9] Gonçalves MJCR. Comportamento ao fogo de elementos estruturais de betão : análise númerica e metodologia (PhD Thesis). Engineering Faculty of the University of Porto, Portugal, (2007).
[10] Costa CRG, Ajala GR, Júnior SÁV, Oliveira MB de, Miller CP. Estudo Comparativo da Utilização da ABNT NBR 15200:2012 e da ABNT NBR 6118:2014. REINPEC - Revista Interdisciplinar Pensamento Científico, 2(1), 2016. https://doi.org/10.20951/2446-6778/v2n1a6

Research on Engineering Structures & Materials
journal homepage: http://jresm.org
Research Group

Research Article

Estimation of the piles axial load in the Public Wharf of Porto Novo during an operation of a port crane

Matheus de Lima Nunes*, [a], Mauro de Vasconcellos Real[b]

Post-graduation program in Ocean Engineering, Federal University of Rio Grande – FURG, Brazil.

Article Info

Article history:
Received 09 Feb 2019
Revised 11 May 2019
Accepted 07 Aug 2019

Keywords:

Port Structures;
Computation modeling;
Wharf design;
Finite Element Method

Abstract

Port structures are usually large and are subject to heavy loads such as the stresses caused by a port crane and other equipment used during a port operation. Therefore, for a meticulous analysis of the internal forces of the port structures, with the intention to optimize and turn more effective the design, is essential the use of computational tools and advanced mathematical methods, as, for example, the Finite Elements Method. The Porto Novo of the Port of Rio Grande moves millions of tons of materials per year, becoming one of the main ports in Brazil. Its structure has gone through two stages of modernization making it possible the use of larger and more efficient port equipment, operation with ships of greater load capacity, and more quantity of mooring berths available for simultaneous operation. This study will be intended to perform the computational modeling of the Public Wharf of Porto Novo of the Port of Rio Grande using the finite element method through the ANSYS software to estimate the axial loads of the wharf piles when a Mobile Port Crane is in port operation.

© 2019 MIM Research Group. All rights reserved.

1. Introduction

The maritime transport sector is growing, with bigger ships and equipment to support the terminals demand. Because of this, it becomes necessary that existing docking structures be revitalized, expanded, and the construction of new cargo terminals [1].

Port is an area for mooring boats and ships, serving as shelter from waves, winds, and currents, allowing access to the coast, aiming at port operations, by docking points. For this activity to occur safely, these areas must have mooring points for the vessels work with minimal efforts and displacements during port operations and fender systems to protect both ship and structure from collision damage. Quay structures are usually large constructions subjected to high-intensity forces [2].

Therefore, to perform a reliable design and with a low-cost construction, it is essential to carry out a rigorous structural analysis with the use of advanced mathematical techniques such as the finite element method (FEM) and the use of computational tools to solve complex structures.

The public wharf of Porto Novo is located in the city of Rio Grande / RS, and it is among the main ports in Brazil, moving millions of tons of materials. Its area has the intended use for military, tourism, roll-on/roll-off, bulks, fertilizers, and container ships. Its structure was modernized in the extension of 1575m of its wharf and increased the depth of mooring berths. This work was carried out in two stages; the first one finished in the year 2004 (450m) and the second one in 2017 (1125m). The objective of this research is to perform

*Corresponding author: matheusnunesrg@gmail.com
[a] https://orcid.org/0000-0002-9723-8175; [b] orcid.org/0000-0003-4916-9133
DOI: http://dx.doi.org/10.17515/resm2019.113ms0209

the computational modeling of the public wharf of Porto Novo of the Port of Rio Grande, using the finite element method through the ANSYS software to investigate the behavior of the structure when it's on the effect of a mobile port crane (Gottwald HMK280E) during a port operation.

2. The computational model

Each wharf modules have the following dimensions 75.00m x 11.20m and the characteristic compressive strength of the concrete used was 40MPa. The infrastructure consists of:

- A line of 12 mixed piles of reinforced concrete with ø71.12 cm (28 ") metal jacket, in the sea parallel to the quay line.

The union of precast structures and in-situ structures in reinforced concrete form the platform (Fig. 1) of the wharf:

- A longitudinal beam called V1, located in the front part of the platform and parallel to the line of the wharf (built part precast concrete and another part concreted in-situ), which transfers its forces to the line of piles;
- A second longitudinal beam called V2 (made in-situ), located on the back of the wharf. Its forces are transmitted to the upper part of the existing quay-wall using sliding supports;
- 22 pre-casted slabs with Pi cross-section;
- 03 blocks built in-situ where the fenders and mooring structures are located;
- A cantilever slab built in-situ after assembly of V1 beams and slabs type Pi.

Also, exist in the posterior part of the platform a vertical plate for soil containment and mobilization of frictional forces and a pavement plate, but they were not considered in the computational model. The construction of the computational model of the structure was performed using ANSYS software, which uses the finite element method for structural analysis.

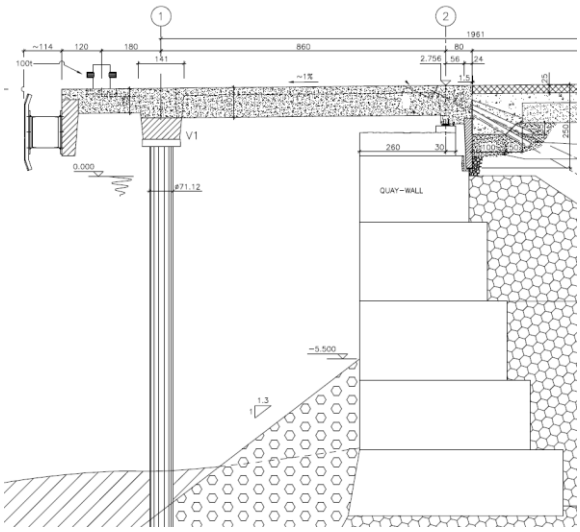

Fig. 1 Cross-section of the wharf

2.1. Platform Modeling

For the modeling of beams V1 and V2, the element BEAM189 (Fig. 2) was used. It is a quadratic element of 3 nodes, having 6 degrees of freedom in each node (displacements in x, y and z, and rotations in x, y, and z). The element BEAM189 is suitable for linear analyzes and can be applied to slender or robust beams.

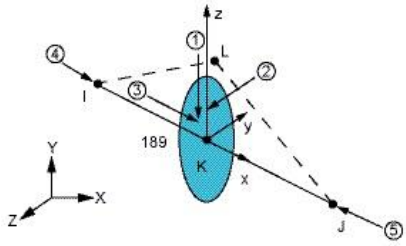

Fig. 2 The element BEAM189 [3]

It was necessary to divide the Pi slabs into one slab, and two beams, because Ansys don't have in its geometry library this type of cross-section (Fig. 3).

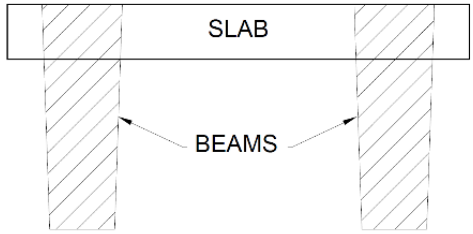

Fig. 3 Pi cross-section divided into three parts

For the beams of Pi cross-section, it was used the element BEAM189 and for the slab the element SHELL281 (Fig. 4). It was used rectangular elements of 8 nodes, having 6 degrees of freedom in each node (displacements in x, y, and rotations in x, y, and z). SHELL281 also used for the cantilever slab and Blocks. This element is suitable for analyzing thin to moderately-thick shell structures and for linear analyzes.

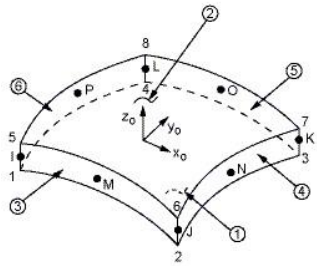

Fig. 4 The element SHELL281 [3]

2.2. Piles Modeling

The piles have a diameter of 71.12 cm and were also modeled using the BEAM 189 element. It was simulated the soil-structure interaction assuming a length, where a pile could be adopted as being perfectly fixed in the soil [4, 5].

$$L_e = L_S + L_U \quad (1)$$

$$L_S = 1.8 \cdot L_0 \quad (2)$$

$$L_0 = \sqrt[5]{\frac{E_P \cdot I}{n_h}} \quad (3)$$

Where L_e is the Cantilever length, L_s is the Buried length, L_U is the free Length of the pile (unearthed), L_0 is the Fictitious length, E_p is Modulus of elasticity of the pile material, I is the moment of inertia of the cross-section of the pile, and n_h is Coefficient of the horizontal reaction of soil [4, 5]. The depth of all the piles was considered the same (Fig. 5).

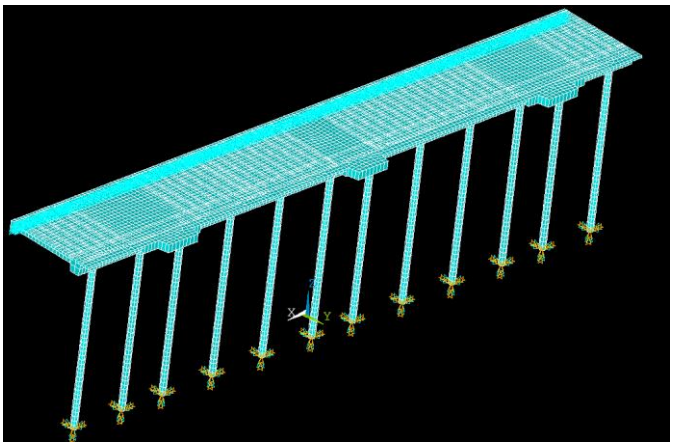

Fig. 5 The computational model

2.3. Test of Mesh Convergence

A mesh size verification test was performed to ensure that there is a convergence of the results for the elements used [6]. A test load was applied (Fz = -1000kN) in the center of the structure, carrying out simulations with mesh sizes 0.75m x 0.75m, 0.50m x 0.50m, 0.25m x 0.25m and 0.10m x 0.10m, in order to ensure that the elements used had a convergence of results.

2.4. Loadings

It was considered the deadweight of the structure, and a load of a mobile port crane model Gottwald HMK280E during a port operation. The crane can be placed in any location on the dock platform and on the deck that exists at the back of the dock. For the crane, several loading situations were tested on the quay with the boom positions of 45 °, 90 °, and 135 °, except for the 0 ° position, since the most loaded stabilizer pads are those arranged on the pavement slab, localized behind the wharf platform (Fig. 6).

Fig. 6 Mobile Port Crane

Table 1 presents values of stabilizer pads loadings for the different positions of the boom in the quay. The stabilizer pads E1 and E2 are arranged on the pavement, and the E3 and E4 are that are on the quay platform (Fig. 7).

Table 1 - Values of stabilizer pads loadings for the different positions of the boom.

Boom angle	E1 (kN)	E2 (kN)	E3 (kN)	E4 (kN)
0°	1410	610	610	1410
45°	620	490	1140	1790
90°	420	500	1670	1460
135°	410	840	1990	800

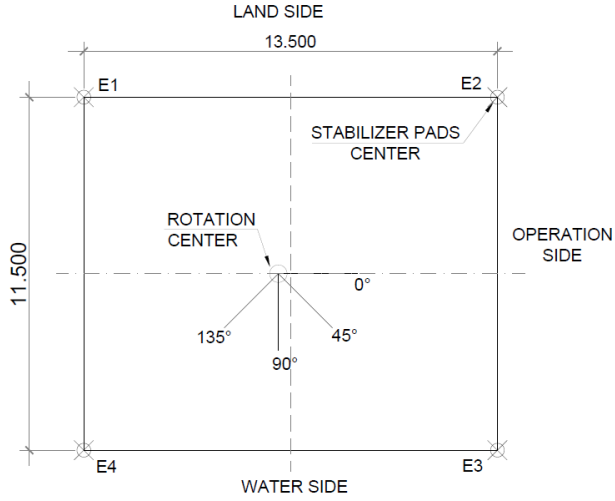

Fig. 7 Sketch of center points of the stabilizer pads and boom angle

4. Results and Discussions

The results obtained in the mesh convergence test were identical for the four mesh sizes, for that reason, the mesh with larger size the values obtained is already satisfactory. However, to get the model mesh with better precision, a value of 0.50m x 0.50m was used for the final simulation mesh.

It was simulated several positions for the port crane during operation, and the worst result is when the following situation occurs:

- The crane is in operation closest to the right corner of the dock;
- The operating side is on the left;
- The rotation center is on the left of the crane axis;
- The front stabilizer pads are over the beam V1 axis, with the stabilizer pad E3 is closest to the right edge of the wharf;
- With the boom operating in the 135° position.

In this case, was obtained the maximum value, which is a compression force of 3164kN for E12 pile (Table 2).

Table 2 Axial load (N) values of piles for the worst operating scenario of the crane

Pile	E1	E2	E3	E4	E5	E6	E7	E8	E9	E10	E11	E12
N (kN)	933	1193	1202	1031	1009	1129	1125	1008	1114	1443	1436	3164

The maximum Z-displacement of the structure for the worst scenario occurs in the region of the slab in the front part of the right edge of the quay, near the crane stabilizer pad E3, with a value of 3mm (Fig. 8).

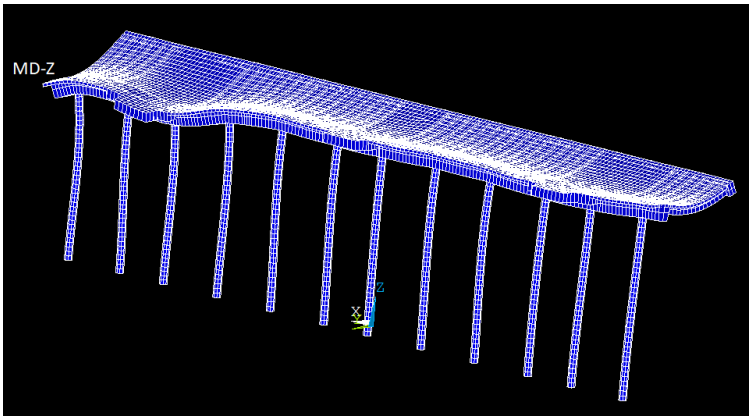

Fig. 8 Color graph of displacements in the worst condition

5. Conclusion

In this study, the computational modeling of the Public Wharf of Porto Novo was carried out with the objective of verifying the axial forces on the piles to the worst position of a port crane during an operation. The results obtained from the mesh convergence, demonstrate the crane load did not show variation for the four sizes of the element used. It is concluded that the computational model performed in the ANSYS software proved to

be quite satisfactory. The worst load situation was obtained when the crane is located on the front of the platform, with the operation side in the same module where the crane is located.

References

[1] Ranga Rao AV, Sundaravadivelu R. A knowledge-based expert system for design of berthing structures. Ocean Engineering, 1999, 26, 653–673. https://doi.org/10.1016/S0029-8018(98)00013-4
[2] Alfredini P, Arasaki E. Obras e Gestão de Portos e Costas. Blucher, São Paulo, SP, Brazil, 2009.
[3] Ansys. Basic Analysis Guide.Ansys Inc, Canonsburg, PA, USA, 2009.
[4] Davisson MT, Robinson K.E. Bending and buckling of partially embedded piles. In 6th ICSMFE, 1965.
[5] Urbano AR. Dimensionamento de Fundações Profundas. Blucher, São Paulo, SP, Brazil, 2003.
[6] Viegas CHH, Real MV, Moura MW. Structural analysis of a container pier through the finite element method. Revista de Engenharia e Tecnologia, 2015, 7: 1 – 12.

Blank Page

Research on Engineering Structures & Materials
journal homepage: http://jresm.org
Research Group

Research Article

Numerical evaluation of the mechanical behavior of an FPSO mooring system fairleads foundations due to maximum environmental loads

Kauê Louro Martins[*,a,1], Vinícius Torres Pinto[b,1], Luiz Alberto Oliveira Rocha[c,2], Elizaldo Domingues dos Santos[d,1], Liércio André Isoldi[e,1]

[1]*Graduate Program in Ocean Engineering (PPGEO), Federal University of Rio Grande – FURG, Rio Grande, RS, Brazil.*
[2]*Graduate Program in Mechanical Engineering, University of Vale do Rio dos Sinos – UNISINOS, Porto Alegre, RS, Brazil.*

Article Info

Article history:
Received 15 Feb 2019
Revised 22 Apr 2019
Accepted 15 May 2019

Keywords:

Mooring System;
Fairleads;
Fairlead Foundations;
Brackets;
Maximum environmental loads

Abstract

The present work aimed to study the mechanical behavior of the fairlead support brackets of a FPSO (Floating, Production, Storage and Offloading) mooring system located in the Campos Basin (22°58'14''S, 42°01'36''O to 20°19'08''S, 40°20'16''O) using numerical simulation. For an inextensible anchor line, the maximum stresses from the environmental loading of waves, winds and currents were determined. The stresses acting on the anchor line were applied to the centroid of the fairlead and the reactions to these, generated in the brackets, were applied in the internal region of the hole that receives the fairlead support axis. The brackets are fixed to the side of the hull by 3 vertical and 1 horizontal points. Their initial proposed geometry was based on models currently in operation on platforms P66 and P67 (Petrobras platforms capable of stocking 1.67 mi oil barrels each, with 288 m of length overall, they are designed to anchor at depth of 2200 m). The numerical simulation process was performed using the Mechanical APDL tool of ANSYS software with a computational model composed by three-dimensional (3D) finite elements. The results indicated that for the proposed geometry the mechanical integrity of the brackets is assured, considering that von Mises maximum stresses did not extrapolate the yielding stress limit of the steel.

© 2019 MIM Research Group. All rights reserved.

1. Introduction

The discovery of petroleum basins in ocean regions with a water layer deeper than 200 m made necessary the use of ships capable to produce and storage that petroleum [1]. The floating solution for the petroleum extraction create the necessity of ensure the permanence of the vessel in the project position. In such context, the mooring system one of the most important systems on the platform.

To solve this problem, the mooring systems were developed to minimize the effects of environmental loads, reducing the offset positioning of platforms. Many types of mooring systems were elaborated and applied, focusing in reduce the surge, sway and heave movements. The preset position has a huge importance and losing that position can cause risk to integrity of the vessel, equipment and environment [2].

[*]Corresponding author: kmartins@furg.br
[a] orcid.org/0000-0001-8441-0848; [b]orcid.org/0000-0002-0977-5086; [c] orcid.org/0000-0003-2409-3152; [d] orcid.org/0000-0003-4566-2350; [e] orcid.org/0000-0002-9337-3169
DOI: http://dx.doi.org/10.17515/resm2019.119ms1502

One of the most used types of mooring applied on the industry is the Spread Mooring. It consists in multiple mooring lines around the vessel. The distribution of the lines gives to the platform the stability to support the environmental loads in every direction, ensuring the set position in any sea condition. The Fig. 1 exemplifies the usual arrangement of equipment from the Spread Mooring.

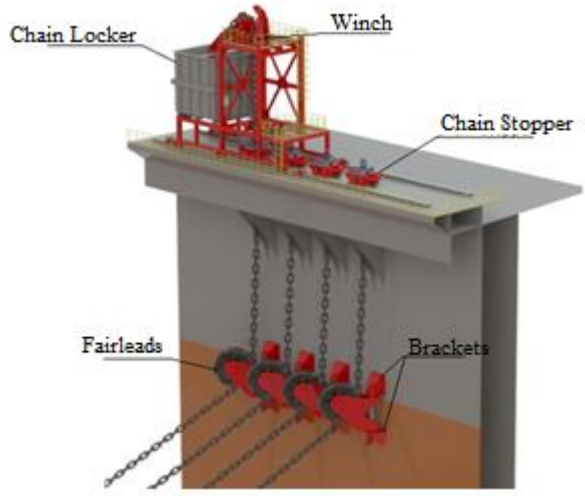

Fig. 1. Example of anchorage system of the Spread Mooring type.

On the side of the hull are the fairleads (see Fig. 1), which have the function of guiding the lines from the ocean side to the main deck level, avoiding the action of torsional loads on the winches and the other equipment on deck.

Consequently, the integrity of all other equipment and the system depends on correct project, manufacture, installation and operation of the fairlead and their foundation (the brackets), as well as of the mooring line.

The mooring system became object of many researches in the last years, but many of them were focused on the line comportment and composition, like Finucane [3], Qiao et al. [4] and Vargas et al. [5]. Although there are researches about brackets or foundations with similar application, as Kumar et al. [6], none of them is focused on naval equipment or fairlead foundations.

The importance of studies about the fairleads is shown by Gordon et al. [7] when it is stated the criticality of the equipment in the system.

The Det Norske Veritas (DNV) [8] stipulates three types of loading that need to be considered on the project of fairleads and their foundations: the Ultimate Limit State (ULS) is the situation with the environmental loads on their maximum value; the Accidental Limit State (ALS) consider the same loads of the ULS, however the number of the mooring lines is smaller since the other lines must maintain the position of the platform in the case of failure of some line; and the Fatigue Limit State (FLS) must be used to analyze the cyclical loads. DNV undertakes classification, certification, and other verification and consultancy services relating to quality of ships, offshore units and installations, and onshore industries worldwide, and carries out research in relation to these functions.

Therefore, the main objective of this paper is analyzing the effects of the environmental loads on the brackets of the fairleads in a mooring system of a FPSO platform, using numerical simulation through the tool Mechanical APDL of ANSYS software. This platform

is placed on Brazilian coast, more specifically on Campos Basin (22°58'14''S, 42°01'36''O to 20°19'08''S, 40°20'16''O). DNV is an autonomous and independent foundation with the objectives of safeguarding life, property and the environment, at sea and onshore.

2. Methodology

As a first stage for the project of the system, adopt the lines as inextensible is a normal premise. Lacerda [9] analyzed the effects of the extensibility on the catenary mooring lines, concluding that the break up loads on the inextensible lines are 40% less than in tensioned lines. It was demonstrated that using inextensible lines is a more conservative approach. Figs. 2 and 3 shows a scheme of an inextensible catenary mooring line and its division on an infinitesimal element.

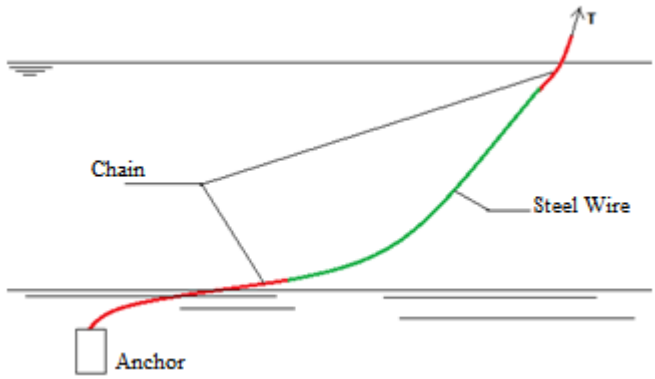

Fig. 2. Line composition commonly adopted in mooring.

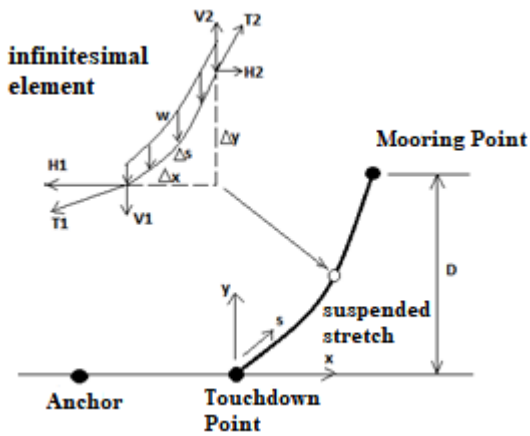

Fig. 3. The infinitesimal element of the catenary mooring line.

To define the loads created by the environment on the lines the methodology proposed by Nazário [10] was adopted. The premises of plane surface on the deep ocean and infinite axial rigidity of the mooring line must be assumed so that the equation is valid. If the sum of horizontal loads is null (see Fig. 3):

$$\Sigma Fh = 0 = H_2 - H_1 \tag{1}$$

where:

$$H_1 = T_1.\cos(\theta_1) \tag{2}$$

$$H_2 = T_2.\cos(\theta_2) \tag{3}$$

Considering the sum of vertical loads equal to zero (see Fig. 3):

$$\Sigma Fv = 0 = V_2 - V_1 - (w.\Delta s) \tag{4}$$

where:

$$V_1 = T_1.\text{sen}(\theta_1) \tag{5}$$

$$V_2 = T_2.\text{sen}(\theta_2) \tag{6}$$

being: w the linear weight of submerged line and Δs the infinitesimal element length.

The boundary conditions application allows to define the relation between the depth (d) and the mooring radius (r). Hence, it is possible to determine the inclination of the line in the fairlead spot.

$$d = \frac{H}{w}.\cosh\left(\frac{w.r}{H}\right) - 1 \tag{7}$$

$$r = \frac{H}{w}.\cosh^{-1}\left(\frac{w.d}{H}\right) + 1 \tag{8}$$

Nazário [10] mentioned the importance of considering the submerged weight on the equations. The submerged weight is the weight of the line subtracted of the buoyancy. This difference of the weight results in a higher mooring radius (r), once the variable values on the equations are only the weight and the environmental loads.

The longest length on the line also creates a different inclination on the line and it affects the loads on the fairleads and brackets.

The environmental loads can be predicted from eight different sources, according with DNV [11]:

- wind;
- waves;
- current;
- earthquakes;
- ice and snow;
- storms;
- extreme temperatures;
- action of animals;
- algae and other marine creatures.

The most common and easier of measurability sources are those generated by winds, currents and waves. In this sense, in this research, the environmental loads were composed by only these three parcels. To do so, the environmental load concerning current or wind can be obtained as:

$$F = \frac{1}{2}.\rho.c.A.v^2 \tag{9}$$

where: ρ is the fluid density (kg/m^3), C is the drag coefficient, A is the platform area suffering the effects of the load (m^2) and v is the incidence velocity of the load (m/s).

All the factors are related to a certain incidence angle of the load. So, Eq. (9), is applicable for both the wind and the current portion, but only the wind load comes from the aerodynamic drag acting on the platform region above the water slide, while the stream portion is generated by the interaction of the flow with the submerged region of the vessel.

The load generated by the waves was obtained through a conservative analysis, proposed by Bergdahl and Kofoed [12], which assumes that their object of study fully reflects the average wave, making their analysis applicable in irregular wave. The equation of the load generated by the waves incidence is given by:

$$F_w = \frac{\rho.g.H_s.Aw}{32} \tag{10}$$

where: g is the gravity acceleration (m/s^2), Aw is the area of the platform that suffer incidence of the load (m^2) and Hs is the average height of the waves (m).

For the case under study, a mixed anchor line was established between ropes of model R4, with a diameter of 120 mm, and Spiral Strand type steel cables, grade 2, class A, galvanized steel A586, with diameter of 102 mm.

DNV proposes angles of incidence for each of the three environmental loads in relation to the others, but in this work the same angle was adopted for all the loads. Figure 4 shows a comparison between the recommendation of the standard, Fig. 4 (a), and what was used in this work, Fig. 4 (b).

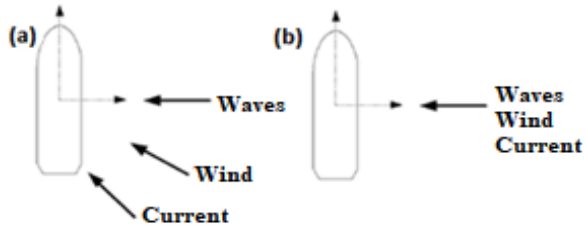

Fig. 4. Comparison between recommended angles of incidence (a) and applied in the study (b). (Adapted from DNV, 2015).

The calculated loads were applied to the centroid of the fairlead and later, through the equations of static equilibrium, applied in the inner region of the bracket hole, which receives the fairlead axis, visible in Fig. 5.

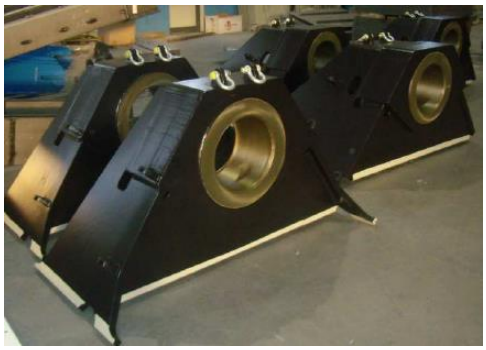

Fig. 5. Bracket used in the P66 and P67 platforms of Petrobras.

The proposed geometry for simulation through ANSYS for the set of brackets is based on the equipment used in the replicating projects of the FPSOs P66 and P67 of Petrobras [13]. The simulation employed the finite element SOLID186, which is composed of 20 nodes, having 3 degrees of freedom per node, being these the translation in the axes *x*, *y* and *z*.

The SOLID186 finite element has a mixed formulation capability, allowing to simulate deformations of elastoplastic materials, although in this study only a linear elastic analysis is performed. The use of this element will provide, in future studies, an elastoplastic analysis of the region where the highest tensions are concentrated [14].

The mesh was generated with finite tetrahedral elements [15]. For the definition of mesh refinement to be adopted, a mesh convergence test was performed. From this, the computational model was verified.

3. Computational Model Verification

To verify the computational model, an example of a three-dimensional bracket with simpler geometry was performed, as shown in Fig. 6. The study proposed by Moussa [16] was replicated by changing only the finite element used in the simulation, from PLANE82 to SOLID186. It is worth to highlight that both elements are available in ANSYS software.

The finite element PLANE82 composed of 8 nodes, has 2 degrees of freedom, allowing translation around *x* and *y* axes, presenting less precision in comparison to the finite element applied in this study (SOLID186).

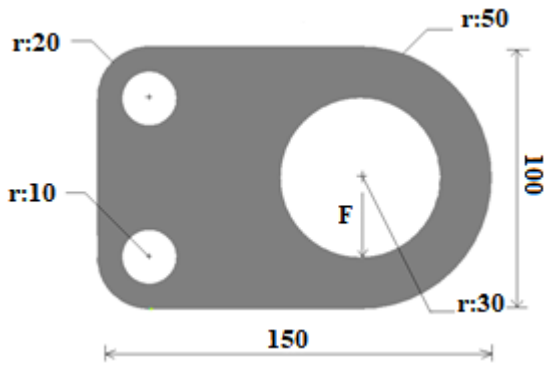

Fig. 6. Bracket used to verify the computational model (dimensions in mm).

The steel plate of the bracket has a thickness of 20 mm and its dimensions of length and maximum height are 150 mm × 100 mm. The inner areas of the two smaller holes are considered clamped and the load (*F*) applied internally to the larger hole is 1000 N. Table 1 presents the results of the mesh convergence test in the current study, with finite element SOLID186.

Table 1. Comparison between the values obtained in the model verification.

Analysis	Maximum displacement (mm)	Maximum von Mises stress (MPa)
1211 nodes	34	15.9
1392 nodes	37	15.5
2016 nodes	38	15.3

The difference in the values obtained among the different meshes shows that the mesh with 2016 nodes is in a region of asymptotic behavior, being considered as independent mesh. The meshes with 1392 and 2016 nodes have a variation of approximately 2% for the maximum displacement and maximum von Mises stress.

The results obtained by Moussa [16] were 33 mm for the maximum displacement and 16.9 MPa for the maximum von Mises stress. Comparing these results with those obtained in the present study it is possible to consider that the model was verified, taking into account that the SOLID186 is a more accurate finite element than PLANE82.

Figure 7 shows a comparison between the von Mises stress distribution obtained in the present study and by Moussa [16]. It is important to note that not only the values found are similar (13.15% for maximum displacement 9.5% and von Mises stress), but also the mechanical behavior of the bracket and the regions with the highest stress concentration are similar.

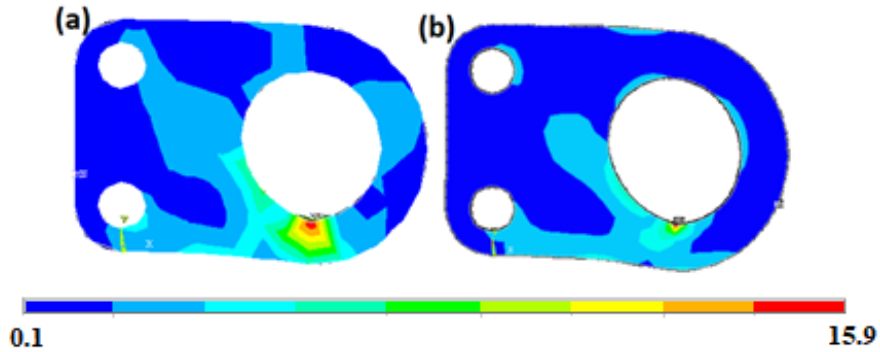

Fig. 7. Distribution of von Mises stress (in MPa) obtained with the present study (a) and the presented in Moussa (b).

4. Results

The environmental loads data on the characteristics of waves, winds and current, in the Campos Basin region, were extracted from the standards of DNV. These data are depicted in Tab.2.

Table 2. Data on the environmental conditions of the Campos Basin (DNV, 2015).

Data	Value
Medium wave height (Hs)	8 m
Medium wave period (Tp)	13 s
Wind velocity (vw)	35 m/s
Current velocity (vc)	1.6 m/s

The depth considered in the study is 1355 m referring to the region of Jubarte field (located on the coast of the brazilian state of Espírito Santo, 76 km from Pontal de Ubu, in the municipality of Anchieta) [17]. The set of brackets and fairlead were arranged 8 m above the level of the water slide and 12 m of deck equipment.

The area of the platform that suffer action of wave and current environmental loads were determined considering the region with deep water characteristics [18]. Thus, for current, the area of action is limited by the deepest height with water particle displacement, determined by:

$$2.Hmpap = L = \frac{g\,.\,(Tp)^2}{2\,.\,\pi} \tag{11}$$

where: $Hmpap$ is the maximum height of particle move to depth water (m), L is the wave length (m), g is the gravity acceleration (m/s^2) and Tp is the period of the medium wave (s).

Considering the synodal movement of the waves the double of the medium height determines the region that suffers action of this specific load. The platform length was adopted as 300 m and its height outside the water as 20 m. The platform draft is of 10 m, within the region of action of the current.

Since each side of the platform is equipped with 12 anchor lines in a traditional Spread Mooring System, the maximum load found is divided by the number of lines. The weight values per meter of the anchor line for the moorings were obtained through the Brasil Amarras [19] catalogs.

Therefore, with the data and assumptions adopted, it was possible to obtain the environmental loading and consequently the tensions for an anchor line. The values obtained are shown in Tab. 3.

Table 3. Environmental loads and loads applied on mooring lines.

Load	Value (MN)
Wind parcel	9.5
Current parcel	7.9
Waves parcel	12.2
Horizontal environmental load per line (H)	2.5

To determine the bracket stresses, the line stresses were applied to the fairlead centroid, located 1.7 m away from the brackets on the x axis and half the distance between the

brackets on the *y* axis. The distance between the brackets is 2.3 m and the 14-ton weight of the fairlead was included in the calculations.

It is important to note that the bracket arranged at the top of the shaft has no restrictions on the movement on the *y* axis, and thus all loads on this axle are supported by the lower bracket.

Figure 8 shows an outline of the free-body diagram of the system under study. The inclination of the fairlead in relation to the hull can vary, according to the need of design and demand of efforts according to the angle of incidence of the environmental loads.

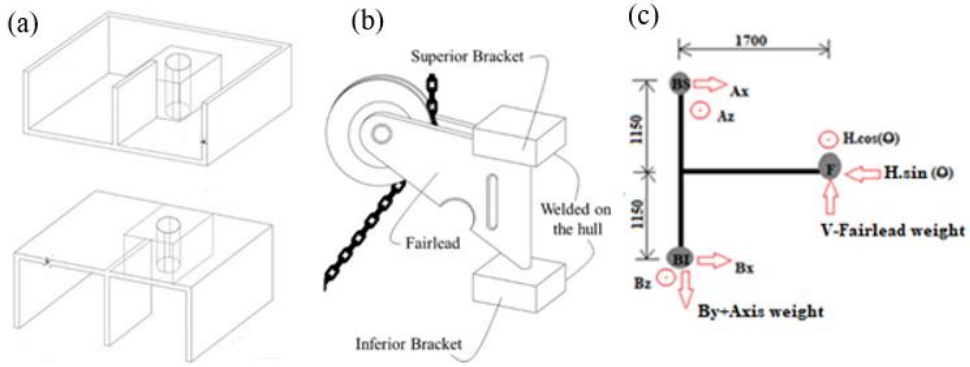

Fig. 8. Sketches of: (a) basic bracket geometry; (b) basic brackets-fairlead assemble; (c) free-body diagram of the problem.

For the analysis an inclination fairlead angle of 15° was adopted, however, even with the inclination of the fairlead, no displacement of the centroid of the equipment with respect to the *z* axis was considered.

We performed separate simulations for each bracket, aiming to propose recommendations about the distribution of stresses and displacements in the lower and upper brackets. In each case a mesh convergence test was carried out. The Tabs. 4 and 5 present the values obtained in the simulations for maximum von Mises stress and maximum displacement for the upper and lower brackets, respectively.

Table 4. Mesh convergence test for the upper bracket.

Nº Elements Mesh	von Mises stress (MPa)	Maximum displacement (mm)
3512	11.34	0.4
4931	13.04	0.4
6185	12.65	0.4
6718	11.85	0.4

Table 5. Mesh convergence test for the lower bracket.

Nº Elements Mesh	von Mises stress (MPa)	Maximum displacement (mm)
3587	57.98	1.7
4343	56.45	1.7
6444	64.08	1.7
6939	59.99	1.7

From Tabs. 4 and 5 it is possible to observe the mesh convergence through the slight variation of the values. The maximum von Mises stress found in the brackets were 11.85 MPa and 64.08 MPa for the upper and lower bracket, respectively, which corresponded to the expectations of the study, considering that they did not exceed the yield limit of the steel (355 MPa for the AH36 steel), which could compromise the structure of the equipment. Figures 9 and 10 illustrate the distribution of von Mises stresses in the upper and lower brackets, respectively.

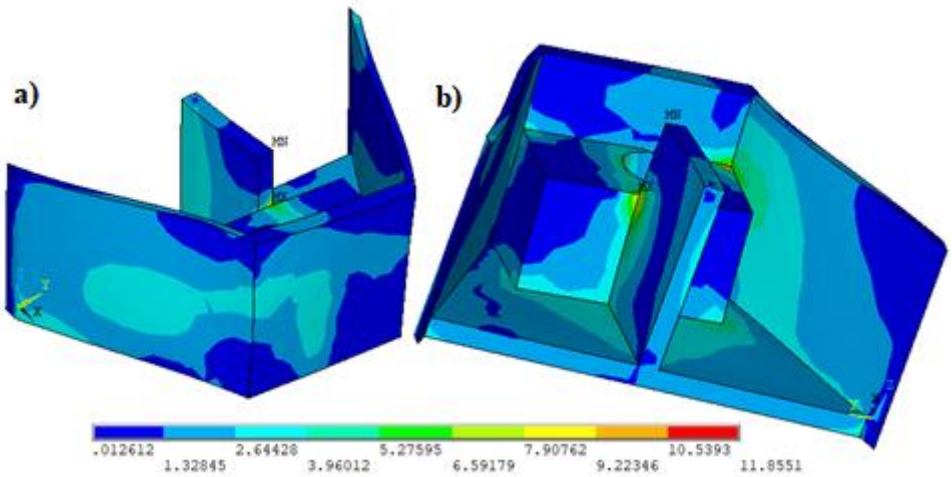

Fig. 9. von Mises stress distribution in upper bracket simulations (in MPa).

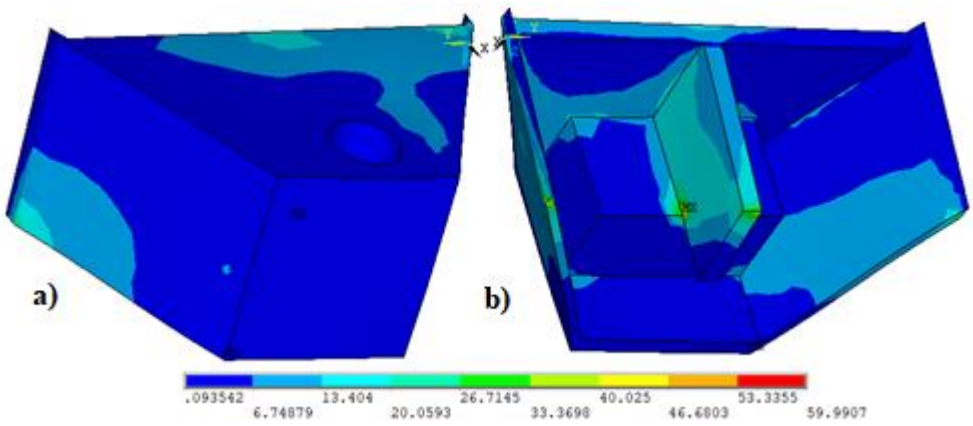

Fig. 10. von Mises stress distribution in lower bracket simulations (in MPa).

It is possible to observe that the spots with higher von Mises stress values are on the join of the solid around the hole, where the loads were applied, and the vertical plates welded on the hull.

5. Conclusion

It was observed through the numerical simulations that the structure did not suffer from mechanical failure risk for the proposed geometry in relation to the maximum environmental load under the imposed conditions of ULS analysis.

The stresses in the brackets did not exceed the yield limit of the steel. This can be justified by the fact that the study considered only the maximum environmental load, and not the other loads proposed by DNV, although it made use of a geometry based on an equipment in which was designed to support all three types of requests.

Finally, it is important to emphasize that the proposal to approach the problem with a 3D model adds precision to the analysis, even more when compared with studies in 2D models, such as that used in the verification of the model of this study.

6. Acknowledgements

K. L. Martins and V. T. Pinto thank Coordenação de Aperfeiçoamento de Pessoal de Nível Superior - Brasil (CAPES) by scholarship research - Finance Code 001. L. A. O. Rocha, E.D. dos Santos and L. A. Isoldi thank CNPq for research grant (Processes: 307847/2015-2, 306024/2017-9, 306012/2017-0).

References

[1] AOGHS, American Oil & Gas Historical Society. Access in: 30th March 2018. https://aoghs.org/offshore-history/offshore-oil-history/.

[2] Kasper F, Barros M, Rossi R, Masetti I, Falkenberg E, Karlsen S, Waclawek I. 1997 DICAS-a new mooring concept for FPSO's. Offshore Technology Conference, 1997. https://doi.org/10.4043/8439-MS

[3] Finucane, Mike. Details of Gryphon incident of 4th February 2011 and lessons learned. Maersk Oil.

[4] Qiao D, Li B, Ou J. Comparative Analysis on Coupling Effects between an Innovative Deep Draft Platform and Different Mooring Models. Brodogradnja: Teorija i praksa brodogradnje i pomorske tehnike, 2012; 63(4), 318-328.

[5] Vargas PM, Hsu TM, Lee WK. Stress concentration factors for stud-less mooring chain links in fairleads. ASME 2004 23rd International Conference on Offshore Mechanics and Arctic Engineering (pp. 909-917). American Society of Mechanical Engineers, 2004. https://doi.org/10.1115/OMAE2004-51376

[6] Kumar KK, Srinivas PS, Rao DS. Modeling and Stress Analysis of Aerospace Bracket Using ANSYS And FRANC3D. International Journal of Engineering Research and Technology, 1(8), 2012.

[7] Gordon RB, Brown MG, Allen EM. Mooring integrity management: a state-of-the-art review. Offshore Technology Conference.

[8] DNV. (2015). OS-301. Offshore Standard, Position Mooring.

[9] Lacerda T. Análise de Sistemas de Ancoragem de Plataformas Flutuantes. Projeto Final de Curso. Departamento de Mecânica Aplicada e Estruturas, 2005.

[10] Nazário VC. Modelagem de Sistemas de Ancoragem Utilizando Catenária Inelástica. Projeto Final de Curso–Departamento de Mecânica Aplicada e Estruturas, 2015.

[11] DNV. (2010). Environmental conditions and environmental loads.

[12] Bergdahl L, Kofoed JP. Simplified Design Procedures for Moorings of Wave-Energy Converters. Structural Design of Wave Energy Devices (SDWED), deliverable, v. 2, 2015.

[13] Petrobras. P-66 deixa o estaleiro rumo ao campo de Lula. Access in: 31 May 2018. http://www.petrobras.com.br/fatos-e-dados/p-66-deixa-estaleiro-rumo-ao-campo-de-lula.htm.

[14] ANSYS, Inc. ANSYS Mechanical APDL Theory Reference. Release 15.0.

[15] Burnett DS. Finite element analysis: from concepts to applications. Prentice Hall, 1987.

[16] Moussa WA. Plane Stress Bracket. Ansys Tutorial. University of Alberta, 2001.

[17] ANP, Agência Nacional do Petróleo, Gás Natural e Biocomb. Access in: 3th April 2018. http://www.anp.gov.br/WWWANP/images/planos_desenvolvimento/Jubarte.pdf.

[18] Dean RG, Dalrymple RA. Water wave mechanics for engineers and scientists. World Scientific Publishing Company, 1991. https://doi.org/10.1142/9789812385512

[19] Brasil Amarras. Access in: 7th April 2018. https://www.offshore-europe.co.uk.

Research on Engineering Structures & Materials
journal homepage: http://jresm.org
MIM Research Group

Research Article

Computational study of the vertical impact coefficient on girders of pier access bridges

Vinícius Avila[*1,a], Mauro Real[2,b], Márcio Moura[2,c]

[1]*Programa de Pós-Graduação em Modelagem Computacional, Universidade Federal do Rio Grande, Rio Grande, Brasil.*
[2]*Escola de Engenharia, Universidade Federal do Rio Grande, Rio Grande, Brasil.*

Article Info

Article history:
Received 28 Jan 2019
Revised 31 March 2019
Accepted 14 May 2019

Keywords:

Bridge;

Moving load models;

Dynamic effects;

Impact coefficient

Abstract

Bridges in Brazil are designed according to design code NBR 7188:2013 [1] and NBR 7187:2003 [2], in which the moving load model is composed of a three-axle vehicle. The configuration of the moving load model follows the pattern of an older version of the code, the NB-6 (1960). Despite the updating of load values, the present moving load model is not appropriate to represent the current traffic effects in Brazilian bridges. The dynamic effects induced by the moving load are taken into account by the impact coefficient, applied in the load model. The static values of the load model are obtained by multiplying its load by this coefficient. The objective of this work is to perform a dynamic analysis of bridge girders, to determine the dynamic effects, to compare with the static effects and to measure the accuracy of the impact coefficient. The results obtained for the beams, showed that for some cases, the impact coefficients had a good approximation to transform the static efforts into dynamic ones. However, in other cases, these coefficients did not show the same result. Through the study it was possible to identify that the impact coefficients provided in the code can be enhanced from new studies taking into account the dynamic analysis of loadings of Brazilian bridges.

© 2019 MIM Research Group. All rights reserved.

1. Introduction

It is called a bridge a construction with the purpose of crossing obstacles to the normal continuity of a way, such as rivers, sea arms, deep valleys, other routes, among other cases. And it is called a viaduct the bridge that has as its objective the transposition of valleys, other ways or obstacles in general not constituted by water [3].

As for the port structures, the construction built on the sea is considered to be a bridge, which provides the connection between the coast and the offshore dock, in order to allow the mooring of ships to loading or unloading and the passage of people and vehicles [4]. An example of such a structure is the port of Açu access bridge (Fig. 1).

Bridges in Brazil are designed according to NBR 7188:2013 [1] and NBR 7187:2003 [2], called "Road and pedestrian live load on bridges, viaducts, footbridges, and other structures" and "Design of reinforced and prestressed concrete bridges - Procedure", respectively. The moving load model is composed of a 3-axle vehicle plus a uniformly distributed load, to be applied in the region outside the vehicle boundaries and multiplied by a dynamic amplification factor, called the vertical load weighting coefficient, which is a function of the bridge span length, number of spans and material used in the structure.

*Corresponding author: vinicius.heidtmann@furg.br
[a]orcid.org/0000-0003-3391-5381; [b]orcid.org/0000-0003-4916-9133; [c]orcid.org/0000-0003-4134-0848
DOI: http://dx.doi.org/10.17515/resm2019.99ms0128

Fig. 1 View of the access bridge port complex Açu [5]

In the study of the structural performance of bridges, the dynamic effects are not included, such as load mobility, vehicle oscillation upon reaching the bridge, impact on the bridge deck due to track irregularities, speed variation among others [6].

In studies of load capacity and dynamic analysis, computational mathematical modeling has become essential, representing the structure as faithfully as possible, to calculate precisely the stress and deformations present in the structural elements [7].

This study intends to compare the dynamic effects and the static effects caused by the moving load model, on a typical pier access bridge. For this, the study seeks to develop numerical and analytical models to simulate the passage of vehicles on some types of bridges.

After the studies, the representative values obtained from the dynamic effects due to the moving load will be compared with the dynamic effects recommended by NBR 7188:2013 [1], when applied to the same bridge systems, in order to evaluate if the code is properly considering the effects of dynamic loading.

2. Methodology

The bridge used was designed with spans of 10 m, 20 m, 30 m, and 40 m. The bridges are 11.50 m wide, have 20 cm slab thickness and four longitudinal girder beams, spaced equally every 310 cm (Fig. 2).

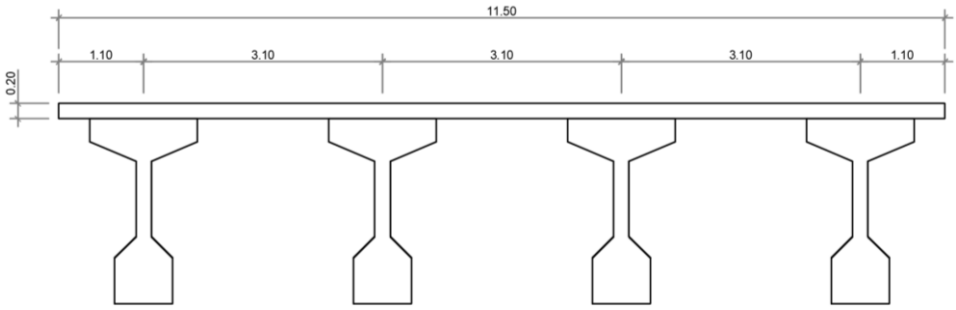

Fig. 2 Cross section of the bridge with 40 m of span. Dimensions in m.

The bridge was considered with the slab simply supported on the beams, non-structural elements were disregarded and for each span of the structure, a different section of the girders was adopted (Fig 3).

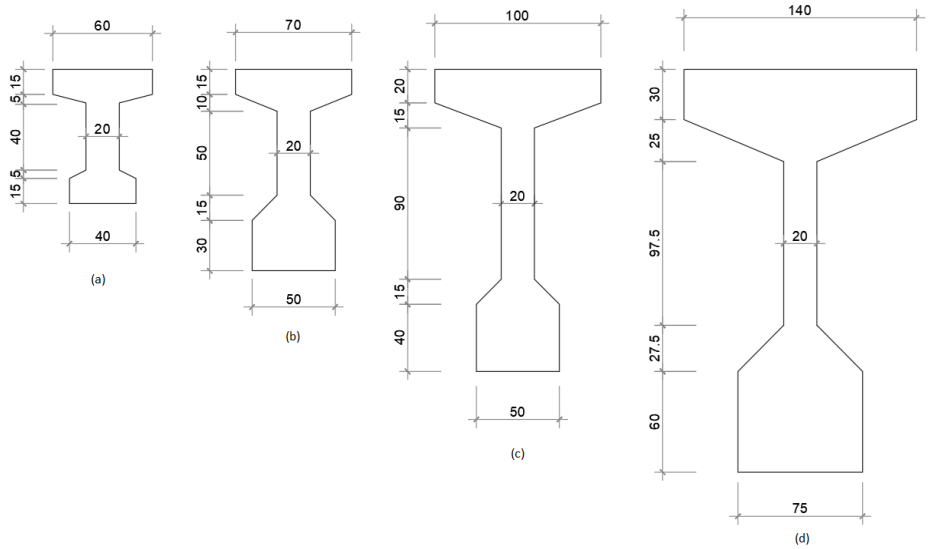

Fig. 3 Cross section of bridge girder beams. Dimensions in cm.

(a) span of 10m, (b) span of 20m, (c) span of 30m and (d) span of 40m.

The numerical-computational model was implemented using the computational tool ANSYS 19.1 Academic version, which analyzed the passage of the vehicle on the structure. Through the software, the usual techniques of discretization using the finite element method were used. The bridge model was made using the grid analogy, in which for both slab and girder were used beam elements, BEAM188 type, which have two nodes and six degrees of freedom per node, being these the translations in the x, y, and z directions and rotations about the x, y, and z directions. Each finite element that constitutes the mesh of the structure has a length of 0.25 m (Fig. 4). Table 1 presents the values of the main properties of the numerical model of the bridge.

Table 1 Properties of the material of the bridges.

Properties	Value Adopted	Unity
Concrete specific mass	2500	kg/m^3
Compressive strength of concrete	30	MPa
Concrete modulus of elasticity	26838	MPa
Concrete coefficient Poisson	0.2	

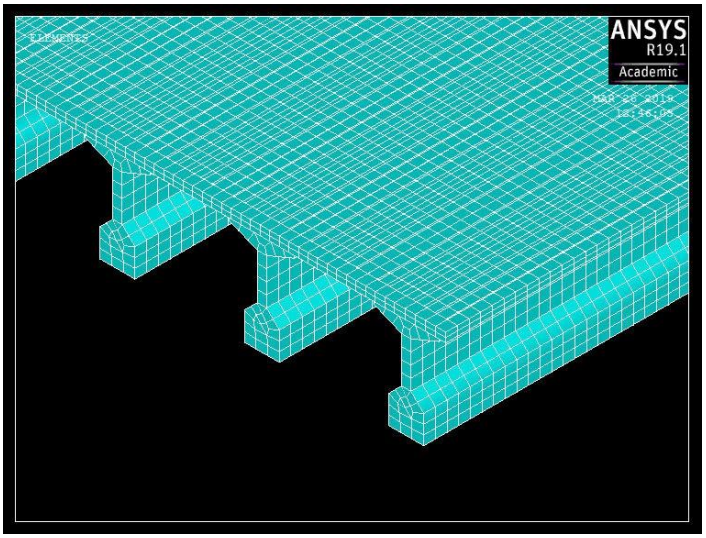

Fig. 4 Finite element mesh, complete perspective

For the moving load, the TB-450 load train (Fig. 5) was considered, which is defined by a three-axle vehicle with a total load of 450 kN, distributed equally on each wheel. It was also considered that the vehicle transits in the most unfavorable position for structure, in order to generate the greatest internal forces, and with a speed of 80 km/h.

For the application of the load from the load train type in the structure, each node of the numerical-computational model belonging to the passage of the vehicle was identified, and, at every 0.5 m, the loads were applied as a function of time.

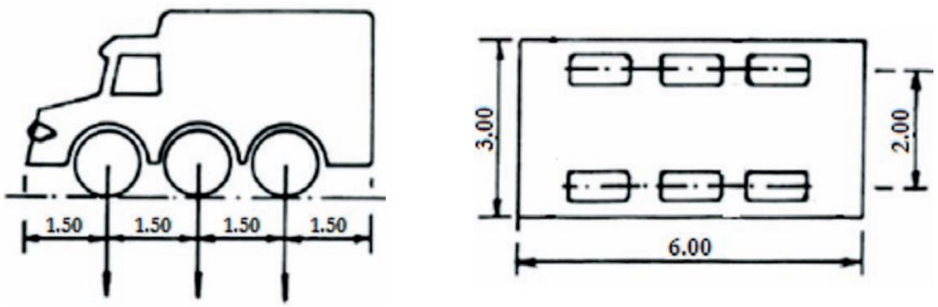

Fig. 5 Truck used in load train type TB-450, according to NBR 7188:2013 [1]. Dimensions in m.

To represent the dynamic interaction between the vehicle and the structure, Eq (1), provided by Fryba [8], was used to represent the harmonic load crossing the bridge.

$$P(t) = P + Q\ sen(\Omega t) \tag{1}$$

Where P is the moving load value in kN, Q is the amplitude in kN, Ω is the circular frequency of the harmonic force in rad/s and t is the time in seconds. According to Melo [9], the value of the oscillation frequency of the vehicle can be between 2.0 Hz and 4.0 Hz, being the last value adopted for the study. A value of 0.10P was also chosen for the amplitude.

For the modeling of damping in the structure, it was used the Rayleigh damping matrix [10], which considers two main plots, α being the contribution rate of the mass matrix, Eq (2), and β rate of contribution of the stiffness matrix, Eq (3). From the most important natural frequencies, ω_1 and ω_2, it is possible to calculate such values.

$$\alpha = 2\xi \frac{\omega_1 \omega_2}{\omega_1 + \omega_2} \tag{2}$$

$$\beta = 2\xi \frac{1}{\omega_1 + \omega_2} \tag{3}$$

Where ξ is damping ratio, where the value of 2% is adopted, and ω_1 and ω_2 are the first and second natural frequencies of the structure in rad/s, respectively.

In order to compare the dynamic effects due to moving load with the dynamic effects recommended by NBR 7188:2013 [1], the dynamic amplification factor (DAF) according to Eq (4) was calculated, so as to check with the correction factor of code.

$$DAF = \frac{Dynamic\ Effort}{Static\ Effort} \tag{4}$$

The correction factor of NBR 7188:2013 [1], due to vertical moving loads, is given by the vertical impact coefficient (CIV), as shown in Eq (5).

$$CIV = \begin{cases} 1.35; L < 10m \\ 1 + \left(\frac{21.2}{L+50}\right); 10m \leq L \leq 200m \end{cases} \tag{5}$$

Where L is the span length for isostatic spans and the average span for continuous bridges.

To verify the transient analysis by means of the computational model, it is used the expression that determines the dynamic coefficient for a simply supported damped beam crossed by a harmonic load, Eq (6), described by Fryba [8], and the result obtained by the symbolic algebraic software wxMaxima is compared to the value of the model in the software ANSYS.

$$\delta = 1 + \frac{Q}{P} \frac{{\omega_{(1)}}^2}{\Omega^2} \frac{1}{\left(\frac{{\omega_{(1)}}^2}{\Omega^2} - 1\right)^2 + 4\left(\frac{\omega^2}{\Omega^2} + \frac{{\omega_b}^2}{\Omega^2}\right)} \left\{ \left[\left(\frac{{\omega_{(1)}}^2}{\Omega^2} - 1\right)^2 + 4\frac{{\omega_b}^2}{\Omega^2} \right]^{1/2} + 2\frac{\omega}{\Omega} e^{-\frac{\omega_b l}{(2c)}} \right\} \tag{6}$$

Where $\omega_{(1)}$, Eq (7), is the circular frequency for the first mode of vibration of the beam simply supported in rad/s; ω, Eq (8), is the load circular frequency in rad/s; ω_b, Eq (9), is the damped circular frequency of the beam simply supported on rad/s; l is the beam span length in m and c is the moving load speed in m/s.

$$\omega_{(1)} = \frac{\pi^2}{l^2} \sqrt{\frac{EJ}{\mu}} \tag{7}$$

Where E is the modulus of elasticity of the material adopted in Pa, J is the moment of inertia of the geometry used in m^4 and μ is the mass of the beam per unit length in kg/m.

$$\omega = \frac{\pi c}{l} \tag{8}$$

$$\omega_b = \frac{\omega_{(1)} \xi}{\sqrt{1 - \xi^2}} \tag{9}$$

3. Results

3.1. Model Verification

A transient analysis was performed for a simply supported beam, with 1 m of height, 40 cm large and 10 m of length, with a modulus of elasticity of 25 GPa and a specific weight of 2500 kg/m^3, subject to a moving load of 100 kN, with amplitude of 10 kN, circular frequency of 30 rad/s and with speed of 60 km/h. For this case, a damping ratio of 5% is considered.

Table 2 shows a good approximation between the numerical-computational model for transient analysis performed in the software ANSYS and the expression that determines the dynamic coefficient for a simply supported damped beam being crossed by a harmonic load, described by Fryba [8].

Table 2 Dynamic coefficient for a damped beam subjected to a harmonic moving load.

Dynamic Coefficient δ		Error (%)
ANSYS	Fryba	
1.121	1.113	0.68

The numerical model analyzed the bridges using the grid analogy. The same bridges were solved, considering them as isolated beams, through software FTOOL, in order to make a comparison between the resolution methods. The value of the maximum bending moment for all beams was calculated for the load applied on beam 1 along with the total bending moment.

The loading is applied in the middle of the girder and it is formed by a concentrated load of 100 kN. Fig. 6 shows an example of loading and the boundary conditions that have been applied to the extremities of the girders of the models.

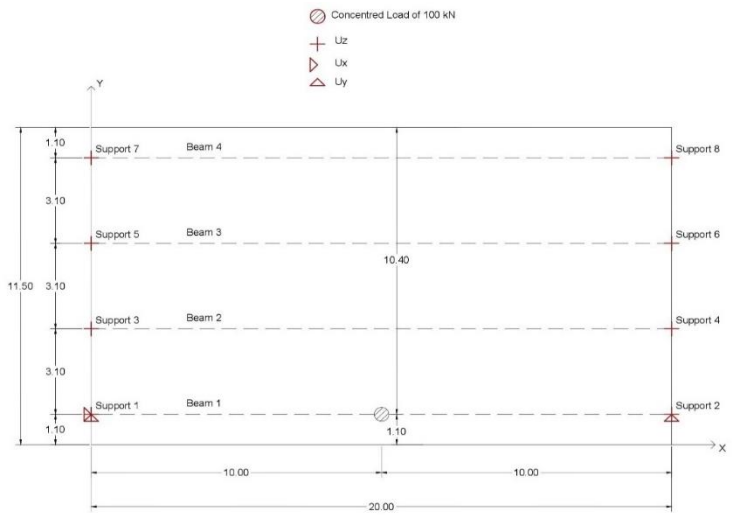

Fig. 6 Example of load model and boundary conditions for the situation of 20 m span, the dimensions in meters

After the definition of loading and boundary conditions, the model was solved using software ANSYS, resulting in the values of maximum normal force (N_i), and maximum

bending moment (M_i) for each girder, as shown in Table 3 to Table 6. The tables also show the calculation used to find the total moment, taking into account the distance from the centroid of the slab to the centroid of each girder (e). Then, they were compared with the results obtained by the software FTOOL, as shown in Table 7. The calculation to obtain the total moment for each beam is constituted by the moment M_i of the precast beam in the central section plus the force N_i multiplied by the distance from the center of the slab to the center of the beam, as shown in Fig. 7, where the point O and the point G are, respectively, the centroids of the slab and the girder [11].

Table 3 Results obtained with loading in the beam 1 for the span of 10 m

Beam	N_i (kN)	M_i (kN.m)	e (m)	Mtotal (kN.m) = Mi + Ni.e
1	3.64	216.37	0.15	216.93
2	-3.91	30.43	0.14	29.89
3	-0.67	-2.41	0.14	-2.50
4	0.94	-0.71	0.15	-0.56
Total Moment				243.75

Table 4 Results obtained with loading in the beam 1 for the span of 20 m

Beam	N_i (kN)	M_i (kN.m)	e (m)	Mtotal (kN.m) = Mi + Ni.e
1	11.66	393.12	0.32	396.83
2	-11.96	103.17	0.29	99.68
3	-4.88	6.82	0.29	5.39
4	5.19	-9.81	0.32	-8.15
Total Moment				493.75

Table 5 Results obtained with loading in the beam 1 for the span of 30 m

Beam	N_i (kN)	M_i (kN.m)	e (m)	Mtotal (kN.m) = Mi + Ni.e
1	15.86	558.52	0.52	566.75
2	-16.11	177.84	0.48	170.05
3	-7.74	26.30	0.48	22.56
4	7.98	-19.39	0.52	-15.25
Total Moment			744.11	

Table 6 Results obtained with loading in the beam 1 for the span of 40 m

Beam	N_i (kN)	M_i (kN.m)	e (m)	Mtotal (kN.m) = Mi + Ni.e
1	17.88	712.98	0.86	728.30
2	-17.76	243.81	0.82	229.28
3	-9.14	51.20	0.82	43.72
4	9.01	-15.27	0.86	-7.55
Total Moment				993.75

Table 7 Results obtained with loading on beam 1

Model	Total Bending Moment		Error (%)
	ANSYS	FTOOL	
10 m	243.75	250.00	2.50
20 m	493.75	500.00	1.25
30 m	744.11	750.00	0.78
40 m	993.75	1000.00	0.62

3.2. Application of the Model

After the verifications, modal and transient structural analysis were performed in order to obtain the values of displacements, shear forces and bending moments in the bridge.

With the modal analysis, the values of the natural frequencies for the first two modes of vibration were obtained, as shown in Table 8.

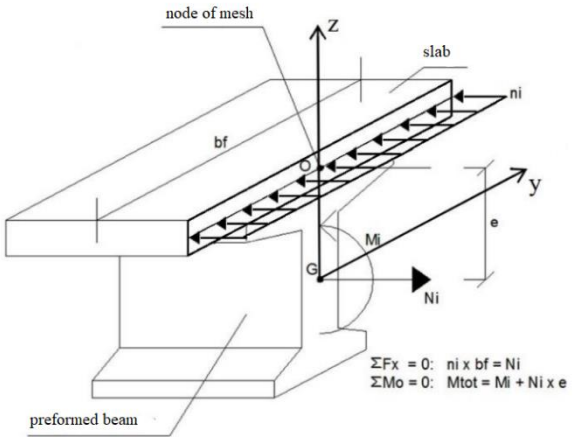

Fig. 7 Loading applied in section [11]

Table 8 Natural frequencies of structures

10 m span bridge		20 m span bridge		30 m span bridge		40 m span bridge	
Mode	Frequency (Hz)	Mode	Frequency (Hz)	Mode	Frequency (Hz)	Mode	Frequency (Hz)
1	9.178	1	5.455	1	3.602	1	2.516
2	12.842	2	5.720	2	3.678	2	2.800

Table 9 shows the parameters α and β used in the transient analysis of the structure, with a rate of damping 2%, for the modeling of the concrete bridges studied.

Table 9 Parameters α and β used in the transient analysis of the structure

Span (m)	Circular natural frequency of the mode 1 (Hz)	Circular natural frequency of the mode 2 (Hz)	Circular natural frequency of the mode 1 (rad/s)	Circular natural frequency of the mode 2 (rad/s)	α	β
10	9.178	12.842	57.667	80.689	1.34525082	0.00028911
20	5.455	5.720	34.274	35.941	0.70174992	0.00056968
30	3.602	3.678	22.634	23.108	0.45737298	0.00087447
40	2.516	2.800	15.807	17.595	0.33306377	0.00119753

Then, by means of static analysis and transient analysis, the maximum internal forces for each situation were determined, as shown in Table 10 to Table 13.

Table 10 Comparison between the dynamic effects due to moving load with the dynamic effects recommended by NBR 7188: 2013 [1], for 10m span bridge

Efforts	Static loading	Dynamic loading	DAF	Correction Factor - NBR 7188: 2013 [1]
Displacement (m)	3.99	4.39	1.10	1.35
Shear effort (kN)	268.92	295.43	1.10	
Bending moment (kN.m)	595.08	643.97	1.08	

Table 11 Comparison between the dynamic effects due to moving load with the dynamic effects recommended by NBR 7188: 2013 [1], for 20m span bridge

Efforts	Static loading	Dynamic loading	DAF	Correction Factor - NBR 7188: 2013 [1]
Displacement (m)	9.20	11.35	1.23	1.30
Shear effort (kN)	292.47	307.32	1.05	
Bending moment (kN.m)	1273.51	1541.98	1.21	

Table 12 Comparison between the dynamic effects due to moving load with the dynamic effects recommended by NBR 7188: 2013 [1], for 30m span bridge

Efforts	Static loading	Dynamic loading	DAF	Correction Factor - NBR 7188: 2013 [1]
Displacement (m)	10.83	14.44	1.33	
Shear effort (kN)	300.48	303.50	1.01	1.27
Bending moment (kN.m)	1920.13	2209.85	1.15	

Table 13 Comparison between the dynamic effects due to moving load with the dynamic effects recommended by NBR 7188: 2013 [1], for 40m span bridge

Efforts	Static loading	Dynamic loading	DAF	Correction Factor - NBR 7188: 2013 [1]
Displacement (m)	8.55	9.76	1.14	
Shear effort (kN)	304.76	304.54	1.00	1.24
Bending moment (kN.m)	2523.14	2822.48	1.12	

In Tables 10 to 13, it is possible to observe that only the passage of a transient load on the structure does not cause increase of the DAF in the middle of the span of the structure, but rather the passage of a transient harmonic load does, where it is able to better represent the vehicle-pavement-structure interaction.

The maximum displacement in the middle of the span calculated on the basis of the Brazilian code presented close results with the values obtained by the transient loads, demonstrating a good conversion of the static to the dynamic forces, except for the 30 m span case.

The maximum shear forces in the supports generated by the transient loads were shown to be lower than those calculated using the Brazilian code, presenting an exaggerated design for this region.

The maximum bending moments in the middle of the span calculated on the basis of the Brazilian code presented close results with the values obtained by the transient loads, demonstrating a good conversion from the static to the dynamic efforts.

4. Conclusion

The vehicle-pavement-structure interaction is directly related to the value of the load amplitude (Q), which takes into account the weight of the vehicle, the effect of the irregularity of the lane or even the overlap of both actions. For future studies, there is a

need for a better understanding of the load amplitude value, in order to develop computational models with greater precision for the studied situations.

The results obtained for the beams showed that, for some cases, the impact coefficients had a good approximation to transform the static efforts into dynamic ones. However, in other cases, these coefficients did not show the same result.

In his studies, Rossigali [12] obtained similar results when comparing the internal forces caused by a real load of a Brazilian road structure to the forces obtained by the increase of the loads by the impact coefficient.

Through this study, it was possible to identify that the coefficients of impact recommended by the code can be improved from new studies taking into account the current loads of the Brazilian bridges.

References

[1] Associação Brasileira de Normas Técnicas. NBR 7188. *Road and pedestrian live load on bridges, viaducts, footbridges and other structures*. Rio de Janeiro: ABNT; 2013.
[2] Associação Brasileira de Normas Técnicas. NBR 7187. *Design of reinforced and prestressed concrete bridges - Procedure*. Rio de Janeiro: ABNT; 2003.
[3] Marchetti O. Pontes de Concreto Armado. São Paulo: Blucher; 2008.
[4] Administração dos Portos de Paranaguá e Antonina. Dicionário básico portuário. Paranaguá: APPA; 2011.
[5] Silva A, Barbosa O. Projeto estrutural e de fundações do Terminal Offshore de Minérios do T1 do Complexo Portuário do Açu. Congresso Brasileiro de Pontes e Estruturas. Rio de Jeneiro; 2018.
[6] Leitão F. Verificação à Fadiga de Pontes Rodoviárias Mistas (Aço-Concreto) [Msc]. Universidade do Estado do Rio de Janeiro; 2009.
[7] Ahi A. Análise de Fadiga em Pontes Rodoviárias de Concreto Armado [Msc]. Universidade do Estado do Rio de Janeiro; 2009.
[8] Fryba L. Vibration of solids and structures under moving loads. Groningen: Noordhoff; 1972. https://doi.org/10.1007/978-94-011-9685-7
[9] Melo E. Interação Dinâmica Veículo-Estrutura Em Pequenas Pontes Rodoviárias [Msc]. Universidade Federal do Rio de Janeiro; 2007.
[10] Soriano H. Introdução à dinâmica das estruturas. Rio de Janeiro: Elsevier; 2014.
[11] Botelho T. Modelagem Computacional de Tabuleiros de Pontes de Concreto [Msc]. Universidade Federal do Rio Grande; 2016.
[12] Rossigali C, Pfeil M, Battista R, Sagrilo L. Towards actual brazilian traffic load models for short span highway bridges. Revista IBRACON de Estruturas e Materiais. 2015;8(2):124-139. https://doi.org/10.1590/S1983-41952015000200005

Blank Page

Research on Engineering Structures & Materials
journal homepage: http://jresm.org
Research Group

Research Article

Constructal design applied to geometrical evaluation of rectangular plates with inclined stiffeners subjected to uniform transverse load

Vinícius Torres Pinto [*a,1], Marcelo Langhinrichs Cunha [b,1], Grégori da Silva Troina[c,1], Kauê Louro Martins [d,1], Elizaldo Domingues dos Santos [e,1], Liércio André Isoldi [f,1], Luiz Alberto Oliveira Rocha[g,2]

[1]*Graduate Program in Ocean Engineering (PPGEO) Federal University of Rio Grande – FURG, Rio Grande. RS, Brazil.*
[2]*Graduate Program in Mechanical Engineering, University of Vale do Rio dos Sinos – UNISINOS, São Leopoldo, RS, Brazil.*

Article Info

Article history:
Received 15 Feb 2019
Revised 04 Apr 2019
Accepted 15 May 2019

Keywords:

Stiffened Plates;
Numerical Simulation;
Constructal Design;
Deflection;

Abstract

This study employs the Constructal Design method associated with the computational modeling (by the Finite Element Method) to evaluate the mechanical behavior related to deflections of stiffened rectangular steel plates submitted to uniform transverse loading. To do so, a rectangular reference plate without stiffeners was used. A material volume portion of this plate was converted into stiffeners through the parameter ϕ, which represents the ratio between the stiffeners volume and the total volume of the reference plate. By adopting ϕ = 0.3, 50 stiffened plates were configured: 25 with orthogonal stiffeners to the plate edges and 25 with stiffeners oriented at 45°. Keeping the total volume of material constant, the influence of the orientation of the stiffeners and the effect of the degree of freedom h_s/t_s (ratio between height and thickness) variation were numerically analyzed. The results showed that variations in the geometry of the stiffeners can increase the rigidity of the plate, reducing its deflection. Further, it has been found that depending on the number of stiffeners, orienting them at 45° may be an alternative to minimize deflections in rectangular plates.

© 2019 MIM Research Group. All rights reserved.

1. Introduction

Plates are straight, flat and two-dimensional structural components because their thickness is much smaller than the other dimensions [1]. In marine structures the plates are used specifically to resist the longitudinal loads advent from the ship's flexion, besides the hydrostatic pressure and the different transported items (static loading) [2].

To increase rigidity, usually, are inserted reinforcements in the longitudinal and/or transverse directions of the plates, called stiffeners. The geometrical proportions of stiffeners have an important role in the performance of these structural components [3].

*Corresponding author: viniciustorreseng@gmail.com
[a] orcid.org/0000-0002-0977-5086; [b] orcid.org/0000-0003-1083-7341; [c] orcid.org/0000-0002-4408-562X; [d] orcid.org/0000-0001-8441-0848; [e] orcid.org/0000-0003-4566-2350; [f] orcid.org/0000-0002-9337-3169; [g] orcid.org/0000-0003-2409-3152
DOI: http://dx.doi.org/10.17515/resm2019.118ms0215

The Fig. 1 shows the cross-section of a ship, where it is possible to observe the stiffened plates that compose the structure, as well as the load that request on it.

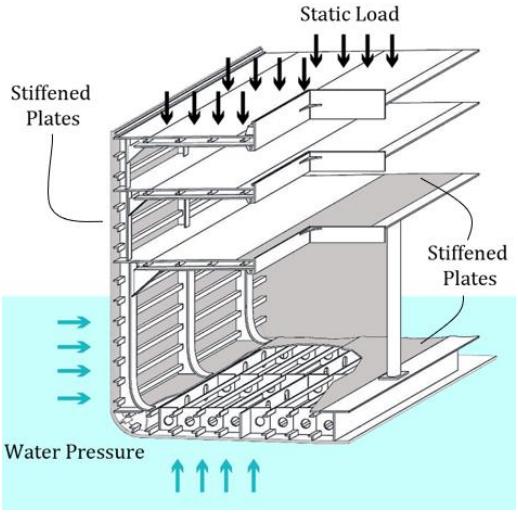

Fig. 1 Cross section of a ship (adapted from [4])

The analysis of the structural behavior of stiffened plates faces the difficulty of establishing analytical solutions due the geometric complexity. The existing proposals can be applied only to cases of simplified geometries, so that numerical methods become an alternative for solving this type of problem.

The Finite Element Method (FEM) was used by Rossow and Ibrahimkhail [5] to apply the Constraint Method in the analysis of stiffened plates with eccentric and concentric stiffeners. Bedair [6] using Quadratic Sequential Programming implemented a method of analysis for stiffened plates, where the structure was idealized considering plate and stiffeners rigidly connected. Peng et al. [7] presented a meshless method to analyze stiffened plates with eccentric and concentric stiffeners, based on the First Order Shear Deformation Theory.

Hasan [8] used the FEM through NASTRAN® software to analyze the better locations of stiffeners in plates under bending with different boundaries conditions. Hosseini and Soltani [9] investigated the structural behavior of square and rectangular plates under bending with different geometries of stiffeners, in concentric and eccentric conditions, using the Meshless Collocation Method.

Stiffened plates of isotropic material under bending were studied by Singh et al. [10]. Using the ANSYS® software, several configurations of stiffeners were analyzed considering different loads and boundary conditions, with the objective of reducing plate deflection. Finally, Troina [11] applied the Construal Design method using the FEM by ANSYS® software in the search for geometric arrangements that minimized the central deflection in plates with rectangular stiffeners.

Thus, the objective of the present study was to numerically evaluate the mechanical behavior related to the deflection of rectangular stiffened plates under uniform transverse loading, regarding the influence of the stiffeners orientation and the variation of the geometric parameter h_s/t_s (ratio between height and thickness of the stiffeners) through the application of the Constructal Design method.

2. Computational Modeling

The computational modeling of the plates analyzed in this study was performed using the ANSYS® software, based on FEM. The FEM is used in physical solution of engineering problems, which usually involve a structure or structural component subject to certain loads [12]. Zienkiewicz [13] explains that finite element analysis basically consists of four steps: creation of model geometry, mesh generation, load and boundary conditions application and problem solving.

According to Madenci and Guven [14], modeling an engineering problem for a static analysis with linear elastic behavior of the material through the FEM, requires the assembly of a global system of equations composed of the characteristic matrixes of the element and the vector of forces:

$$[K] . \{u\} = \{F\} \tag{1}$$

where $[K]$ is the global stiffness matrix; $\{u\}$ is the vector of unknown nodal displacements and $\{F\}$ represents the vector of external loads.

2.1. Computational Modeling Verification

To verify the computational model, it was simulated through ANSYS® the simply supported stiffened plate shown in Fig. 2. The plate was subjected a uniform transverse load of 0.006895 kN/cm^2 and its material has a Poison's ratio of 0.3 and Young's modulus of 20,684.27 kN/cm^2.

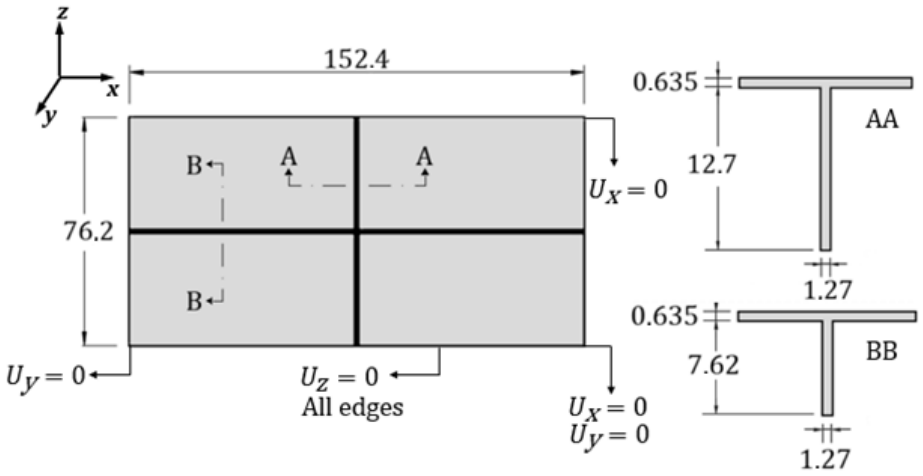

Fig. 2 - Rectangular plate with two orthogonal stiffeners (in cm).

To solve this problem, it was adopted the triangular finite element SHELL281, totalizing 30,400 elements after the mesh convergence test presented in Fig. 3. The results of central deflection U_z, as well, the results of other authors to the same plate model can be observed in Table 1.

There was a meaningful difference comparing the result found in this verification using the element SHELL281 with the results found by Rossow e Ibrahimkhail [5] and Peng et al. [7]. This can be justified considering the precision of the current model, which due to the available computational power, allows a greater refinement of mesh in the numerical model discretization.

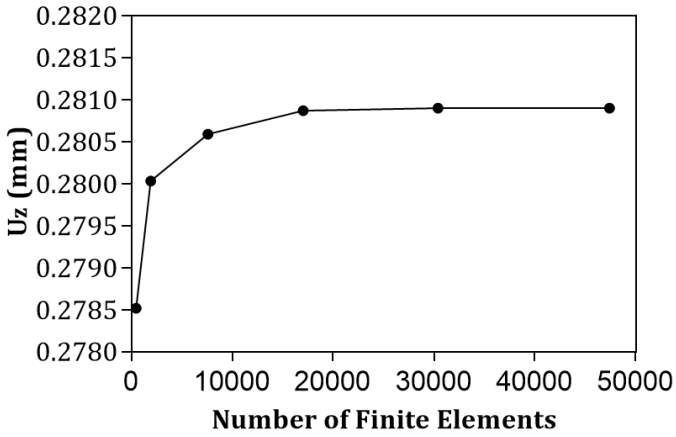

Fig. 3 - Results of mesh convergence test for computational model verification

Table 1 - Computational Model Verification

Authors	U_z (mm)	Difference (%)
Rossow e Ibrahimkhail [5]	0.2245	20.07
Peng et al. [7]	0.2185	22.20
Troina [11]	0.2781	0.99
Present Study	0.2809	--

In addition, comparing with the result found by Troina [11], which was obtained using the 3D finite element SOLID95, one can note a good agreement. This small difference can be explained because the element SOLID95 considers all components of stress and strain of the three-dimensional solid; while the two-dimensional element SHELL281, have some simplifications relative to the plane state of stress and strain. So, the proposed model can be considered as verified.

3. Constructal Design Method

According to Bejan and Lorente [16] the Constructal Law dictates that flow systems (river basins, lungs, atmospheric circulation, vascularized tissues, etc.) should evolve over time, acquiring better and better configurations to provide more access for the currents that flow through them.

The Construtal Design method is the way in which the Construtal Law is applied in practical situations, it is the generation of the flow architecture. The performance of a system is global and carries fixed global constraints, which may include the space allocated to the system, available material and components, ranges temperature limits, pressure or stress. Thus, the designer gathers all the components and optimizes the arrangement, so that can develop the flow architecture that achieves the better performance [17]. Bejan and Lorente [16] explain that in the analysis of mechanical structures the Constructal Law is applied in a similar way to any flow system, when subjected to a load the mechanical arrangements work as networks in which the stress flow through their components.

To apply the Constructal Design method, a rectangular reference plate without stiffeners was adopted. So, the volumetric fraction ϕ, presented in Eq. (2) and Eq. (3), was established for orthogonal stiffeners to the plate edges and stiffeners oriented

at 45°, respectively. The parameter ϕ represents the ratio between the material volume of the stiffeners and the total material volume of the reference plate. In this study, ϕ = 0.3 was considered, i.e., 30% of the material volume of the reference plate was removed from the thickness and transformed into stiffeners.

$$\phi = \frac{V_s}{V_r} = \frac{N_{sx}(ah_st_s) + N_{sy}[(b - N_{sx}t_s)h_st_s]}{abt} \quad (2)$$

$$\phi = \frac{V_s}{V_r} = \frac{\sum_{d=1}^{n}[(d_1 + d_2 + d_3 \dots d_n)h_st_s] - (N_{int}h_s{t_s}^2)}{abt} \quad (3)$$

where V_s is the volume of reference plate transformed into stiffeners; V_r is the total volume of the reference plate; a = 2000 mm, b = 1000 mm and t = 20 mm are, respectively, the length, width and thickness of the reference plate; h_s and t_s are, respectively, the height and thickness of the stiffeners, common to all configured plates. Exclusively for the geometric arrangements formed with stiffeners oriented at 45°, the parameters d_1, d_2, d_3, d_n, represents the length of the stiffeners, being n the total number of stiffeners and N_{int} the number of intersections among them. It is important to observe that all stiffeners thicknesses adopted in this study were based on commercial plates.

Just for the plates with stiffeners oriented at 45° an auxiliary coordinate system *x'*, *y'* and *z'* was considered. Then, was adopted the format P(N_{sx}, N_{sy}) and P'$(N_{sx'}, N_{sy'})$, for orthogonal stiffeners to the plate edges and stiffeners oriented at 45°, respectively. Being $N_{sx'}$ and $N_{sy'}$, respectively, the number of stiffeners in *x'* and *y'* directions, as well, N_{sx} and N_{sy} represents, respectively, the number of stiffeners in *x* and *y* directions.

Thus, from the reference plate were configured 25 stiffened plates with orthogonal stiffeners to the plate edges (non-inclined) and 25 stiffened plates with stiffeners oriented at 45° (inclined). The Figs. 4 and 5 show the plates P(3,3) e P'(3,2), respectively.

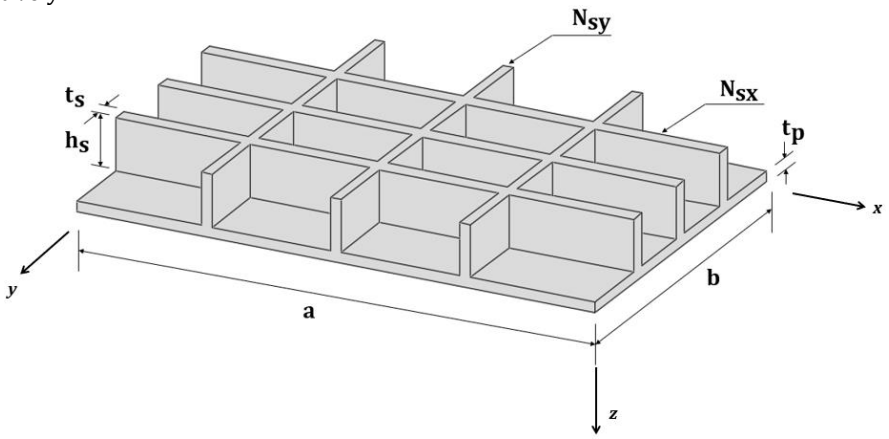

Fig. 4 - Plate P(3,3)

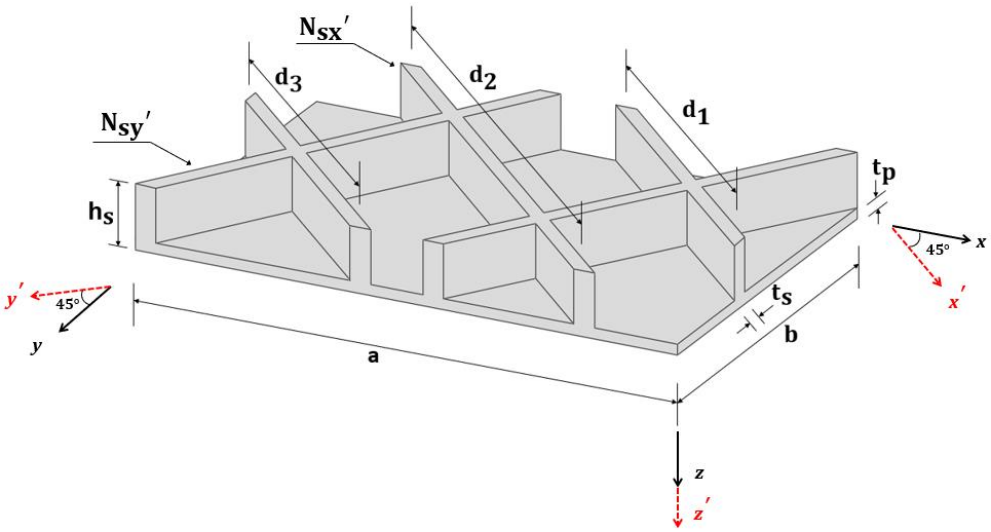

Fig. 5 - Plate P'(3,2)

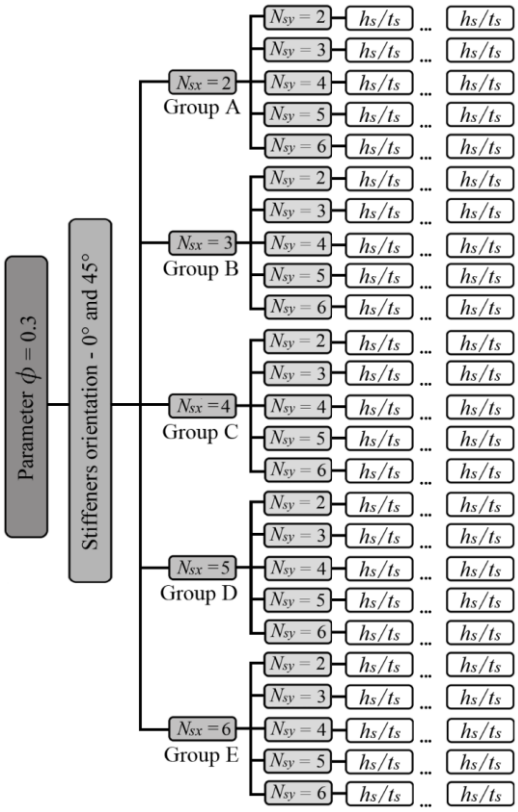

Fig. 6 - Plates arrangements analyzed

To facilitate the organization of the results presented in this study all proposed geometric configurations were divided into groups, as shown in Fig. 6. In addition, to avoid excessive

disproportion between the dimensions of the plate and the dimensions of the stiffeners, the maximum stiffener height was limited to 300 mm.

In order to evaluate the influence of the degree of freedom h_s/t_s on the mechanical behavior of stiffened plates in relation to the deflection, for each new considered thickness, a new height was formed, maintaining constant the total material volume. The length of the reference plate a = 2000 mm and its width b = 1000 mm were preserved; however, its thickness t = 20 mm became t_p = 14 mm after material removal to create the stiffeners.

4. Mesh Convergence Test

A mesh convergence test was performed to define the size of the finite elements that would be used in the simulations. For this, the plate with greater geometric complexity P'(6,6) with h_s/t_s = 92.275 was chosen. The spatial discretization was done with SHELL281 finite element in its triangular shape, due to the geometric complexity of the plates with inclined stiffeners.

Six mesh configurations were analyzed, in each analysis the size of the finite elements was reduced successively as shown in Table 3. According to Fig. 7, it can be observed that from the third simulation the value of the center (U_z) and maximum (U_{zMax}) deflections of the plate were kept constant. It is important to highlight that in this geometric configuration used for the convergence mesh test $U_z = U_{zMax}$. Hence, the mesh M3 with finite element size of 25 mm was adopted, as can be viewed in Fig. 8.

Table 2 - Convergence mesh test

Meshes	Finite element size	Number of finite elements	Deflection U_z=U_{zMax} (mm)	Relative difference (%)
M1	100	1560	0.0181	2.162
M2	50	5090	0.0185	0.537
M3	25	20478	0.0186	0.000
M4	16,67	47338	0.0186	-
M5	12,5	84502	0.0186	-
M6	10	132322	0.0186	-

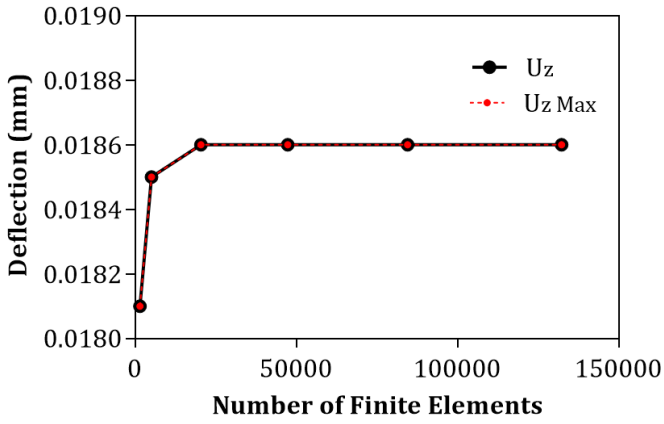

Fig. 7 - Result of mesh convergence test

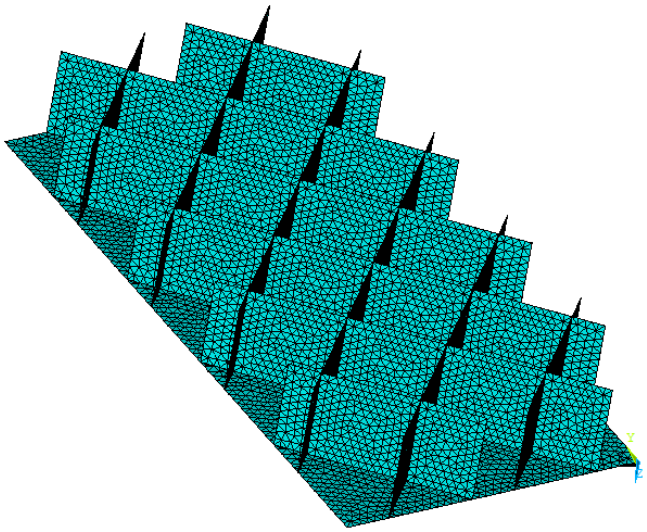

Fig. 8 - Discretization of the computational model for plate P'(6,6) with h_s/t_s = 92.275

5. Results and Discussions

For all plates simulated in this study, a uniform transverse load of 10 kN/m^2 was adopted. The material of plate is A-36 steel with modulus of elasticity E = 200 GPa and Poisson's ratio ν = 0.3.

Firstly, it was observed that transforming part of the volume of the reference plate into stiffeners always promote an improvement of the mechanical behavior concerning the deflections. The reference plate presented central and maximum displacement equal to $U_z = U_{zMax} = 0.697$ mm. Therefore, all proposed geometric configurations for the stiffened plates have central and maximum displacements lower than 0.697 mm.

Another observation was that for some geometric configurations of stiffened plates the central and maximum displacements are equal; while for other geometries different values for central and maximum deflections are obtained. This is due to the distribution of stiffeners. In the plates with orthogonal stiffeners, the distribution was carried out in function of the length and the width of the plate. However, for the plates with inclined stiffeners, the distribution was performed regarding the plate diagonal. Thus, whenever a stiffener crosses the center of the plate its central displacement is less than its maximum displacement.

For discussion purpose, only the results of groups A and D were presented, which showed distinct behaviors. That way, it was possible to analyze the influence of the stiffeners orientation, as well as the effect of its geometry variation. The other results of this study are presented in Appendix A. Moreover, for presentation purposes, the values of the center and maximum displacements were considered in the opposite direction of the z axis.

Observing the Fig. 9, it's noted that all plates of group A with orthogonal stiffeners to the edges (non-inclined) presented better performance (lower displacements) if compared to the plates with stiffeners oriented at 45°. The plates with the best results in this group were: P(2,5) with h_s/t_s = 59.409 and P'(2,5) with h_s/t_s = 62.891. The plate P(2,5) showed reductions of 34% for the central displacement and 40% for the maximum displacement, when compared with the plate P'(2,5).

However, all plates of group D with stiffeners oriented at 45° presented better results, both for the central displacement and maximum, when compared with orthogonal stiffened plates (see Fig. 10). The plates that presents better performances were: P(5,3) with h_s/t_s = 41.137 and P'(5,3) with h_s/t_s = 58.129 The plate P'(5,3) with stiffeners oriented at 45° showed a reduction of 50.2% for the central displacement and 34.2% for de maximum displacement, when compared with the plate P(5,3).

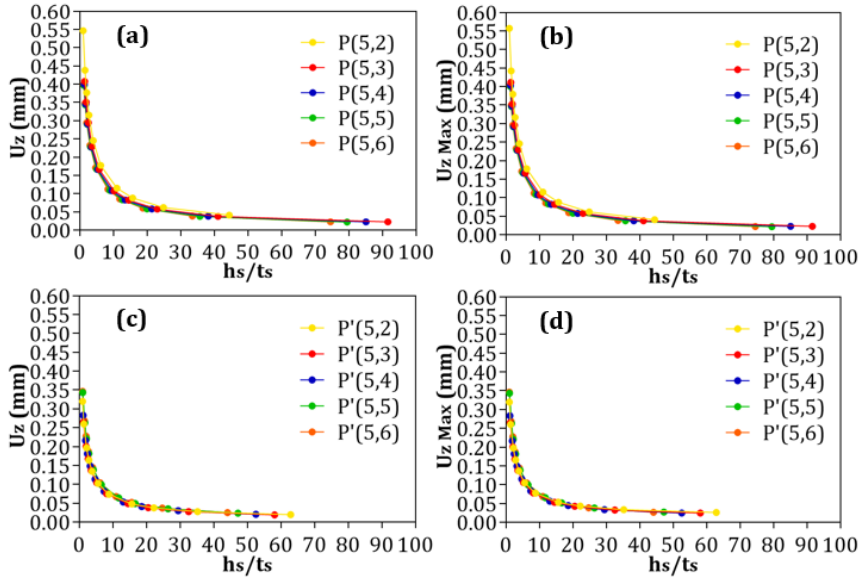

Fig. 9 - Group A - Central and maximum displacements – (a) and (b) Orthogonal stiffeners to edges; (c) and (d) stiffeners oriented at 45°

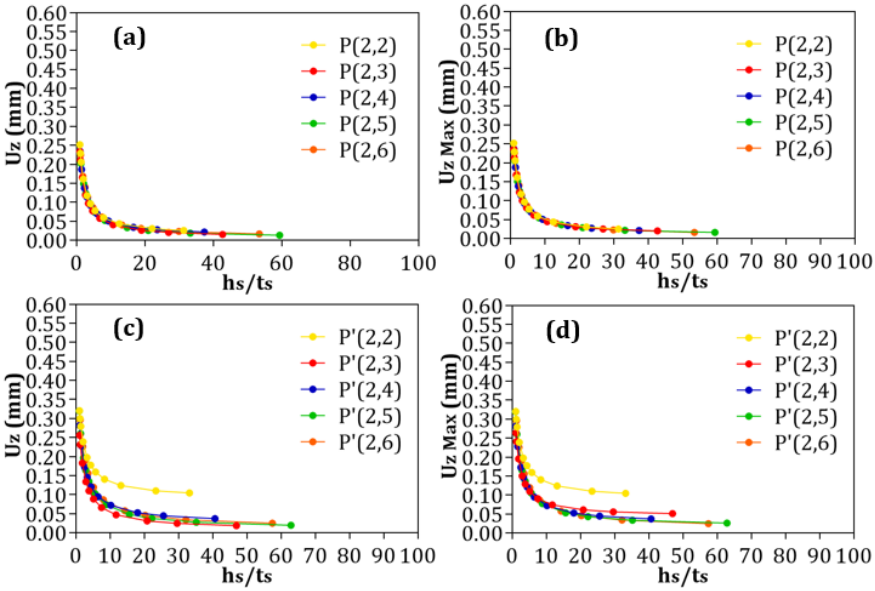

Fig. 10 - Group D - Central and maximum displacements – (a) and (b) Orthogonal stiffeners to edges; (c) and (d) stiffeners oriented at 45°

The displacements distribution of the best performing plates in Group A and D are showed in Figs. 11 and 12. It is interesting to note that the plates with orthogonal stiffeners to the edges have a uniform displacement pattern, while in the plates with stiffeners oriented at 45° the displacement is presented of irregular way.

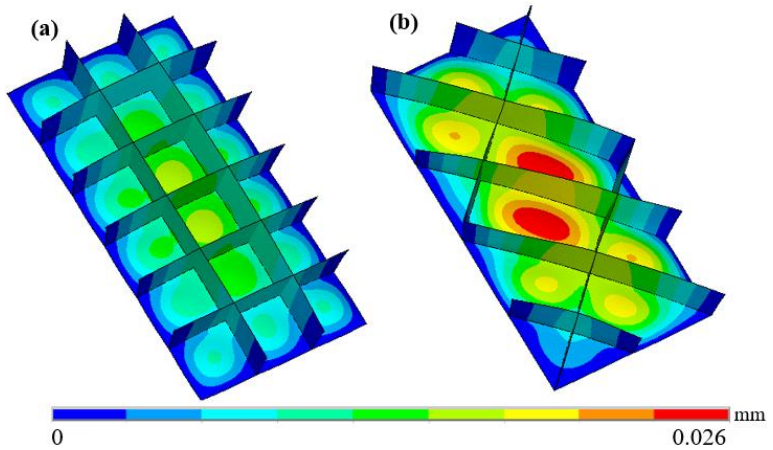

Fig. 11 - Group A - Displacements distribution: (a) P(2,5); (b) P'(2,5)

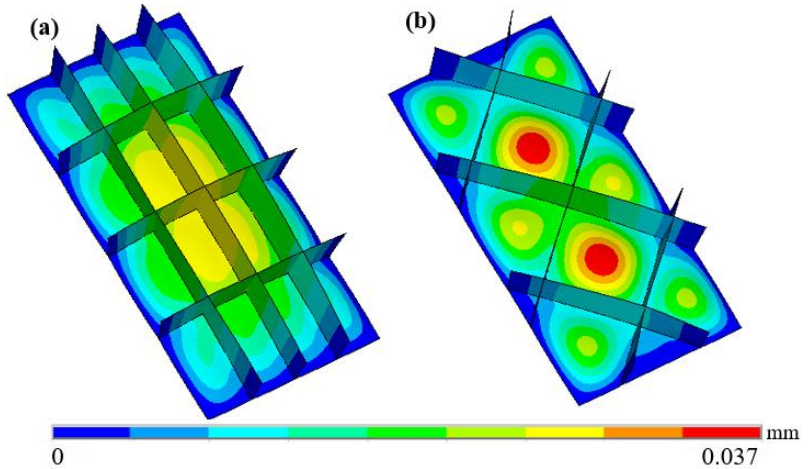

Fig. 12 - Group D - Displacements distribution: (a) P(5,3); (b) P'(5,3)

Another important observation indicates that a greater number of stiffeners does not necessarily reduce the deflections. This trend is valid for both investigated stiffeners orientations. The fact of keeping constant the total material volume of the plate, makes that in plates with a greater number of stiffeners the stiffener height is smaller, hence reducing its moment of inertia.

6. Conclusion

It was observed that transform part of the reference plate material into stiffeners always promote a reduction in the central e and maximum deflections, if compared the stiffened

plate and the reference non-stiffened plate. In its turn, the increasing of the ratio h_s/t_s in stiffened plates always conduct to a reduction of central and maximum deflections. In other words, the rearrangement of material while keeping constant the volume of plate material may increase its stiffness.

Regarding the stiffeners orientation, it has been observed that orienting the stiffeners at 45° can lead to smaller displacements depending on the number of stiffeners. In addition, the results indicated that a greater number of stiffeners does not mean smaller deflections in both cases of plates, with stiffeners oriented at 45° and orthogonal to the edges of the plate.

The results also showed that for plates with two stiffeners in the *x'* direction (Group A), independent of the number of stiffeners in the direction *y'*, oriented them at 45° is not advantageous in reducing the central and maximum deflections. However, for three or more stiffeners in the *x'* direction, independent of the number of stiffeners in the direction *y'*, significant reductions in the central and maximum displacements can be obtained by orienting the stiffeners by 45°.

Therefore, the use of the Construtal Design method associated with computational modeling is an effective tool for the analysis of mechanical behavior of plates. In addition, modification of the orientation and geometry of the stiffeners can lead to an improvement in the mechanical behavior of hardened rectangular plates. In some cases, reaching a reduction of greater than 60% in relation to their deflections. For instance, the plates P(6,2) with h_s/t_s = 5.373 and P'(6,2) with h_s/t_s = 8.094. The plate P'(6,2) with stiffeners oriented at 45° showed a reduction of 64.8% for the central displacement and 64.8% for de maximum displacement, when compared with the plate P(6,2).

In future works, it is worth investigating stiffened plates with other orientations and amounts of stiffeners. As well as, other values of ϕ, i.e., other ratios of material transformed into stiffeners from the reference plate. It is also possible to evaluate the influence of the degrees of freedom considered in this study in the stress distribution from the uniform transverse loading.

Acknowledgement

This study was financed in part by the *Coordenação de Aperfeiçoamento de Pessoal de Nível Superior - Brasil* (CAPES) - Finance Code 001.

The authors thank to CAPES (Coordination of Superior Level Staff Improvement – Brazil, FAPERGS (Foundation for Research Support of the State of Rio Grande do Sul, and CNPq (Brazilian National Council for Scientific and Technological Development)

APPENDIX A

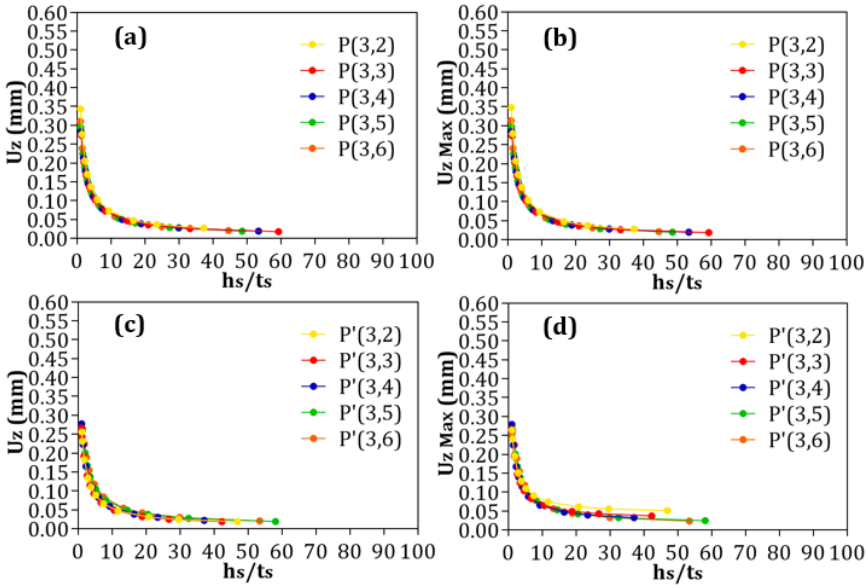

A. 1 - Group B - Central and maximum displacements – (a) e (b) Orthogonal stiffeners to edges; (c) e (d) stiffeners oriented at 45°

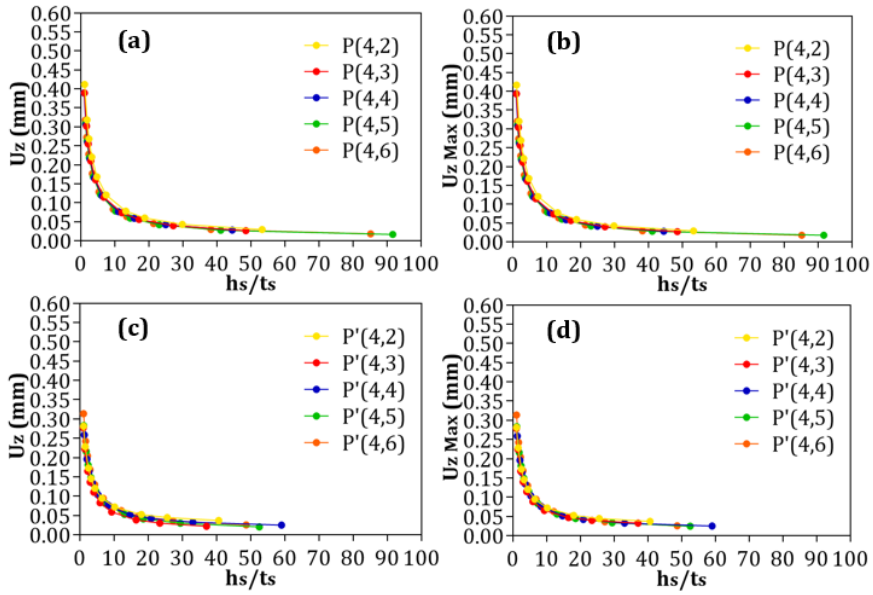

A. 2 - Group C - Central and maximum displacements – (a) e (b) Orthogonal stiffeners to edges; (c) e (d) stiffeners oriented at 45°

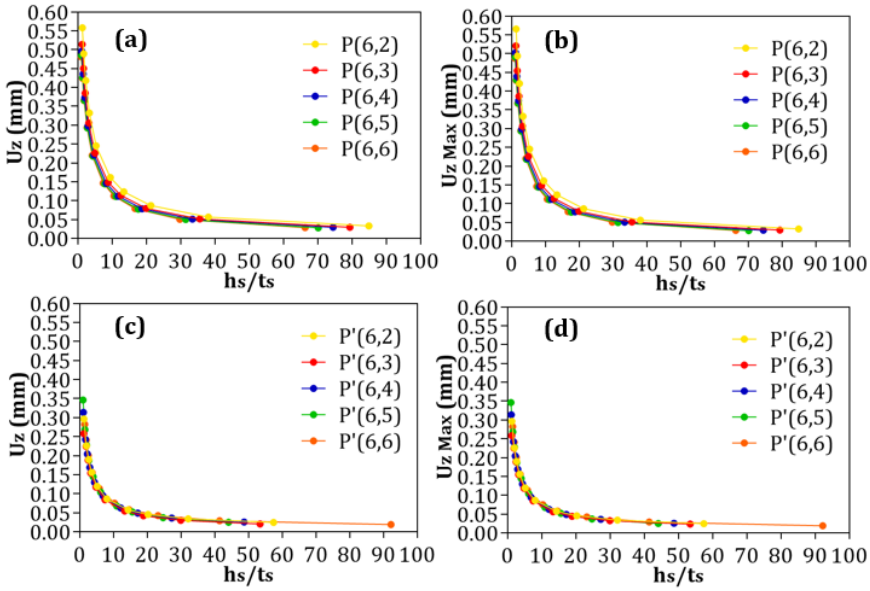

A. 3 - Group E - Central and maximum displacements – (a) e (b) Orthogonal stiffeners to edges; (c) e (d) stiffeners oriented at 45°

References

[1] Szilard R. Theories and applications of plate analysis: Classical numerical and engineering methods. 1ª ed. Hoboken: Wiley, 2004. https://doi.org/10.1002/97804701728722

[2] Manrique LJC. Colapso de painéis planos enrijecidos. Dissertação de Mestrado em Engenharia Oceânica. Universidade Federal do Rio de Janeiro, Rio de Janeiro,1989.

[3] Bedair OK. Analysis and Limit State Design of stiffened plates and shells: A world view. Applied Mechanics Reviews, v. 62, p. 01-16, 2009. https://doi.org/10.1115/1.3077137

[4] Ghavami K, Khedmati MR. Nonlinear large deflection analysis of stiffened plates. Finite Element Analysis - Applications in Mechanical Engineering. IntechOpen, 2012. https://doi.org/10.5772/48368

[5] Rossow MP, Ibrahimkhail AK. Constraint method analysis of stiffened plates. Computers and Structures, v. 8, p. 51-60, 1978. https://doi.org/10.1016/0045-7949(78)90159-1

[6] Bedair OK. Analysis of stiffened plates under lateral loading using sequential quadratic programming (SQP). Computer and Structures, v. 62, p. 63-80, 1997. https://doi.org/10.1016/S0045-7949(96)00281-77

[7] Peng LX, Kitipornchai S, LIew KM. Analysis of rectangular stiffened plates under uniform lateral load based on FSDT and element-free Galerkin method. International Journal of Mechanical Sciences, v. 47, p. 251–276, 2005. https://doi.org/10.1016/j.ijmecsci.2004.12.006

[8] Hasan MM. Optimum design of stiffened square plates for longitudinal and square ribs. Al-Khwarizmi Engineering Journal, v. 3, p. 13-30, 2007.

[9] Hosseini SH, Soltani B. Analysis of Rectangular Stiffened Plates Based on FSDT and Meshless Collocation Method. Journal of Solid Mechanics, v. 9, n. 3, p. 568-586, 2017.

[10] Singh DK, Duggal SK, Pal P. Analysis of Stiffened Plates using FEM – A Parametric Study. International Research Journal of Engineering and Technology, v. 2, n. 4, p. 1650-1656, 2015.

[11] Troina GS. Modelagem computacional e método design construtal aplicados à otimização geométrica de placas finas de aço com enrijecedores submetidas a carregamento transversal uniforme. Dissertação de Mestrado em Engenharia Oceânica. Universidade Federal do Rio Grande, Rio Grande, 2017.
[12] Bathe K. Finite Element Procedures. 1ª ed. Upper Saddle River, New Jersey: Prentice-Hall, 1996.
[13] Zienkiewicz OC. The finite Element Method in Engineering Science, 2º ed. London: McGraw- Hill, 1971.
[14] Madenci E, Guven I. The Finite Element Method and Applications in Engineering Using ANSYS. 1ª ed. New York: Springer, 2006. https://doi.org/10.1007/978-1-4899-7550-8_122
[15] ANSYS Academic Research Mechanical, Release 19, Help System, Element Reference, ANSYS, Inc.
[16] Bejan A, Lorente S. Design with Constructal Theory. 1ª ed. Hoboken: Wiley, 2008. https://doi.org/10.1002/9780470432709
[17] Reis AH. Constructal theory: from engineering to physics, and how flow systems develop shape and structure. Applied Mechanics Reviews, v. 59, p. 269-281, 2006. https://doi.org/10.1115/1.2204075

Research on Engineering Structures & Materials
journal homepage: http://jresm.org
Research Group

Research Article

Computational modeling and constructal design method applied to the geometric evaluation of stiffened thin steel plates considering symmetry boundary condition

Rodrigo Reis Amaral[*1,a], Grégori da Silva Troina[2,b], Carolina Martins Nogueira[2,c], Marcelo Langhinrichs Cunha[4,d], Luis Alberto Oliveira Rocha[3,e], Elizaldo Domingues dos Santos[1,2,f], Liércio André Isoldi[1,2,g]

[1] *Programa de Pós-Graduação em Modelagem Computacional (PPGMC), Universidade Federal do Rio Grande (FURG), Brazil*
[2] *Programa de Pós-Graduação em Engenharia Oceânica (PPGEO), Universidade Federal do Rio Grande (FURG), Brazil*
[3] *Programa de Pós-Graduação em Engenharia Mecânica, Universidade do Vale do Rio dos Sinos (Unisinos), Brazil*
[4] *Escola de Engenharia (EE), Universidade Federal do Rio Grande (FURG), Brazil*

Article Info

Article history:
Received 04 Feb 2019
Revised 14 May 2019
Accepted 15 May 2019

Keywords:

Stress minimization;

Deflection minimization;

Plate with stiffeners;

Geometric evaluation

Abstract

The present article presents a geometric evaluation of stiffened plates employing the symmetry boundary condition. The computational models were developed in the software ANSYS, based on the Finite Element Method, using the SHELL281 finite element. As expected, the numerical simulations considering the symmetry demonstrated a gain in computational processing because of the possibility of developing the models in a quarter of a plate rather than simulating the entire plate, without accuracy loss. The geometric configurations are obtained through the application of Constructal Design. For this, some geometric parameters are varied (degrees of freedom) and others are kept fixed (restrictions). After that, these plates with different geometries are numerically simulated and their mechanical behaviors (deflection and stress) are compared to each other through the Exhaustive Search Technique. Then, it is possible to define the stiffened plate that has the best mechanical behavior. For this, a reference plate without stiffeners was used. In this plate part of its volume of material was transformed into stiffeners by reducing the thickness of the same, thus maintaining the value of the length and the value of the width as constants. The objective here is to determine the geometric configurations that minimize the maximum deflection and the maximum von Mises stress of the stiffened plates. The obtained results showed that, by transforming part of the volume of the reference plate into stiffeners, structural stiffness gains can be achieved in the stiffened plates when compared with the values of deflection and stress reached by the reference plate.

© 2019 MIM Research Group. All rights reserved.

1. Introduction

Plates or panels are flat and three-dimensional structural components that may be subject to transverse loads that cause them to deflect. These structures, when have a thickness ten times smaller than their length or width, can be classified as thin plates. Thus, the analysis of displacements, deformations and stresses will go from a three-dimensional problem to

[*]Corresponding author: rodrigo_amaral_23@hotmail.com
[a] https://orcid.org/0000-0001-9035-5806; [b] orcid.org/0000-0002-4408-562X; [c] orcid.org/0000-0002-1847-8446; [d] https://orcid.org/ 0000-0003-1083-7341; [e] https://orcid.org/ 0000-0003-2409-3152; [f] https://orcid.org/ 0000-0003-4566-2350; [g] https://orcid.org/ 0000-0002-9337-3169
DOI: http://dx.doi.org/10.17515/resm2019.112ms0204

a two-dimensional problem, according to Kirchhoff's Thin Plate Theory (Bhaskar & Varadan [1]).

According to Szilard [2], some hypotheses must be respected for the use of this theory, being:

- The material should be homogeneous, isotropic and linear elastic.
- The plate, in its initial state, should be flat.
- The middle surface of the plate remains unrestricted during the deflection.
- The transverse deflections w (x,y) must not exceed one-tenth the thickness of the plate.
- The shear deformations γ_{yz} and γ_{xz} must be very small and neglected.

In order to improve the stiffness of the thin plates, there are attached to them reinforcements called stiffeners. These reinforcements are usually positioned longitudinally, transversely or in both directions relative to the plate. So, investigations involving the mechanical behavior of the stiffened plates were performed, such as: Orozco [3] made a comparison between two methodologies, Orthotropic Plate Method and FEM, of stiffened plates submitted to a transverse load and determined which of the two methodologies presents the best behavior of the dimensionless deflection and stress parameter curves; Silva [4] determined the influence of the eccentricity on the structural behavior in stiffened plates through the use of computational models developed in the ANSYS software; Bhaskar & Pydah [5] presented an analytical solution for stiffened plates that consider the shear force and rotational inertia in order to quantify the individual contribution of the plate and the stiffeners in the total deformation of the structure; and Troina [6] developed 3D and 2D computational models of stiffened plates subjected to uniform transverse loading in ANSYS and evaluated the influence of stiffener height by stiffener thickness and transformation of a volume fraction of material into stiffeners in a central deflection analysis.

Normally, the researches considered the whole plate as the computational domain, not using the symmetry boundary condition. The symmetry, when possible, allows to work with half or a quarter of the plate as computational domain. The symmetry boundary condition can be adopted if the structural component presents symmetry of: geometry, loading, support conditions and material properties. When applying the symmetry boundary condition it is assumed that the out-of-plane translations and in-plane rotations are set to zero (ANSYS [7]).

Therefore, the present article presents a geometric evaluation by means a computational model using the symmetry boundary condition in a quarter of stiffened plates subjected to a uniform transverse loading and clamped in its edges. The computational model to numerically simulate its mechanical behavior was elaborated in the software ANSYS 18.2 academic version with the SHELL281 finite element. The study analyzed the maximum deflection and the maximum von Mises stress of the different geometric configurations of plates that were generated from the application of the Constructal Design Method (Rocha, Lorente & Bejan [8]). They were defined by varying the number of longitudinal (N_{ls}) and transversal (N_{ts}) stiffeners; and by the use of different height-to-thickness ratios of stiffeners (h_s/t_s). All the geometric configurations were then numerically simulated, allowing the identification of the one that minimized the maximum deflection and the maximum von Mises stress, characterizing a process of geometric optimization through the Exhaustive Search Technique.

2. Computational Modeling

The software ANSYS, based on FEM, was used to generate the numerical models presented in this work. According to Stolarski, Nakasone & Yoshimoto [9], the ANSYS package can be used to numerically solve a wide variety of mechanical problems involving static or dynamic structural analysis, both of which can be linear or non-linear; problems involving heat transfer or fluid transfer; acoustic problems; electromagnetic problems, among others.

These computational models adopted the SHELL281 finite element (Fig. 1). According to ANSYS [7], the element is composed by eight nodes, having in each node six degrees of freedom (three translations in directions x, y, z, and three rotations around the axes x , y, z); and its use is suitable for the analysis of shell and plate structures that are thin to moderate in thickness.

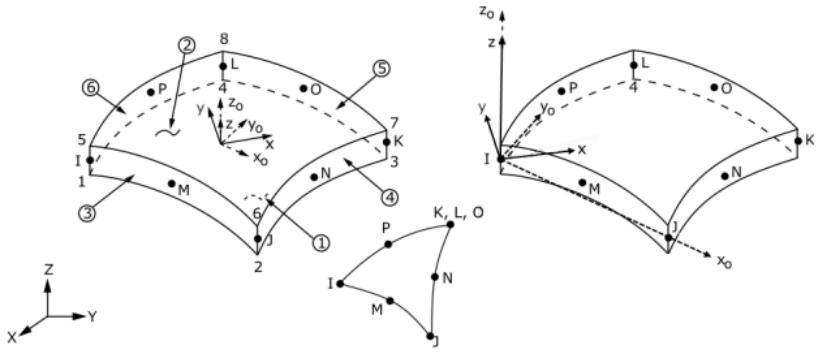

Fig. 1 Illustration of SHELL281 finite element (ANSYS [7])

In relation to FEM, its definition is given as the discretization of a mathematical model in a finite number of parts, whose geometry, boundary condition and load imposed on the model are defined according to the proposed physical problem. The accuracy of the method is directly related to the size of the elements, because the smaller the size, the greater the number of finite elements for the discretization of the computational domain and, consequently, the greater the precision of the results; but longer is the computational processing time required to develop the simulations. Also, tests that evaluate the minimum number of elements are necessary due to the low variation of result that the computational models present from a certain point, characterizing, thus, the stabilization of a mesh convergence test. Regarding the solution obtained by this method, this will only occur from the assembly of the global matrix of elements that will allow the nodal solution and the values of displacement and stress suffered by each element. In order to exemplify this explanation, for cases involving linear elastic behavior problems, the global matrix is represented by (Zienkiewicz [10], Rao [11]).

$$[K] \cdot \{u\} = \{F\} \tag{1}$$

where $[K]$ is the stiffness matrix of the structure, $\{u\}$ is the vector of unknown nodal displacements and $\{F\}$ is the external forces vector. The stiffness matrix of the system is obtained through the strain-displacement relations of the structure, from the discretization of the model and the properties of the material.

3. Constructal Design Method and Exhaustive Search Technique

The Constructal Law, the basic law of the Constructal Theory, deals with the design forecast (the flow configuration) and its evolution over time. Also, it is a way of seeing, as it teaches that the evolution of the flow system can be observed at all-time scales. That is, it is not only a principle from which the geometric form and the structure are deduced in nature, but also an engineering method (Design Construtal) used to optimize the paths of the flows through open systems of finite size. In this way, the Construtal Law indicates that the best flow architecture is one that minimizes the resistance of global flow or maximizes access to the global flow (Rocha, Lorente & Bejan [8]).

Therefore, the Constructal Design is a method that allows the obtaining of a geometry that gives the best performance of systems when submitted to some kind of flow. For this, the flow must be ajustable and the geometry must be deduced in order to maximize overall performance. In addition, global constraints and variations of certain degrees of freedom must be subjected to geometry (Bejan [12]). About the Exhaustive Search Technique, according to Khoury [13], refers to any search algorithm that analyzes a range of solutions until it finds the most adequate solution or reaches the maximum number of pre-established attempts.

The use of the Constructal Design Method in this article has the purpose to set the search space by changing the geometric parameters, so that the volume of the material does not change. For this purpose, a non-stiffened plate of length a, width b and thickness t was adopted as reference. After that, a fraction of its volume ϕ is transformed into stiffeners by reducing its thickness, maintaining the length and width with constant values (Fig. 2). Consequently, all the analyzed geometries have the same amount of material, allowing a comparative evaluation of the structural performance of these plates. The improvement of the mechanical behavior will be considered in the definition of the optimized geometric configuration. In addition, the volume fraction of the material is a constraint parameter of the Constructal Design Method and can be defined by:

$$\phi = \frac{V_s}{V_r} = \frac{N_{ls}\,(a\,h_s\,t_s) + N_{ts}\cdot[(b - N_{ts}\,t_s)\,h_s\,t_s]}{abt} \tag{2}$$

where V_s is the volume of the plate transformed into stiffener and V_r is the volume of the plate used as a reference, N_{ls} is the number of longitudinal stiffeners, N_{ts} is the number of transversal stiffeners, h_s is the height of the stiffeners and t_s is the thickness of the stiffeners. As for degrees of freedom, according to [6], for problems involving stiffened plates, it is possible to consider: height-to-thickness ratios of stiffeners h_s/t_s, the number of longitudinal stiffeners N_{ls} and the number of transverse stiffeners N_{ts}.

The analysis involved plates formed by 10 combinations of longitudinal and transverse stiffeners, obeying the P(N_{ls},N_{ts}) format, varying the following degrees of freedom: $N_{ls} = 2, 3$ and $N_{ts} = 2, 3, 4, 5, 6$. Therefore, in this study the following plates were analyzed: (2,2), P(2,3), P(2,4), P(2,5), P(2,6), P(3,2), P(3,3), P(3,4), P(3,5) and P(3,6). On the stiffeners, they have a rectangular cross section and commercial values of thicknesses of steel plates were adopted. In addition, two geometrical constraints are imposed: the height of the stiffeners cannot be greater than 0.3 m, in order to avoid geometric disproportions between the height of the stiffener and the lateral dimensions of the plate; and the ratio h_s/t_s must be greater than 1 to avoid that the thickness of the stiffener be greater than its height, a reason that would de-characterize the stiffener that should have a height greater than its thickness.

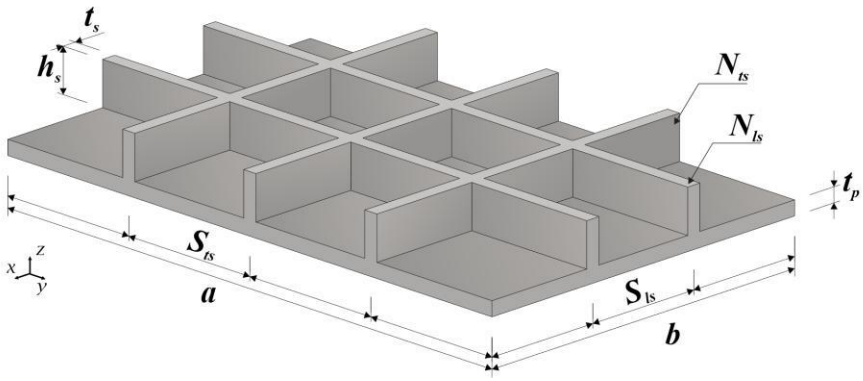

Fig. 2 Stiffened plate with 'its' variables

The adopted reference plate has a length of 2.00 m, width of 1.00 m, thickness of 0.02 m, and is of structural steel A-36 with modulus of elasticity of 200 GPa and Poisson coefficient of 0.3. The ratio of the volume of material transformed in stiffeners to the volume of the reference plate is ϕ = 0.3, that is, 30% of the volume was used in the stiffeners. The reference plate and the stiffened plates were considered to be clamped in the four edges, being subjected to a uniformly distributed transverse loading of 10 kPa.

4. Results and Discussions

Initially, two verifications were performed. The first one, through a comparison of the results of the central deflection of the stiffened plates P(2,5), and P(2,6), with simply support and subject to uniform transverse loading, with numerical results presented by Troina [6]. The second verification was a comparison between the deflection results and the von Mises stress of a stiffened plate (whole, without considering the condition of symmetry) in relation to a quarter of the plate considering the symmetry boundary condition, both with simply supported on its edges.

Figure 3 shows the first verification, so that the central deflection results obtained with SHELL281 finite element (used in this study) were compared with the SOLID95 finite element (used by [6]). The verification showed coherent results, since the largest difference between the displacements was 5.54%, found on the plate P(2,6) with h_s/t_s equal to 1.2337. While the smallest difference was 0.97% in the plate P(2,5) with h_s/t_s equal to 59.4087. The variation of the accuracy of the results may be due to the SOLID95 being an element that considers all the components of the stress and strain state as a three-dimensional system of a solid body, whereas the shell element SHELL281 has some simplifications in the components of its plane of stress and deformation.

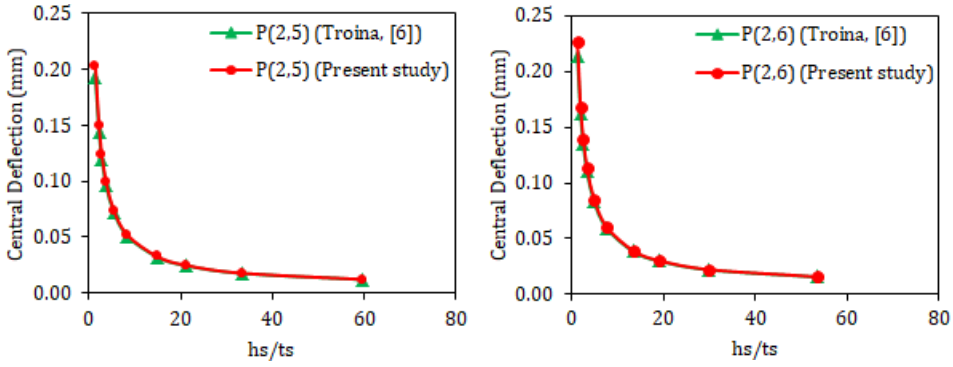

Fig. 3 Comparison of the numerical results of the central deflection of the stiffened plate due to the variation of degree of freedom h_s/t_s

The second verification was exposed in a mesh convergence test, shown in Tabs. 1 and 2. The objective here was to compare the stabilization of the displacement and von Mises stress results for the plate with greater geometric complexity among all simulated cases, that is, the plate P(3,6).

Table 1 Mesh convergence test for entire stiffened plate P(3,6)

Element size (mm)	Number of elements	w (mm)	σ_{vM} (MPa)
352	73	0.007	3.363
176	292	0.009	4.317
88	804	0.009	4.813
44	2631	0.009	5.552
22	9978	0.009	6.598

Table 2 Mesh convergence test for stiffened plate P (3,6) with symmetry

Element size (mm)	Number of elements	w (mm)	σ_{vM} (MPa)
376	34	0.008	3.416
188	80	0.009	4.317
94	222	0. 009	4.813
47	796	0.009	5.553
23.50	2718	0.009	6.568
11.75	9970	0.009	7.692

One can observe that the symmetry plate model (Tab. 2) presented similar results to the simulations that treated the entire plate (Tab. 1), which verifies the proposed computational model. In addition, it can be seen that for a deflection analysis it was possible to determine the independent mesh solution, as seen in Tabs. 1 and 2. In its turn, for the von Mises stress the results indicated the need for continuity of the mesh convergence test, i.e., the use of more refined meshes. However, the academic version of the software ANSYS 18.2 limits the simulations to a maximum use of 32000 nodes. Meshes with element sizes smaller than 11.75 mm in the symmetric model (see Tab. 2) exceed this node limit.

A solution for this problem on the mesh convergence test of the von Mises stress would be if it was used an elasto-plastic analysis rather than an elastic linear analysis. This new analysis could solve this problem because, in this case, the yielding of the material would occur at this point. Then, there would be a limit to the value of the von Mises stress at this stress concentration point. Thus, the maximum value of the von Mises stress will be used as a means of comparison, and not as an absolute value.

Then, the case study was performed using the computational model with the symmetry boundary condition. To do so, based on the results of Tab 2, the regular meshes were generated with quadrilateral SHELL281 finite elements with size of 11.75 mm. Figure 3 shows the numerical results obtained for the maximum deflection and in Fig. 4 for the maximum von Mises stress of the stiffened plates with symmetry subjected to the distributed uniform transverse loading. Besides, the reference plate was also numerically simulated. A maximum displacement of 0.1739 mm and a maximum von Mises stress of 11.047 MPa were obtained, being included in Figs. 4 and 5, respectively.

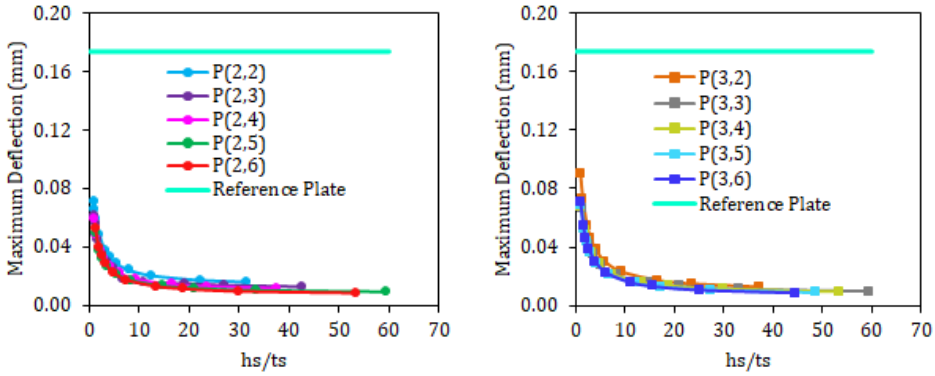

(a) (b)

Fig. 4 Variations of the maximum deflection in relation to h_s/t_s for: (a) N_{ls} = 2; and (b) N_{ls} = 3

The results of Fig. 4 indicate that the transformation of 30% of reference plate material into stiffeners always leads to an improvement over deflection, i.e., all the stiffened plates have a maximum deflection smaller than that of the reference plate. However, for the maximum von Mises stress, it can be noted that geometric configurations with values of h_s/t_s greater than approximately 5 (Fig. 5 (a)) and 10 (Fig. 5 (b)) show mechanical behavior superior to the plate and reach lower stresses; while for smaller values of h_s/t_s there was an increase in the maximum stress and, consequently, a worsening in the mechanical behavior.

Another aspect observed is that as the value of h_s/t_s increases, the deflection (Fig. 4) and the von Mises stress (Fig. 5) of the stiffened plates decrease. Table 3 shows the best geometric configuration, that is, the one with the lowest deflection and lowest von Mises stress for each combination of longitudinal and transverse stiffeners.

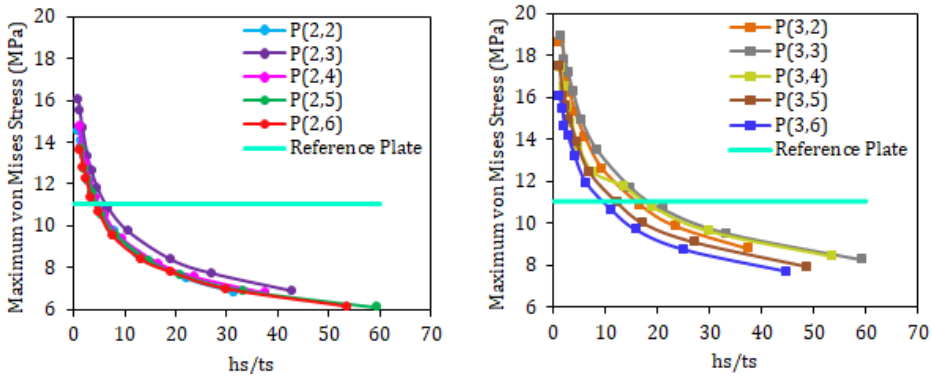

(a) (b)

Fig. 5 Variations of the maximum von Mises stress in relation to h_s/t_s for: (a) N_{ls} = 2; and (b) N_{ls} = 3

Table 3 Better geometric configurations that minimize displacements and stresses

Plate	h_s/t_s	w (mm)	σ_{vM} (MPa)
P(2,2)	31.4176	0.0158	6.5167
P(2,3)	42.7470	0.0126	6.6846
P(2,4)	37.4378	0.0115	6.5674
P(2,5)	59.4087	0.0091	6.0334
P(2,6)	53.4905	0.0083	6.0244
P(3,2)	37.3781	0.0128	8.5811
P(3,3)	59.3771	0.0098	8.2325
P(3,4)	53.4905	0.0096	7.7104
P(3,5)	48.6658	0.0089	7.8466
P(3,6)	44.6394	0.0087	7.6923

The stiffened plate that presented the smallest displacement was P(2,6) with h_s/t_s = 53.4905 (see Tab. 3). Its maximum deflection is 95.23% smaller than the deflection obtained by the reference plate without stiffeners and 4.82% smaller than the plate P (3,6) with h_s/t_s = 44.6394 (lower displacement reached by the degree of freedom N_{ls} = 3). Also, it has been noted that as the degree of freedom N_{ts} increases, overall the maximum deflection of the plates decreases, as can be seen in Fig. 6 (a).

In relation to the stresses (see Table 3), the geometric configurations generated by the degree of freedom N_{ls} = 2 presented a greater reduction of von Mises stress than the geometries generated by the degree of freedom N_{ls} = 3, as can be seen in Fig. 6 (b). Thus, among the studied cases, the geometric configuration that minimized the maximum stress was the plate P(2,6) with h_s/t_s = 53.4905, whose stress presented a value 45.46% lower than the reference plate and 27.69% lower than the plate P (3,6) with h_s/t_s = 44.6394 (lower stress reached by degree of freedom N_{ls} = 3).

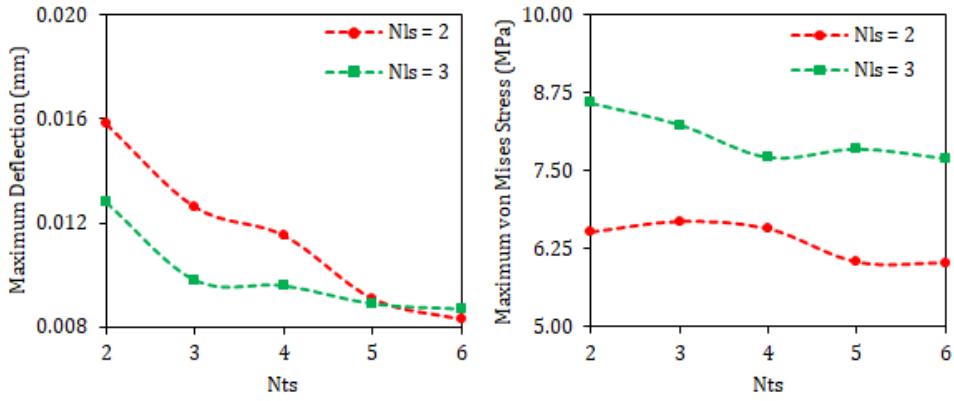

(a) (b)

Fig. 6 Variation of (a) maximum deflection; and (b) Maximum von Mises stress in relation to Nts

5. Conclusion

Different geometric configurations of plates with stiffeners, generated from the application of the Constructal Design Method, were numerically simulated. The obtained results for the maximum deflection and for the maximum stress were compared with each other, in order to determine the optimized geometric configuration, by means the Exhaustive Search Technique. It is understood as optimal geometry the one that minimizes maximum deflection and minimizes maximum stress.

The study allowed determining a reduction in the computational processing time of the simulations that use the symmetry boundary condition in a quarter of the plate in the analysis of the deflection, because they reduce the computational domain of the problem and, as a consequence, they need less finite elements for their spatial discretization. For example, for the plate with 3 longitudinal stiffeners, 6 transverse and h_s/t_s = 44.6394 with element size of 22 mm, it was observed a reduction of 71.22% in the computational processing time to calculate the results in the simulation that employs the symmetry boundary condition (2876 elements) when compared with the simulation that uses the computational domain as entire (9978 elements). Also, it was noted that the symmetry boundary condition enables the use of more refined meshes with respect to simulations that consider the entire plate in the ANSYS software academic version. This is an important aspect, since the academic version of ANSYS has a limitation on mesh refinement.

About the results, it has been observed that the transformation of part of the volume of a non-stiffened plate into longitudinal and transverse stiffeners generally results in an improvement of structural mechanical performance.

The optimum geometric configuration for the cases studied was the plate with 2 longitudinal stiffeners, 6 transverse and h_s/t_s = 53.4905 ratio that provided reductions in maximum deflection and maximum von Mises stress of respectively 95.23% and 45.46% relative to the reference plate.

For the plates with N_{ls} = 3, the maximum stress reduction was 30.36% in relation to the reference plate. However, in the use of stiffeners with h_s/t_s of less than 5, a stress increase of 71.73% was found for the plate with 3 longitudinal stiffeners, 3 transversal stiffeners and h_s/t_s = 1.3618 ratio, that is, a worsening relative to the reference plate. Thus, it is clear

that not always the inclusion of stiffeners leads to an improvement in the mechanical behavior of the plates, evidencing the importance of the geometric evaluation in this type of structural component.

Acknowledgment

This study was financed in part by the *Coordenação de Aperfeiçoamento de Pessoal de Nível Superior - Brasil* (CAPES) - Finance Code 001. The authors also thank to the Brazilian funding agencies *Fundação de Amparo à Pesquisa do Estado do Rio Grande do Sul* (FAPERGS) and *Conselho Nacional de Desenvolvimento Científico e Tecnológico* (CNPq) for the financial support.

References

[1] Bhaskar K, Varadan TK. *Plates Theories and Applications*. Ane Books Pvt. Ltd., New Delhi, India, 2013. https://doi.org/10.1002/9781118894705
[2] Szilard R. *Theories and applications of plate analysis: classical, numerical and engineering methods*. Hoboken: New Jersey, USA, 2009.
[3] Orozco JCG. Contribuição ao estudo de painéis reforçados: comparação entre o método da chapa ortotrópica e o método dos elementos finitos. Masters dissertation, Universidade de São Paulo, Brasil, 2009. (in Portuguese)
[4] Silva, HBS. Análise numérica da influência da excentricidade na ligação placa-viga em pavimentos usuais de edifícios. Masters dissertation, Universidade Federal de São Carlos, Brasil, 2010. (in Portuguese)
[5] Bhaskar K. Pydah A. An elasticity approach for simply-supported isotropic and orthotropic stiffened plates. International Journal of Mechanical Sciences, 2014; 89: 21-30. https://doi.org/10.1016/j.ijmecsci.2014.08.013
[6] Troina G. da S. Modelagem computacional e Método Design Construtal aplicados à otimização geométrica de placas finas de aço com enrijecedores submetidas a carregamento transversal uniforme. Masters dissertation, Universidade Federal do Rio Grande, Brasil, 2017. (In Portuguese)
[7] ANSYS, Inc. ANSYS® Academic Research Mechanical, Release 18.2, Help System, Element Reference.
[8] Rocha LAO, Lorente S, Bejan A. *Constructal Law and the Unifying Principle of Design. Springer*. Science+Business Media, New York, NY, USA, 2013. https://doi.org/10.1007/978-1-4614-5049-8
[9] Stolarski T, Nakasone Y, Yoshimoto S. *Engineering Analysis with ANSYS Software (2nd ed.)*. The Boulevard, Langford Lane, Kidlington, Oxford OX5 1GB, United Kingdom, 2018.
[10] Zienkiewicz OC, Taylor RL. *The Finite Element Method – Volume 1: The basis*. Butterworth-Heinemann, Oxford, 2000.
[11] Rao SS. *The Finite Element Method in Engineering*. Elsevier Inc., Burlington, 2011. https://doi.org/10.1016/B978-1-85617-661-3.00001-5
[12] Bejan A. *Shape and Structure, from engineering to nature*. Cambridge University Press, Cambridge, 2000.
[13] Khoury R, Harder DW. *Numerical Methods and Modelling for Engineering*. Springer International Publishing, 2016. https://doi.org/10.1007/978-3-319-21176-3

Research on Engineering Structures & Materials
journal homepage: http://jresm.org
Research Group

Research Article

Finite element evaluation of notch effect on partial penetration T-joints subjected to distinct toe-grinding processes

Gabriel Funes*[a,1], Priscila Amaro [b,1], Paulo Teixeira[c,1], Kleber Bianchi[d,1]

[1]*School of Engineering, Federal University of Rio Grande - FURG, Brazil*

Article Info

Article history:
Received 07 Feb 2019
Revised 15 Apr 2019
Accepted 15 May 2019

Keywords:

Welded structures;

Toe grinding;

Finite Element Analysis;

Notch effect

Abstract

Toe grinding process is widely employed for increasing fatigue life of welded structures with high dimensions, which are very usual in civil, naval and offshore industries. In these cases, costs related to the application of an additional manufacturing process are naturally justified. However, code recommendations referred to toe grinding process are quite conservatives, which justifies investigations on the applicability of more effective and efficient procedures. This work presents an alternative toe grinding procedure for application in a partial penetration T-joint with fillets subjected to a longitudinal load. Such alternative was analyzed by comparison of results of Finite Element Analysis applied over modeled specimens corresponding to three cases: i) original configuration (no grinding process had been applied), ii) tip rib contouring groove (code based procedure) and iii) straight grinding groove. This last case was proposed because the manufacturing procedure is considerably simplified and easily adaptable for automated production. After performing the FE analysis, results indicated that notch effect is very similar for both grinding cases. This result supported the choice of the simplified grinding process for manufacturing a set of real specimens, assigned for fatigue testing. In a resume, this work indicates that a simple and adaptable for automated manufacturing procedure may provide similar fatigue performance of the relatively complex method preconized by standard codes.

© 2019 MIM Research Group. All rights reserved.

1. Introduction

Ribs and gussets are widely employed for improving strength and rigidity of engineering structures, especially where shell and plate components are employed. Although these reinforcements are used in a wide range of applications, from small laboratory devices to offshore platforms, in some areas they are especially important, as in the naval industry, for example. Hulls, decks and other naval structures and components are usually assembled by plate and ribs joining, which is made by welding procedures [1-2-3]. Even though this building philosophy is very successful and well consolidated, some important aspects related to fatigue phenomena are frequently neglected. A first important issue is related specifically to the welded joints, which naturally are the weakest links in the structure. High levels of residual stress and the presence of discontinuities represented by several flaws emerged during the welding process, associated with geometry and notch effect aspects, are responsible for a remarkably poor fatigue performance of welded joints [4-5-6-7-8-9]. A second issue is related to the variation of compliance caused by inserting a partial rib in a structural component, which propitiates a greater mechanical strength and rigidity in relation to the region without rib. Consequently, when load is applied, there

*Corresponding author: funes.gx@gmail.com
[a] orcid.org/0000-0002-9869-5781; [b] orcid.org/ 0000-0002-6378-3933; [c] orcid.org/0000-0003-0773-6865; [c] orcid.org/0000-0001-6961-8595;
DOI: http://dx.doi.org/10.17515/resm2019.114ms0207

is a stress concentration at the interface of these regions. It is worth to emphasize that such effect happens even in the case of a non-loaded rib (i.e., the force is applied in the base plate). Finally, ribs aligned with the flux of force have their beads and fillets subjected to longitudinal stress, in which case, even lower fatigue performances are expected.

Along the structural assessment phase, joint designers are frequently in face of a concerning problem: the overall aspect of the structure and the main structural components are yet established, giving no space for changing in favor of welded joints. In this case, some alternatives are available. The first one is prescribing higher levels of quality control, by non-destructive examination of critical regions of beads and fillets. Another alternative involves welding process optimization for providing a shape, in bead or fillet reinforcement, more favorable to the flux of loads, or simply for lowering the degree of inhomogeneity of the weld affected region. A third approach encompasses several post-welding processes responsible for increasing fatigue response. Thermal stress relief is preponderantly employed in small parts but, in case of the great civil, naval and offshore structures, its application is impracticable. In these cases, several post welding processes can be applied for promoting a better surface geometry, for wiping off potentially dangerous flaws at critical points on the beads or fillets and, finally, for providing stress relief or inserting localized compressive stress. Hammer peening, toe grinding and TIG dressing are the most employed procedures in case of big structures, but other processes, like shot peening and surface rolling may be circumstantially employed [4-10-11]. As a result, significant fatigue performance increases may be achieved. However, any of these processes are time and money consuming, as well as craftsmanship dependent.

Several studies evidenced that, after an ordinary but careful welding procedure is applied, in order to achieve a usual weld quality level, bead geometry aspects are of greater relevance in relation to material and metallurgical characteristics [12-13]. Fig. 1 shows the transversal cut of an idealized bead, where any material inhomogeneity is purposely omitted. In other words, this figure represents a plate of an isometric and homogeneous material with localized face protuberances that correspond to the bead reinforcements. A clear notch effect is observed, both in the face and in the root toes. Such effect is responsible for a localized level of stress usually well above the yield strength value. Fortunately, because of the high toughness characteristic of ordinary structural steels, such localized stresses are mitigated by microscale yielding. Geometrical parameters like the height of reinforcement *h* and the toe angle φ are employed for characterizing the notch effect at the face and root toes. Finally, these observations are also valid for fillet welds.

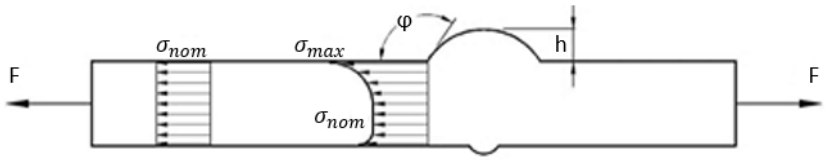

Fig. 1 Notch effect in face and root reinforcements in a butt-joint [8]

By means of the simplified image shown in Fig. 1 it is possible to comprehend some important aspects related to fatigue performance of welded joints, which in turn depends on the superposition of following pernicious facts concerned to the toe region: *i)* the previous presence of process resulted in sub-millimeter cracks, *ii)* the high level of tensile residual stress and *iii)* the notch effect yet described. A fourth issue is the high metallurgical inhomogeneity in the weld affected region, however, as already said, in

conventional structural steels joined by arc welding processes, the presence of cracks, residual stress and the notch effect are more relevant.

Considering that the life achieved by a structural part in a fatigue test is dependent on the superposition of the described effects, it is possible to figure why a very low performance and a high scatter of results is always observed. Summarizing, the high level of variability in such effects is responsible for the strong likelihood characteristic of fatigue phenomena in welded joints.

In order to provide a robust assessment approach, international standards contain S-N diagrams that effectively represent the lower bound, usually corresponding to 95% of survival probability, of the whole set of structural materials and arc welding processes for the most common joint configurations. Eurocode 3 – section 1.9: Fatigue, AWS D1.1 and the IIW Recommendations [14-15-16] are examples of reference codes for welded joints assessment. Such codes are also referenced inside other standardized procedures. For example, ABS - Rules For Materials And Welding [17] adopts AWS D1.1 specifications for welded joints evaluations.

After this general explanation, it would be worth returning to the notch effect subject, but now focusing on a fillet in a cruciform or T-joint. Fig. 2 schematically shows a somewhat different but convenient definition of geometrical parameters, to be used instead of the ones presented in Fig. 1. In a fillet joint, toe angle θ (the counterpart of φ angle in Fig. 1) and the concordance radius *r* at the toe are employed.

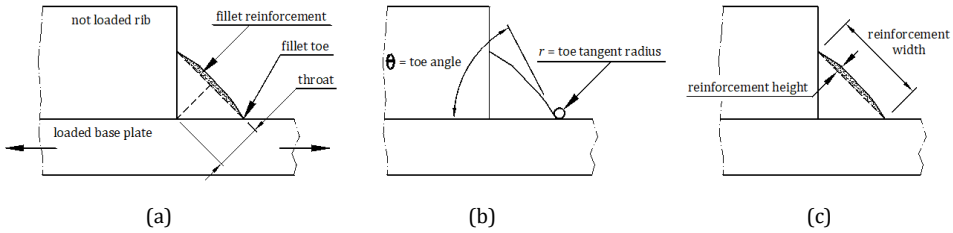

Fig. 2 Geometrical parameters for notch effect characterization in a fillet: a) fillet associated nomenclature, b) toe angle and toe radius and c) reinforcement height and width.

As already cited, toe grinding is frequently employed for fatigue life improving. The process consists of a grinding or eventually milling process applied by means of an electric or pneumatic manual device. A specifically developed tool with a blunted tip and several cutting edges, usually of high-speed steel, is adopted in the cutting process.

Fig. 3 shows a double fillet, complete penetration T-joint, after the grinding process was applied at left and right toes. At the left fillet, the final groove did not achieve the necessary depth for sub-millimeter crack removal, but groove on the right fillet was successfully applied instead. Fig. 3 also evidences that the grinding process is not able to efface cracks positioned in the weld root region.

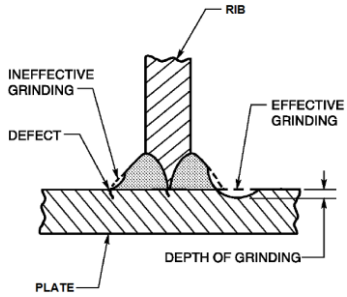

Fig. 3 Geometrical aspects related to toe grinding process [15]

Previously existent cracks at the toe are considered responsible for suppressing the nucleation period of fatigue phenomenon, which in ordinary (no-welded) parts, frequently corresponds to high percentiles (sometimes greater than 80%) of overall life. So, by effectively erasing those previously existent cracks, a nucleation period is supposedly attached to the whole fatigue life of the welded joint.

Studies evidenced that welding process associated cracks have a length inside a range flanked by an upper bound of 0.5 mm, while the lower flank is conveniently assigned to the resolution of the nondestructive inspection method employed (usually 0.1 to 0.2 mm). In order to effectively erase potentially dangerous flaws, toe grinding depth should overpass the measured crack length in at least 0.5 mm. Consequently, if any inspection procedure is going to be applied, a groove depth value of 1 mm is ordinarily specified. Such value can be a problem in case of thin plates, because of the important decrement caused in the resistance area. In such cases, an even lower fatigue response could be achieved by applying the toe grinding process. However, in case of thick plates and ribs, as the ones ordinarily employed in naval and offshore industry, the decrement in cross area is irrelevant and, oppositely, an important fatigue life increase is usually achieved [4].

Fig. 4 and Table 1 present the summary of design dimensions with respective recommended values in accordance with employed references.

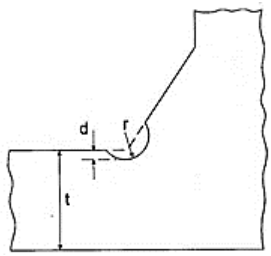

Fig. 4 Geometrical parameters related to toe grinding process [11]

Furthermore, some degree of residual stress relief is also assigned to the toe-grinding process. Such an effect is very difficult to quantify however, being completely neglected in assessment procedures.

Finally, whatever the geometry of a welded joint, loads acting on fillets and beads can be classified in longitudinal, transversal or the combination of both cases.

Table 1 Recommended geometrical parameters for the toe grinding process [11][15].

Reference	d_{min} (mm)	d_{max} (mm)	r_{min} (mm)
AWS D1.1	0.8 to 1 below plate face or 0.5 to 0.8 mm below deepest crack	greater value between 2 or 5% of plate thickness	5 mm(2) 6 mm(3)
IIW	0.5 mm below the deepest crack	7% of plate thickness(1)	≥ t/4

(1) for plate thickness ≤ 40 mm
(2) for plate thickness < 20 mm
(3) for 20 mm ≤ t ≤ 29 mm

Figure 5 shows a ribbed part with a longitudinal load applied to the base plate (note that the rib is not directly loaded). In this case, fatigue life is lower than the one expected for transversal loading, because of the uneven distribution over the throat or leg area in the longitudinal case. As the weakest link points are the extremities, any post-welding process for fatigue life improving is directed to these regions. So, Fig. 5 also shows the advised groove extension in case of toe grinding application.

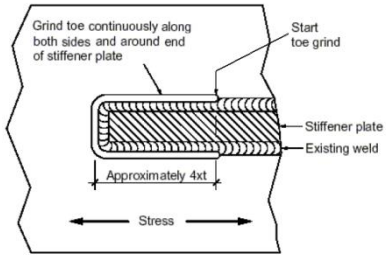

Fig. 5 Recommended contouring toe-grinding [11]

The cited reference codes seem to adopt a conservative approach in defining the geometrical parameters of the groove. However, in field or even in shop floor welding, some level of misalignment between rib and direction of the load may occur, resulting in a predominant but not exclusive longitudinal stress. Because of that, as observed in Fig. 5, the extension of the groove prolongs well beyond the critical stress region at the rib tip. Nevertheless, doubts about the ideal length to be employed naturally arise.

Finally, even though the grinding process is costly and dependent on operator hand skills, in the other sense it is clearly prone to be automated.

In face of such context, this work presents a study focused on the suitability of an alternative toe-grinding procedure, proposed for partial penetration T-welded joints subjected to longitudinal loading on the fillets. The proposed groove is applied only in the extreme point of the fillet, having a straight shape, instead of the contour shown in Fig. 5. Such proposal aims to investigate a procedure able to provide production advantages, i.e., manufacturing of a smaller and straight groove, easily adaptable for automated machining with a standard ball end milling tool, instead of a more complex but standard groove geometry. For guessing the possibility of success of such a proposal, preliminary studies on FEA software had been made in order to compare the notch effect related to original and proposed configurations.

2. Methodology

2.1. Specimen definition

The overall geometry of the T-joint specimens had been defined mostly to enable a simple machining process of the toe-grinding groove, which means that base and rib should present dimensions (and specially thickness) sufficiently high. So, base and rib were taken from a 9.53 mm (3/8 in) - AISI 316L steel plate. Other dimensions, directly correlated with plate thickness, were defined in accordance with AWS D1.1 [15] and ASTM E466 standards [18]. Rib length was defined in order to propitiate a greater length than 40 mm, as advised by NBR 8800 [19]. Fig. 6 shows the final shape and dimensions adopted in the specimen. As observed, a contour fillet with leg length of 9 mm was specified and, consequently, the joint is characterized as presenting partial penetration.

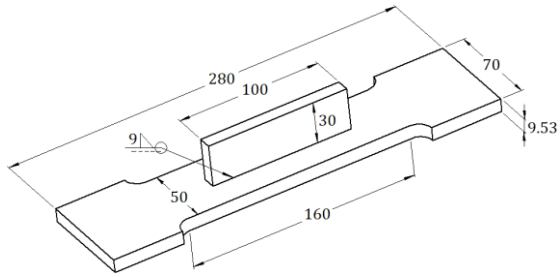

Fig. 6 Shape and principal dimensions of the specimen (mm).

2.2. Definition of Groove Geometry

Based on the specimen geometry shown in the previous section, three study cases had been defined: *i)* ordinary specimens (no grinding process was applied), *ii)* specimens that underwent a standardized grinding process (as shown in Fig. 5) and *iii)* specimens subjected to the simplified, straight grinding process. Fig. 7 shows the model elaborated in SolidWorks Education Edition software for the second case. Radius and groove depth had been defined in accordance with Tab. 1. Fig. 8 shows part of the model of the third case specimen. Radius and depth of the groove are the same as the previous case.

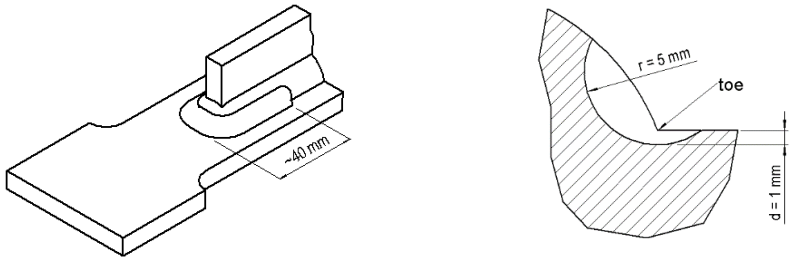

(a) (b)

Fig. 7 Groove geometry of the second study case: a) overall geometry and b) cross cut of the groove.

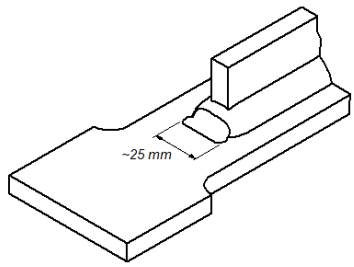

Fig. 8 Detail of the straight groove region.

2.3. Mathematical Model

2.3.1 Finite Element Meshes

A Finite Element Analysis was implemented to compare the level of stress concentration at the critical points in the contour fillet (as already explained, in the tips of the rib) considering the three cases explained in the previous section. Additional effects associated with fillet surface geometry, residual stress and any welding discontinuity probable to exist at the toe region were omitted. So, the central idea was comparing the level of notch effect mitigation propitiated by both toe-grinding procedures (standardized and alternative) in comparison with the ordinary case (without grinding).

Structural analysis was implemented in the Workbench module of software Ansys, version R15.0. The first step consisted in inserting mechanical properties of the material (in this case, Young Modulus of 193 GPa, yield strength of 207 MPa and ultimate strength of 586 MPa). Afterward, FEA meshes were automatically created by means of "Use advanced size function" command, inside "fixed" mode, allied to "sizing" method. Such set of commands enables to choose regions of interest, where a more refined mesh is necessary. In such approach, linear tetrahedral elements with four nodes were automatically generated with a user-defined main dimension.

Final mesh composition was determined by means of a convergence evaluation procedure consisting of a sequence of running and refinement steps. The resulting data was considered satisfactory when the maximum normal stress (in the X direction of the adopted coordinate system) remained in a range of variation of 5% of previous analysis value. A final main dimension of 0.8 mm for the linear tetrahedral elements of all meshes analyzed propitiated the desired result in this stage of convergence evaluation. Table 2 presents a summary of results attained in the convergence test for the original mesh (without groove). Table 3 reports the final mesh related data for all the cases of study.

Table 2 Mesh convergence history corresponding to original case (without toe grinding).

Element size (mm)	Maximum normal stress (MPa)	N. Nodes	N. Elements	Variation (%)
3	271.8	34711	21706	-
2	308.6	62689	41300	13.5
1	363.9	202972	140221	17.9
0.9	387.8	242742	168508	6.50
0.8	390.6	298064	207662	0.75

Table 3 Mesh related data.

Geometry	N. of Nodes	N. of Elements
Without toe grinding	298064	207662
Contouring toe grinding	355210	247442
Straight toe grinding	318232	247442

Fig. 9 sequentially shows the original (no grinding) mesh, followed by the standardized and simplified meshes generated. In second and third cases, adopted values of radius and depth of the groove were the ones presented in Fig. 7.

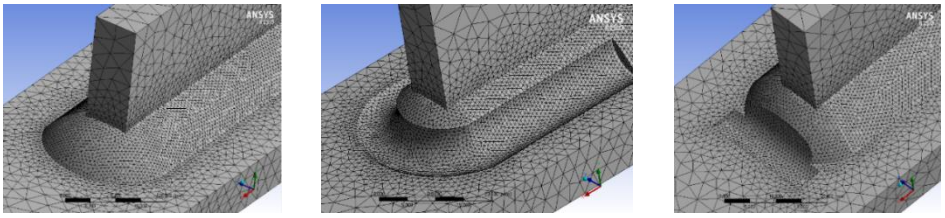

(a) (b) (c)

Fig. 9 Resulting meshes: a) without toe grinding, b) with a contouring toe grinding and c) with straight toe grinding.

2.3.2 Boundary Constraints and Loading Definition

Before running the analysis, boundary constraints had to be specified. So the elements pertaining to one of the plate extremities were completely constrained to translation, while supports constraining one of the transversal displacements had been associated with the face plate elements. A monotonic load with a maximum value of 75 kN was applied over the face of this second longitudinally free extremity. Corresponding nominal stress value for the maximum load case is 157.4 MPa, an intermediate value to be adopted on fatigue tests phase. Fig. 10 shows a vision of the boundary step implemented inside software Ansys: A) crimped face B) with constraints on Y and Z axis and C) face where a distributed force is applied.

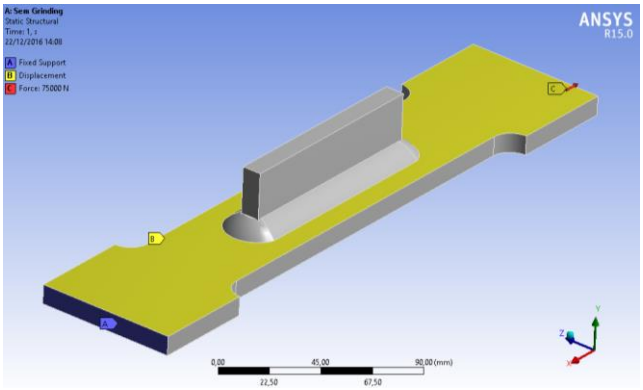

Fig. 10 Boundary conditions taking the no-grinding specimen as an example.

3. Results and Discussion

Fig. 11 shows a view of the post-processing result obtained for the no-grinding case. As observed, the toe of the rib tip fillet presents maximum normal stress, which is in accordance with experimental results reported in several welded joints assessment codes. In the performed analysis, maximum normal stress value attained is approximately 391 MPa, corresponding to a notch factor of ~2.5.

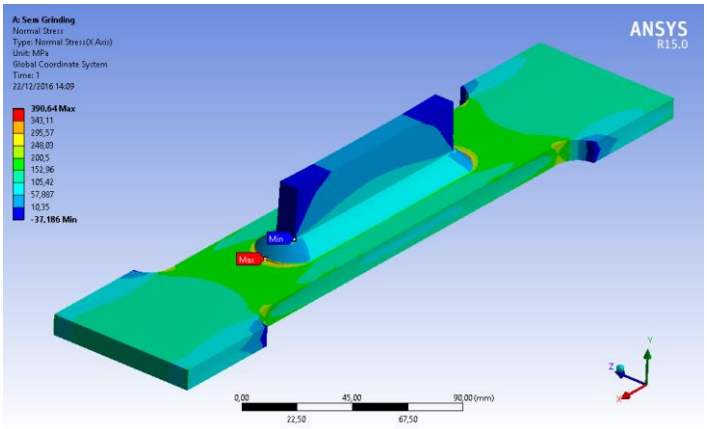

Fig. 11 Post-processing image obtained for the no-grinding case.

Fig. 12 presents a similar figure for the case of the standardized contour groove, as preconized in reference codes consulted. In this case, maximum normal stress value attained is approximately 327 MPa, corresponding to a notch factor of ~2.1. Such value represents a reduction of approximately 20% in relation to the original case.

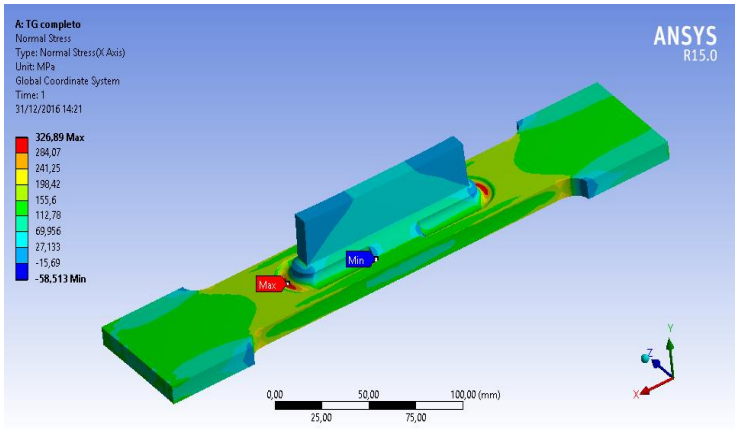

Fig. 12 Obtained results for the case of contour groove at the rib tip

Finally, Fig. 13 presents the attained results for the simplified, straight groove at the tip of rib fillet. In this case, a peak stress value of approximately 310 MPa was attained, which corresponds to a notch effect value of ~2.

These results indicate that notch effect mitigation achieved by the simplified version of toe-grinding is very similar to that attained by standardized case. The small difference

between peak values of stress in both cases is inside the 5% interval of acceptance previously established.

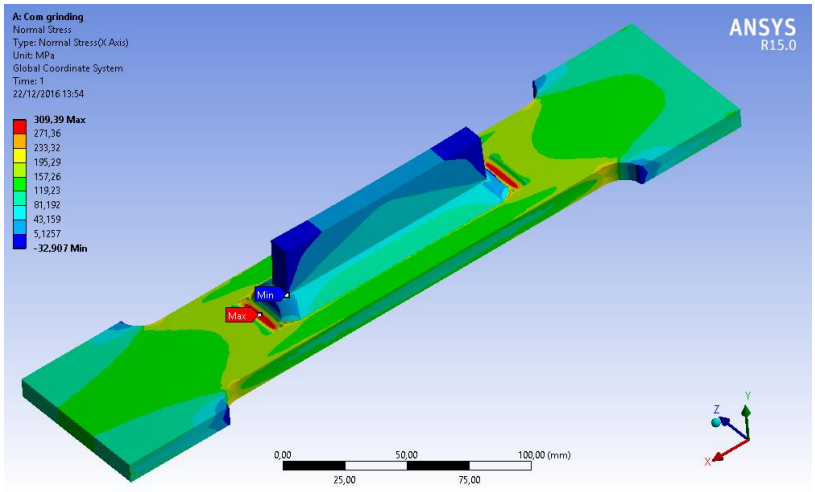

Fig. 13 Obtained results for the case of a straight groove at the rib tip.

4. Concluding and Remarks

Attained results confirm that partial penetration T-joints subjected to longitudinal loading have the toe of fillets on rib extremities as critical points of fatigue phenomena, because of the high level of localized stress. So, any post-welding procedure for increasing fatigue life shall have this region in focus.

Analyzing the reference codes and recommendations about the toe-grinding application, a clear conservative approach was observed. Such fact opened space for an alternative, more simplified procedure for grinding implementation.

By means of the analysis performed in this study, it was possible to verify that a simplified toe-grinding procedure, consisting in a straight groove, propitiates a very similar notch effect of the contouring case preconized by reference codes. In this way, a relatively simple Finite Element Analysis was very effective on describing the level of stress achieved in the structural parts, evidencing that this design tool gives support for production and manufacturing changes that may cause huge impacts on costs of naval and offshore industry.

Finally, it is worth to say that, after finishing this study, fatigue tests were made on real specimens, with stress ratio $R = \sigma_{min}/\sigma_{max} = 0$, of original (no grind) and straight groove configurations, evidencing a remarkable fatigue life increment. Actually, the attained results remained above the ones expected for the contouring groove case. Discussion of such results will be explored in a second paper.

Evaluation of a straight grinding procedure, like the one implemented in this work, shall be extended to the case of specimens with some degree of misaligned in the ribs. In such case, the apparently conservative contouring grinding procedure so far advocated by engineering codes is justified. Such future study would permit, for example, to define some level of acceptability to the misalignment of the ribs in relation to the load.

References

[1] Moehring HC, Brecher C, Abele E, Fleischer J, Bleicher F. Materials in machine tool structures. CIRP Annals, 2015; 64(2): 725-748. https://doi.org/10.1016/j.cirp.2015.05.005

[2] Odot - Ohaio Department of Transportation. On-line Bridge Maintenance Manual Preventive Maintenance/Repair. Guidelines for Bridges and Culverts 2008. Available in: https://www.dot.state.oh.us/Divisions/Engineering/Structures/bridge%20operations%20and%20maintenance/PreventiveMaintenanceManual/BPMM/beams/sbeams.htm

[3] Roy J, Munro B, Walley S, Meredith A. Longitudinal versus Transversely Framed Structures for Large Displacement Motor Yachts. In 20th International HISWA Symposium on Yacht Design and Yacht Construction, Amsterdam, The Netherlands, 2008.

[4] Branco CM, Fernandes AA, Castro PMST. *Fadiga de Estruturas Soldadas*, Fundação Calouste Gulbenkian, Lisboa, PT, 1999.

[5] Blondeau R. *Metallurgy and Mechanics of Welding*, Processes and Industrial Applications. John Wiley & Sons Inc, Hoboken, NJ, USA, 2008.

[6] Lassen T, Récho N. *Fatigue Life Analyses of Welded Structures: Flaws*, ISTE, Londres, ENG, 2006. https://doi.org/10.1002/9780470612149

[7] Suresh S. *Fatigue of materials*, Cambridge university press, Cambridge, ENG, 1998.

[8] Hicks J. *Welded joint design*, Industrial Press, New York, NY, USA, 1999.

[9] Maddox SJ. Fatigue Strength of Welded Structures. 2nd Ed. Woodhead Publishing Ltd and The Welding Institute. Cambridge, 2002.

[10] Kirkhope KJ, Bell R, Caron L, Basu R I, Ma K-T. Weld detail fatigue life improvement techniques. Part 2: application to ship structures. Marine Structures, 1999; 12: 477-496. https://doi.org/10.1016/S0951-8339(99)00031-3

[11] Haagensen PJ, Maddox SJ. Recommendations on Post Weld Improvement of Steel and Aluminium Structures. IIW Doc, 2006; 13: 1815-00.

[12] Funes GX. Evaluation of a modified version of the toe grinding technique in the fatigue life improvement for longitudinally loaded T joints made AISI 316 L stainless steel. Msc. Dissertation, Federal University of Rio Grande – FURG, Rio Grande, 2017.

[13] Silva MSda. Comparison of fatigue life of microlight structural steel joints welded by Gas Metal Arc Welding - GMAW and Flux Cored Arc Welding - FCAW. Msc. Dissertation, Federal University of Rio Grande – FURG, Rio Grande, 2018.

[14] Eurocode 3. Design of steel structures – Part 1.9: Fatigue, CEN, Brussels, BEL, 2003

[15] American Welding Society. AWS D1.1/D1.1M:2010: Structural Welding Code – Steel. Miami, 2010.

[16] Hobbacher A. Recommendations for Fatigue Design of Welded Joints and Components. IIW Doc, 2008; Review of 13: 1539-96 and 15, 945-96.

[17] American Bureau of Shipping. Rules For Materials And Welding – PART 2. Houston, TX, USA, 2010.

[18] American Society for Testing and Materials. ASTM E466-07, Standard practice for conducting force controlled constant amplitude axial fatigue tests of metallic materials. ASTM International, West Conshohocken, PA, 2007.

[19] Brazilian Association of Technical Standards, ABNT NBR. 8800 Design of Steel Structures and Mixed Structures of Steel and Concrete for Buildings. Rio de Janeiro, RJ, Brazil, 2008.

Blank Page

Research on Engineering Structures & Materials
journal homepage: http://jresm.org
Research Group

Research Article

Damage progression in rubble-mound breakwaters scale model tests, under a climate change storm sequence

Conceição J.E.M. Fortes [*a,1], Rute Lemos [b,1], Ana Mendonça[c,1], Maria Teresa Reis[d,1]

[1]*Department of Hydraulics and Environment, National Laboratory for Civil Engineering (LNEC), Portugal*

Article Info

Article history:
Received 18 Dec 2018
Revised 05 Apr 2019
Accepted 14 May 2019

Keywords:

Damage progression;

Rubble-mound breakwaters;

Climate change;

Stereo-photogrammetric techniques

Abstract

This paper describes the two-dimensional (2D) physical model tests of a rock armor breakwater, performed at LNEC´s experimental facilities, under the framework of the HYDRALAB+ project. The aim of the present work was to evaluate damage evolution under future climate change scenarios, by using different damage evaluation techniques. The tested wave conditions simulated a storm sequence where two water levels (low water and high water) were considered, as well as an increase of the wave height. The water levels and the wave heights were chosen to simulate extreme events forecasted on climate change scenarios. Damage evaluation was based on the traditional counting method and on stereo-photogrammetric techniques. Test results are presented in terms of the damage parameter S and in terms of the percentage of removed armor units. The analysis is focused on the damage progression during the scale model tests, for the imposed storm sequence. The damage presents an oscillating behavior with two main damage areas corresponding to the active zones for each level, due to the variation of the water level between low-water and high-water. This behavior differs significantly from that found for the common storm sequences usually tested, where the water level does not change. Both measuring techniques lead to an intermediate damage of the cross-section breakwater. However, the damage parameter assessment with the stereo-photogrammetric technique allows a more versatile evaluation, since it is possible to characterize damage in representative zones of the cross-section

© 2019 MIM Research Group. All rights reserved.

1. Introduction

Most climate change scenarios predict, in addition to mean-sea-level rise, the increase of sea storminess, more frequent extreme events and changes of the dominant wave direction [1]. However, the actual failure probability of existing structures under such conditions is not known. To ensure an adequate performance of rubble-mound breakwaters in such scenarios, adaptive structures have to be designed, aiming at not increasing significantly the breakwaters' dimensions and the associated costs. This means that it is mandatory to characterize and measure further the response of these structures to climate change, in what concerns wave run-up, wave overtopping and hydraulic stability (damage), as well as how altered run-up/overtopping conditions impact the stability of both the main and the rear armors [1].

Project HYDRALAB+ (H2020-INFRAIA-2014-2015) gathers an advanced network of environmental hydraulic institutes in Europe, which provides access to a suite of

*Corresponding author: jfortes@lnec.pt
[a]orcid.org/0000-0002-5503-7527; [b]orcid.org/0000-0003-0380-391X; [c]orcid.org/0000-0002-4060-2650; [d]orcid.org/0000-0003-3878-1634
DOI: http://dx.doi.org/10.17515/resm2019.82ms1218

environmental hydraulic facilities that through physical experiments plays a vital role in the development of climate change adaptation strategies, by allowing the direct testing of adaptation measures and by providing data for numerical model calibration and validation. The use of physical (scale) models allows the simulation of extreme events as they are now, and as they are projected to be, under different climate change scenarios.

Task 8.2 of RECIPE, one of the Joint Research Activities of the HYDRALAB+ project, entitled "Damage characterization under variable and unsteady test conditions", has as main objective to develop new innovative experimental techniques, methods and protocols to characterize damage evolution on structures under extreme events. Damage can be assessed using visual observation, profilers and/or photographic techniques. Digital overlay techniques are employed to assess rock and concrete unit movements. Photographs (taken before and after the test) and videos are also used to assess structural/toe stability. However, the success of each technique relies on the setting conditions (light conditions, camera characteristics, etc.), on the experience of the technician and on the need of emptying the flume to use the technique.

In this framework, LNEC's HYDRALAB+ team performed a set of physical experiments to simulate 2D damage and overtopping tests with a rock armor slope for extreme events (climate change). Overall, those tests aimed at developing and comparing different methodologies/techniques to measure and quantify the most important responses of hydraulic structures (wave run-up, wave overtopping and hydraulic stability) to the altered wave/water-level conditions due to climate change.

The main goals of the present work were to simulate a cumulative storm sequence, where the water levels (alternating low-water with high-water levels) varied with an increase of wave heights, and to study the damage evolution throughout the tests. To achieve these goals, two different measuring techniques were applied: displacement counting method and photogrammetric techniques.

In relation to damage characterization, note that some of the most commonly used damage indicators are the percentage of damage for all armor, N_d, the number of displaced blocks per width of one block, N_{od} (both based on counting the number of individual units that have been dislodged) and the dimensionless erosion area, S (based on determining the volumetric change in areas where armor units have been displaced) [2], [3] and [4]. Critical values of N_d, N_{od} and S for varying materials (rock, concrete armor units) and varying armor thicknesses are presented in the Rock Manual [3] and in the Coastal Engineering Manual [2].

This paper begins with the description of damage assessment and stereo-photogrammetric techniques. Then the physical model tests are described, and their results and discussion presented. Some conclusions are drawn in the final section of the paper.

2. Materials and Methods

2.1. Damage assessment

Damage in physical scale models of rubble-mound breakwaters can be characterized by two methods: counting the number of displaced units and measuring the eroded area of the profile. In the last case, Broderick & Ahrens [5] and Van der Meer [6] defined a dimensionless damage parameter, $S=A_e/(D_n)2$, where A_e is the eroded cross-sectional area around the still water level (SWL) (Figure 1) and D_n is the nominal diameter of the armor units.

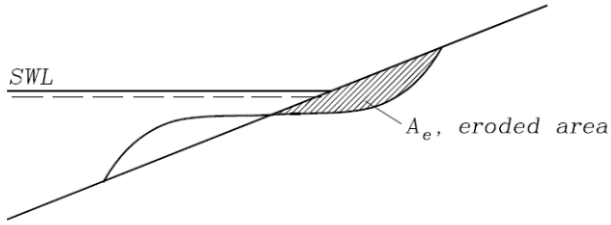

Fig. 1 Eroded cross-sectional area (A_e) [2]

Several measuring techniques can be used for the two damage assessment methods (number of displaced units or eroded area of the profile), such as, visual observation and stereo-photogrammetry. These techniques have the main advantage that they do not require emptying the flume/basin before measurements are taken. However, visual observation can only be applied to identify the unit displacements and movements, and it is very dependent on the technician experience. Stereo-photogrammetry can be applied to both damage progression methods since the counting method can be achieved by photos and the eroded area can be determined through comparison of cross-section profiles.

2.2 Stereo-photogrammetry

Stereo-photogrammetry consists of identifying depth from two different views of the same scene (stereo image pairs).

Stereopsis is the base of reconstructing a three-dimensional (3D) scene from a pair of images acquired from two slightly different locations. In the present study, the profile surveys were carried out with a fixed separation of 16 cm between the centers of the camera lenses.

The available software package allows a complete 3D reconstruction environment, using stereo image pairs as input. It consists of two distinct applications implemented in MATLAB™ [7], each with a specific objective:

- Camera calibration, which consists of identifying the parameters describing the projective cameras and their position and orientation within the observed world;
- Scene reconstruction, which consists of identifying depth from two different views of the same scene.

The output of the package consists of a (x, y, z) file describing the cloud of surveyed points. This is a standard file format that can be imported by various modelling tools. By using a MATLAB™ algorithm [8] and [9], it is possible to create regular grids, enabling to extract the breakwater surveyed surface, as well as profile definition, in order to quantify the eroded area (A_e) and, subsequently, the non-dimensional damage parameter S.

Since the used scene-reconstruction software rectifies the distortion introduced by the air-water interface, it is possible to reconstruct both the emerged and submerged scenes without emptying the flume/basin.

3. Physical Model Tests

3.1 Physical model setup and equipment

LNEC´s experiments were performed at the Ports and Maritime Structures Unit (NPE) of the Hydraulics and Environment Department (DHA), in a wave flume (COI 1) approximately 50 m long, with an operating width and an operating water depth of 80 cm (Figure 2). The flume is equipped with a piston-type wave-maker that combines both irregular wave generation and dynamic absorption of reflected waves.

Fig. 2 COI1 wave flume

The structure is a rubble-mound breakwater, with a 1:2 rock slope and a trapezoidal core covered by two rock layers with a porosity of ~37% and a rock nominal diameter, D_n, of 0.045 m (model scale).

The physical model was constructed and operated according to Froude's similarity law, with a geometrical scale of 1:30, to ensure reduced scale effects (with wave heights that lead to values of the Reynolds number, $Re = (\sqrt{gH_s}D_n)/\nu$, were higher than $3x10^4$, where g is the acceleration due to gravity (m/s^2) and ν is the kinematic viscosity of water ($= 10^{-6}$ m^2/s).

The construction of the physical model began with the implementation at the flume of a foreshore slope of 2%. Then, the breakwater cross-section was built (Figure 3, top), with 0.80 m width. The slope of the breakwater was divided in three main parts, with the rocks painted with three different colors (red, yellow and blue). This procedure facilitates the identification of rock falls/movements and helped also the photogrammetric surveys. Finally, the experimental equipment was placed in the wave flume. The experimental setup is presented in Figure 3, bottom.

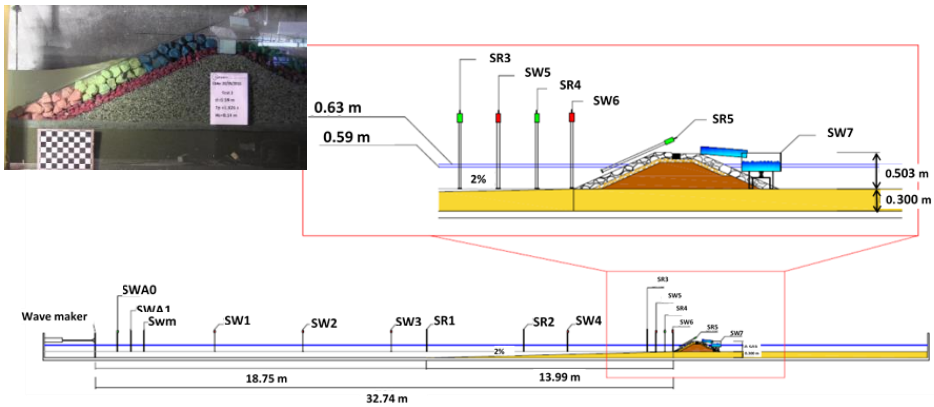

Fig. 3 COI1 wave flume

The flume was equipped with twelve resistive-type wave gauges deployed along the wave flume, to measure the free surface elevation (Figure 4, left). In order to measure run-up levels, an additional gauge was placed on the armor layer slope (Figure 4, right).

Fig. 4 . Measuring equipment. Left: wave gauges to measure free surface elevation; right: run-up wave gauge

As referred previously, for damage assessment, two methods were used. The counting of falls and movements of the armor units was performed by visual observation and by taking some photos of the breakwater cross-section with a common camera. The stereo-photogrammetric technique used two cameras mounted side by side in a support structure and able to photograph the same scene simultaneously (Figure 5, top). Throughout the tests herein described, two digital SLR cameras (Canon EOS 600D) were fitted with fixed focal length lenses (Canon EF 35mm ƒ/2). This setup is capable of acquiring images ranging from 3.5 to 18 megapixel). All tests were filmed with 2 video cameras, one located above the model and the other placed next to the flume side wall (Figure 5, bottom). These cameras were used for run-up and damage measurements.

Fig. 5 Top: Photographic equipment. Bottom: Video camera for damage evaluation

3.2 Incident Wave Conditions

In the present work, a cumulative storm build-up was simulated. It represents a cumulative test series with constant wave period, alternating low-water and high-water levels, and increasing wave heights. The values of water levels and wave heights correspond to extreme events related with climate change scenarios.

In detail, the test conditions for Tests 10-17 are presented in Table 1, in which d represents the water depth at the toe of the structure, where low and high water levels correspond to d=8.1 m and d=11.1 m, respectively. Hs represents the significant wave height at the toe of the structure and T_p the peak period of the JONSWAP wave spectrum, with a peak enhancement factor of 3.3.

At the end of the test series 10-17, Test 16, was repeated three times, herein called Tests 16Rep1, 16Rep2 and 16Rep3. The test duration was 2400 s for the prototype peak period of 12 s (around 1000 waves).

Table 1. Test conditions at structure toe.

Test	Prototype			Model		
	d (m)	T_p (s)	H_s (m)	d (m)	T_p (s)	H_s (m)
10	11.1	12	3.2	0.37	2.191	0.107
11	8.1	12	3.2	0.27	2.191	0.107
12	11.1	12	3.7	0.37	2.191	0.123
13	8.1	12	3.7	0.27	2.191	0.123
14	11.1	12	4.2	0.37	2.191	0.140
15	8.1	12	4.2	0.27	2.191	0.140
16	11.1	12	4.7	0.37	2.191	0.157
17	8.1	12	4.7	0.27	2.191	0.157
16Rep1	11.1	12	4.7	0.37	2.191	0.157
16Rep2	11.1	12	4.7	0.37	2.191	0.157
16Rep3	11.1	12	4.7	0.37	2.191	0.157

4. Results and Discussions

4.1 Counting method

Figure 6 presents an overview of the cross-section before Test 10, after Test 16 and after Test 16Rep3, respectively.

Fig. 6 Overview of the cross-section before Test 10 (left), after Test 16 (center) and after Test16Rep3 (right)

With the photos taken with the photogrammetric cameras it was much easier to count the number of rocks that fell down than by using visual observation. These values are presented in Table 2.

Table 2. Number of displaced blocks (N) and relative displacement (D) for Tests 10 to 17 and repetitions of Test 16.

Test	10	11	12	13	14	16	17	16 Rep1	16 Rep2	16 Rep3
N	5	6	8	8	9	11	13	14	14	15
D (%)	4.0	4.8	6.5	6.5	7.3	8.9	10.5	11.3	11.3	12.1

Figure 7 presents the cumulative damage curve in terms of percentage of displaced blocks (N) over the total number of blocks of the active zone, D (%).

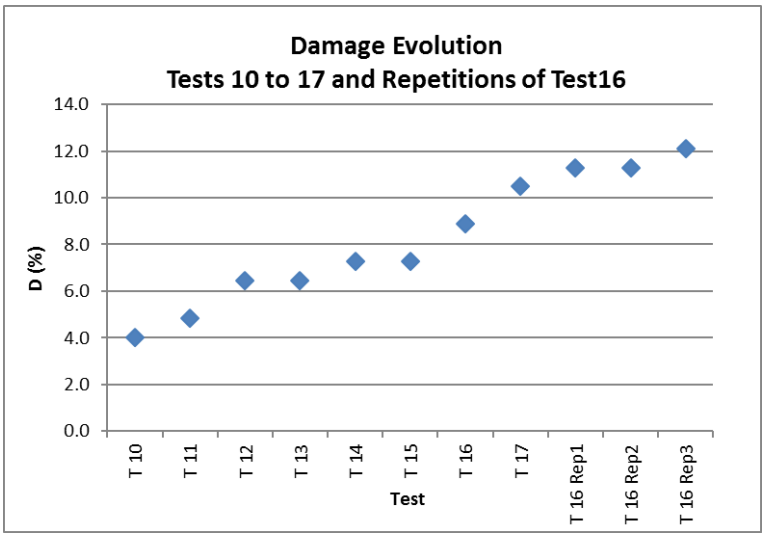

Fig. 7 Damage in terms of percentage of displaced blocks

According to the damage classification referred in the Coastal Engineering Manual [2], the cumulative damage at the end of Test 17 and Test 16Rep3 corresponds to an intermediate damage (units are displaced but without causing exposure of the under or filter layers to direct wave attack).

From the analysis of the damage curve one can infer that damage progression increases with the wave height, with some stabilization during tests with the low-water level. During the repetitions of Test 16, a damage stabilization is visible between Tests 16Rep1 and 16Rep2, and a slight increase with Test 16Rep3, mainly due to an additional displaced block near the active zone for the high-water level.

Figure 8 (left) illustrates image comparison, using an image analysis algorithm, between photos taken before Test 10 and after Test 16, with a modified area of 1327.1 cm^2 (9.6% of the photo total area). Figure 8 (right) depicts damage evolution between Tests 16 and 16Rep3, with a modified area of 1240.4 cm^2 (9.0% of the photo total area).

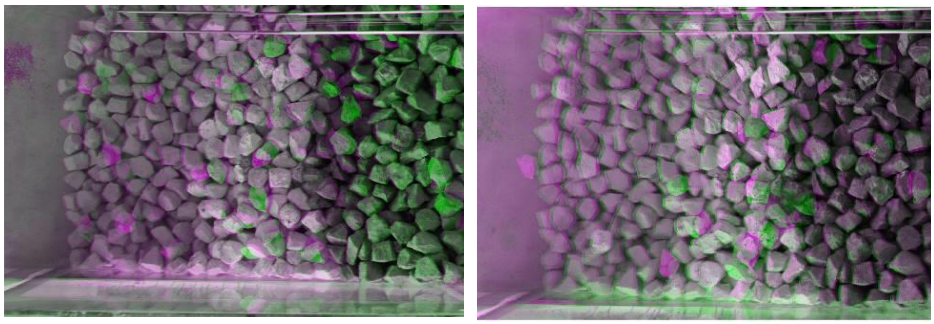

Fig. 8 Left: Differences between photos taken before Test 10 and after Test 16.
Right: photos taken after Tests 16 and 16Rep3

The algorithm overlaps final image (magenta) with initial image (green), calculating the area of the changed zones of the photos. This calculation is proceeded by calibration of the area of a square of a checkerboard.

Although this algorithm does not distinguish between erosion and accretion areas, it was a helpful tool for detecting stone displacements. Furthermore, the damage evolution trends calculated both with the photo modified area and with add up of displaced blocks are similar.

4.2 Calculation of the non-dimensional damage parameter (S)

For a better damage characterization, the armor layer was divided in five profiles, 10 cm apart (Figure 9). During the test series, a survey of the undamaged profile was carried out (T0) and 7 surveys (T10 to T17) were conducted to compare the eroded area between consecutive surveys. Furthermore, three repetitions of Test 16 were conducted, in order to infer on the reliability of the measurements (T16Rep1, T16Rep3 and T16Rep3). Due to problems with photo acquisition during Test 15, its results are not presented.

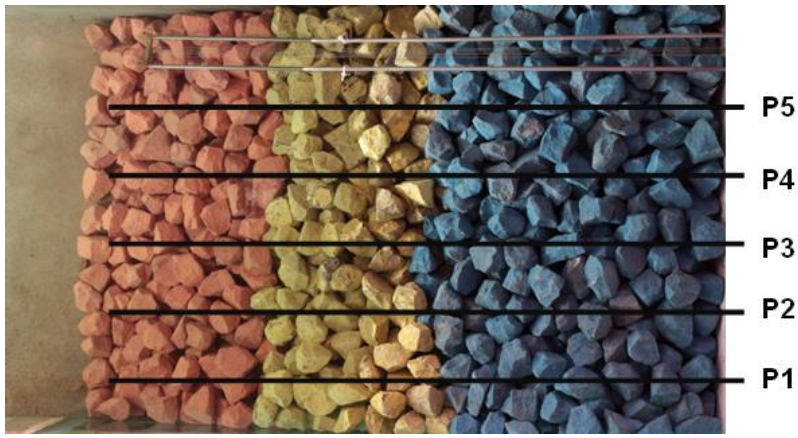

Fig. 9 Location of surveyed profiles

To obtain the eroded area for all the profiles, a MATLAB™ code [8], was used, having as input the point clouds resulting from the reconstruction files. It enables to extract the pre-defined profiles for all the surveys, including the initial survey (undamaged profile, T0). The second step of the code compares all the profiles with their initial surveys and measures the corresponding eroded areas. Finally, the last step of the code consists in the calculation of the S parameter.

The most relevant eroded area occurred around the SWL, between x=0.35 m and 0.7 m. Figure 10 (left) and Figure 10 (right) present the surveys at profiles P2 and P4, respectively, where x is the cross-shore distance and z the elevation of the profiles. These two profiles were the most representative profiles of damage since they do not suffer the influence of the flume side walls (friction conditions between units and glass are different

than friction between units). Figure 11 illustrates the non-dimensional damage parameter (S) evolution for profiles P1 to P5 during the test sequence.

The main advantage of this technique is the fact that one can choose the number and the position of the profiles even after finishing the survey.

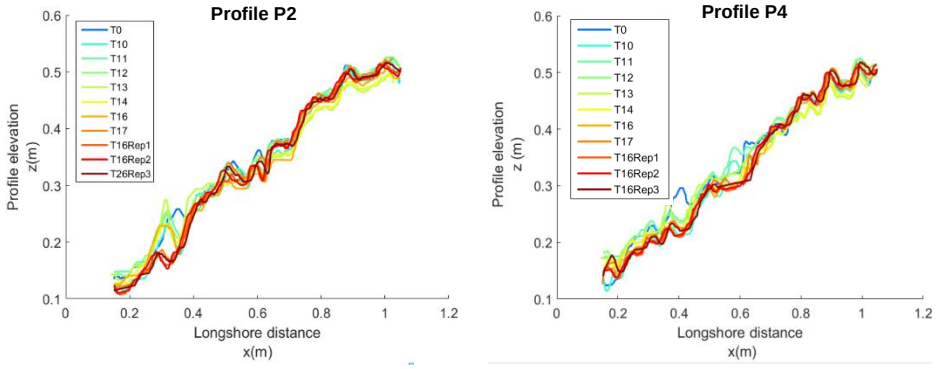

Fig. 10 Profile P4. Surveys for Tests 10 to 16Rep3 for Profile P2 (left) and for Tests 10 to 16Rep3 (right)

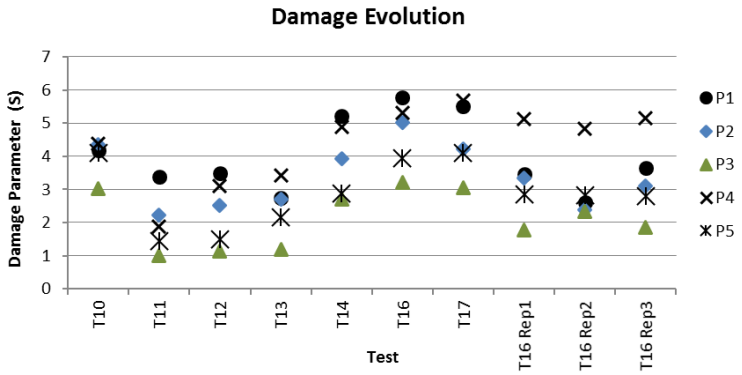

Fig. 11 Non-dimensional damage parameter, S, for Profiles P1 to P5

The analysis of Figures 10 and 11 shows a clear influence of the water-level variation between tests with low-water and high-water levels. There are two main eroded areas corresponding to low and high tides (Figure 10). There are significant damage differences between the profiles during the test series, since the central area of the cross-section (profiles P2 to P4) is the zone where there is more damage (although P3 presents lower damage than the other profiles) and it does not suffer the influence of the flume side walls, as P1 and P5 do.

Table 3 summarizes the non-dimensional damage parameter S obtained for each profile at the end of Test 16Rep3.

Table 3. Damage obtained at the end of Test 16Rep3.

Profile	P1	P2	P3	P4	P5
S	3.65	3.10	1.85	5.15	2.80

The average of the damage parameter for the five profiles at the end of Test 16Rep3 is 3.3, which, according to the damage classification proposed by Van der Meer [6] (Table 4), for a 1:2 rock slope, corresponds to initial/ intermediate damage. Nevertheless, P4 (S=5.15) is in intermediate damage.

Table 4. Damage level by S for a two-layer rock armor [6].

Armor Slope	Initial Damage	Intermediate Damage	Failure
1:1.5	2	3-5	8
1:2	2	4-6	8
1:3	2	6-9	12
1:4-1:6	3	8-12	17

The average damage only for profiles whose damage may represent the whole section damage (P2, P3 and P4, because they do not suffer the influence of the flume walls) is 3.36, which is quite similar to the one obtained with the five profiles.

5. Conclusions

This paper describes two-dimensional physical model tests of a rock-armor breakwater to characterize the damage evolution under future climate change scenarios, by using different damage evaluation techniques, such as counting the number of armor blocks that fall/move and the damage parameter S, which is the ratio between the eroded cross-sectional area around the still water level and the square of the nominal diameter of the armor units, $S=A_e/(D_n)^2$.

Cumulative test series with a constant wave peak period, varying between high-water and low-water levels, and increasing wave heights were simulated. Two different measuring techniques were applied to calculate the number of falling blocks and the damage parameter S. In the last case, five profiles were considered.

One noticed that due to the fact that the water level alternates between low-water and high-water, the damage also presents an oscillating behavior, with two main damage areas corresponding to the active zones for each level. This behavior differs significantly from that found for the common storm sequences usually tested, where the water level does not change.

Both measuring techniques lead to an intermediate damage of the cross-section breakwater. However, the damage parameter assessment with the stereo-photogrammetric technique allows a more versatile evaluation, since it is possible to characterize damage in representative zones of the cross-section.

Although in the present work only five profiles were considered for the average damage, one can assume that this can lead to some errors in the evaluation of the eroded area. So, it is recommended to use a higher number of profiles or, alternatively, one can measure

the eroded volume and divide it by the length of the section [10]. This still needs further research, since it may not be applicable in cases where the damage is much localized.

6 Acknowledgements

This work was developed under the framework of task 8.2 of RECIPE sub-project of the H2020 project HYDRALAB+ Adapting Climate Change, EC contract no. 654110

The authors also acknowledge the scientific and financial support by the Portuguese Foundation for Science and Technology (FCT) for project BSAFE4SEA - Breakwaters Safety control through a Forecast and decision support System Analysis, Ref. PTDC/ECI-EGC/31090/2017 and To-SE Alert - Wave overtopping and flooding in coastal and port areas: Tools for an early warning, emergency planning and risk management system, Ref. PTDC/EAM-OCE/31207/2017.

References

[1] HYDRALAB+ (2017). Deliverable: Task 8.1 Critical Review of Challenges for Representing Climate Change in Physical Models. Report of HYDRALAB+ project - EC contract no. 654110.
[2] USACE - U.S. Army Corps of Engineers (2006). Coastal Engineering Manual. Engineer Manual 1110 2 1100, U.S. Army Corps of Engineers, Washington, D.C. (6 volumes).
[3] CIRIA/CUR/CETMEF (2007). The Rock Manual. The Use of Rock in Hydraulic Engineering (2nd edition). C683, CIRIA, London.
[4] IAHR (2011). Users Guide to Physical Modelling and Experimentation: Experience of the HYDRALAB Network. IAHR.
[5] Broderick, L., & Ahrens, J. P. (1982). "Rip-rap stability scale effects," Technical Paper 82-3, U.S. Army Engineer Waterways Experiment Station, Vicksburg, MS.
[6] Van der Meer, J. W. (1988). Rock Slopes and Gravel Beaches Under Wave Attack. Ph.D. thesis, Delft University of Technology, The Netherlands; also Delft Hydraulics Publ. 396.
[7] Ferreira, R., Costeira, J.P., Silvestre, C., Sousa, I., & Santos, J.A. (2006). Using stereo image reconstruction to survey scale models of rubble-mound structures. Proc. CoastLab 2006. Porto, Portugal, pp. 107-116.
[8] Lemos, R. (2013). Aplicação da Modelação Computacional em MATLAB ao Pós-processamento de Dados de Levantamentos Estereofotogramétricos em Modelos Físicos de Quebra-Mares de Taludes. HIDRALERTA Report 04/2013 (in Portuguese).
[9] Lemos, R., & Santos, J.A. (2013). Photogrammetric profile survey in scale model tests of rubble-mound breakwaters. Proc. 6th SCACR – International Short Course/Conference on Applied Coastal Research.
[10] Pedro, F., Bastos, M., Lemos, R., Fortes, C.J.E.M., & Santos, J.A. (2015). Toe berm damage progression analysis using a stereo photogrammetric survey technique. Proc. 7th SCACR – International Short Course/Conference on Applied Coastal Research.

Research on Engineering Structures & Materials
journal homepage: http://jresm.org
Research Group

Research Article

Analysis of a dolphin by analogy of grid, finite element method with plate element and equivalent frame method

Weslley Lopes [*a], Márcio Moura[b], Carlos Viegas[c], Mauro Real[d]

Escola de Engenharia, Universidade Federal do Rio Grande, Brazil.

Article Info

Article history:
Received 16 Feb 2019
Revised 23 Apr 2019
Accepted 15 May 2019

Keywords:

Port structures;
Breasting Dolphin;
Equivalent Frame Method;
Finite Element Method

Abstract

Port structures are usually composed of large structural elements and support heavy loads. The determination of the maximum and minimum internal forces generated by these loads is very important for the design of these harbor constructions. Therefore, the structural analysis of these structures must be rigorous, using robust numerical methods in order to obtain safety level in the design. Furthermore, this work aims the analysis of a breasting dolphin, composed of twenty steel piles, which are joined by a reinforced concrete block. The structural analysis was carried out in the dolphin's block through the following methods of analysis: Finite Element Method; Grid Analogy; and Equivalent Frame Method. As a result, a comparison was established between a maximum and minimum internal force (normal compressive force and bending moment) given by the three methods. Due to the level of simplification of the structure, the equivalent frame models presented the greatest internal forces, followed by the grid analogy model and finally, the finite element model.

© 2019 MIM Research Group. All rights reserved.

1. Introduction

The ports have been, over the years, entrance and exit points for goods and people, due to its function of connecting the continent to the sea. In this way, ports have contributed to the stable development of industries and to the development of people's lives by ensuring exchanges of goods with other partners around the world. The port operations involved in these exchanges must ensure the safety of cargo, ships, berthing structure, equipment and especially of the personnel involved in the work. Concomitantly, the berthing structure must satisfy the safety levels for the entire process may occur in a safe manner. [8]

Unlike conventional civil engineering constructions, the berthing structures have some characteristics related to their geometry and loading that highlight them. "In particular, we must emphasize the high values of horizontal loads due to the impacts of ships or traction on the mooring ropes [6]. Also, according to Mason [6], to resist the impact of large ships is feasible the adoption of dolphins, when it is convenient to the build, because these elements are characteristic of discrete structures, which each element do a specific function to ensure the approach, berthing and mooring of ships and vessels.

Due to the importance of these structures, the determination of the maximum and minimum internal forces must be made by methods that guarantee that the peculiarities

*Corresponding author: weslley.camargo.lopes@hotmail.com
[a] http://orcid.org/0000-0001-6014-7475; [b] orcid.org/0000-0003-4134-0848; [c] orcid.org/0000-0003-0812-5599; [d]orcid.org/0000-0003-4916-913
DOI: http://dx.doi.org/10.17515/resm2019.120ms0216

of the structure can be considered, about its geometry, behavior of materials, external loads and supports. To achieve this goal, it is necessary introduce robust methods, such as Finite Element Method (FEM), in according with methods simpler, which might offer basis of comparison of results and design tools, such as Grid Analogy and Equivalent Frame Method.

This work aims the determination of the maximum and minimum internal forces in the dolphin block, by the three methods of analysis mentioned before.

2. Presentation of The Structure

Dolphins are port structures formed by a monopile or a set of piles joined by a block. Piles can be performed in reinforced concrete or steel and may be constructed vertically aligned or have a slope in relation to the zenith, a feature that helps in absorbing horizontal forces. Its function can be only mooring or berthing, or it can perform both functions: mooring and berthing of vessels.

The dolphin analyzed in this work is displayed in the Fig. 1 and performs the berthing function of ships. Twenty (20) steel piles with cross sections double "I" profile, welded side by side by flanges and a rigid block reinforced concrete that unites the piles, compose the structure. All piles have a slope 1:4 (h:v) and are embedded in a depth of 17.2 m.

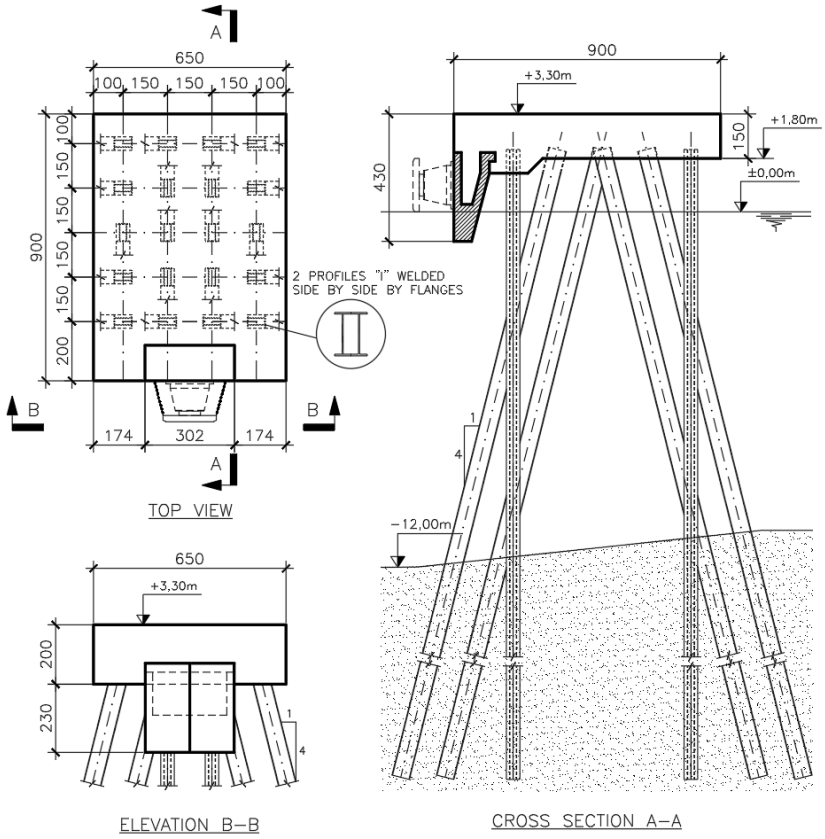

Fig. 1 General scheme of the breasting dolphin. Dimensions in centimeters (cm)

The characteristic dimensions of the dolphin that were used for the models are:

- Block dimensions: 9.0×6.5 m;
- Block surface area: A=58.5 m^2;
- Block Height: h=1.50 m;
- Pile spacing: s=1.50 m

2.1 Materials and properties

The dolphin is composed of the materials presented in Table 1.

Table 1. Materials used in the structure

Component and material	Property of Materials				
	Resistance (MPa)	Modulus of elasticity (GPa)	Poisson coefficient	Coefficient of thermal expansion ($°C^{-1}$)	Specific weight (kN/m^3)
Block: Reinforced Concrete	$f_{ck} = 40$	30.1	0.2	1.0×10^{-5}	25.0
Pile: ASTM A572 Grade Steel 50	$f_y = 345$ $f_u = 450$	200	0.3	1.2×10^{-5}	76.5

2.2 Loads in The Structure

The loads acting on the structure, which were considered for the construction of the models, are due to the deadweight of the block, live load and berthing load. The first two ones must always be considered in the design and the last one, which was considered only the impact of the ship, are typical of breasting dolphins lied in the sheltered area, where the wave effects are not important. The deadweight of the block (pp) is calculated according to the specific weight of the reinforced concrete (γc) and the dimensions of the block. For live load (*Qsc*) was adopted a value of 40 kN/m^2. The berthing load acts in the position of the dolphin fender in the direction of the largest side of this structure (y direction) with a value of 901 kN. This value was taken of table for Super Cone type fenders from the catalog of the Fentek [4], for an impact energy equal to 465 kNm, which was calculated according to the PIANC [7].

3. The Methodology

In order to determine the internal forces in the dolphin's block, three methods of calculation were chosen for this work: Grid Analogy; Finite Element Method and Equivalent Frame Method. The three models developed were limited to represent the dolphin's block by beams supported on the piles, whose axes are oriented according to the lines of piles of the dolphin. Based on this, the structural analysis was carried out to obtain the normal compression force and bending moments in these beams. All materials used in the models was idealized as elastic-linear. There for, was employed the linear elastic structural analysis.

For the solution of the three-dimensional models by the Grid Analogy and Finite Element Method, was used the software SAP2000. In addition to the SAP2000, the Ftool program was used to solve the two-dimensional models by the Equivalent Frame Method.

3.1 Grid Analogy

According to Araújo [1], the method can be used for analysis of polygonal slabs in different forms and may calculate the efforts on the whole pavement. Thus, this method is based on replacing the dolphin's block with an approximate equivalent grid. According to Araújo [1], this is done by a discretization of the block in two sets of evenly spaced lines.

The block was discretized according to the lines of piles of the dolphin, then was possible to obtain the equivalent grid presented in Fig. 2. The grid bars are all evenly spaced at 1.50 m and are positioned belong to the reference plan situated at 1.20 m below the top of the block, since in this position is lied the top of the piles. The points 1 and 2 in Fig. 2 indicate the position of the fender. Note also in this same figure that the plan containing the block is the x-y plane, so the z-axis is orthogonal to this plane, oriented upward.

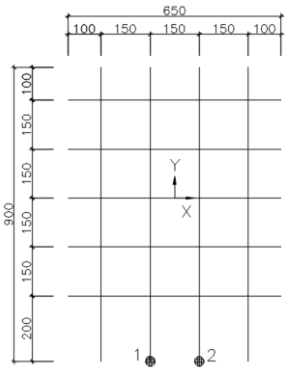

Fig. 2 Equivalent grid. Top view. Dimensions in centimeters (cm)

3.1.1 Grid model geometry

The geometry of the three-dimensional model of grid is given according to Fig. 3. In this model are represented the 20 piles and the block of the dolphin, modeled by the equivalent grid. The length of the grid bars is shown in Fig. 2. All piles have a length equal to 17.7 m.

The cross section of the bars representing the piles was modeled as presented in Fig. 4-a. The grid bars have a rectangular cross section with a base of 1.00 m and a height of 1.50 m, as illustrated in Fig. 4-b.

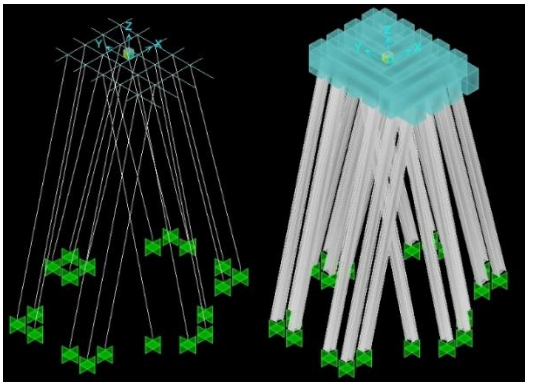

Fig. 3 Three-dimensional model of grids in SAP2000

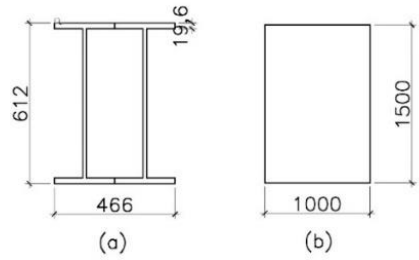

Fig. 4 (a) Cross section of the piles. (b) Cross section of the grid bars. Dimensions in millimeters (mm)

3.1.2 Loads on the grid model

Vertical loads resulting from the deadweight ($\boldsymbol{Q_{PP}}$) and live loads ($\boldsymbol{Q_{SC}}$) were uniformly distributed along the length of the bars of the grid, respectively: $\boldsymbol{Q_{PP} = \gamma_c \cdot h \cdot A/l}$ and $\boldsymbol{Q_{sc} = sc \cdot A/l}$, where A=6.5×9=58.8 m^2 is the surface area of the block, h=1.50 m is the height of the block and l=4×9+5×6.5=68.5 m is the sum of the lengths of the grid's bars. The berthing load was divided between points 1 and 2 of the equivalent grid in Fig. 2, with a value of 450.5 kN at each point. The moment of the forces is equal to 540.6 kNm, which the lever arm of the force is equal to 1.20 m.

3.2 Finite Element Method with Plate Element

The Finite Element Method is a numerical method of great application in the Structural Engineering topics, for reticulated structures, structures bi-dimensional and tree-dimensional.

It uses concepts of "discretization" of the continuum and "interpolation matrix" that provides the displacements at a point inside the element depending on their nodal displacements. The term discretization refers to a model with a number finite of unknowns (nodal displacements in the model nodes) for analysis of continuous in contrast to the analysis with an infinite number of variables as those made by the theory of elasticity that uses continuous functions, that is, with endless unknowns as a solution. [9].

In order to set up the finite element model, plate elements were applied in the grid model for modelling the block of the dolphin. In addition, in order to apply the berthing load, two bars were placed in the position of the fender. The entire mesh of the block was built in order to satisfy the conditions of compatibility, so, the nodes of the bars and plates are coincidental.

3.2.1 Finite element model geometry

The geometry of the three-dimensional finite element model is presented in Fig. 5. In this model are represented the 20 piles, the block and the support of the fender with 1.20 m length. Information about the finite element mesh of the SAP2000 is displayed in Table 2.

Table 2. Finite element mesh on SAP2000

Component	Element	Size	Number of elements
Block: Plate	Plate	50x50 cm	234
Block: Bar	Beam	50 cm	137
Support	Beam	1.20 m	2
Pile	Beam	17.70 m	20

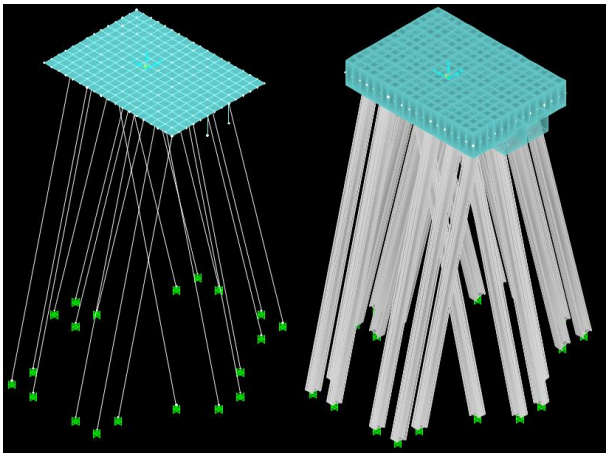

Fig. 5 Three-dimensional model of finite elements in SAP2000

The cross sections of the bars representing the piles and bars of the block are the same as those presented in Fig. 4-a and 4-b, respectively. The board was modeled with a thickness of 1.50 m, equal to the height h of the block.

3.2.2 Load on the finite element model

The deadweight ($\boldsymbol{Q_{PP}}$) of the block was applied uniformly distributed loads on the board, with a value equal to $\boldsymbol{Q_{PP} = \gamma_c \cdot h}$, where $\boldsymbol{\gamma_c = 25\ kN/m^3}$ is the specific weight of the reinforced concrete and h=1.50 m is the height of the block. Similarly, the live load was applied to the board, with a value equal to $\boldsymbol{Q_{sc} = sc = 40\ kN/m^2}$, as per section 2.2. In this model, the berthing load was again divided (two forces with the equal value of 450.5 kN each) and applied in the bars that represent the element that support the fender, as shown in Fig. 6.

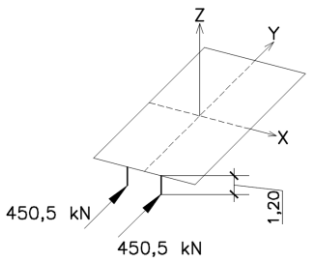

Fig. 6 Berthing load applied to the fender's bars

3.3 Equivalent Frame Method

As said by NBR-6118[2] (Brazilian Norm), the analysis of flat slabs supported on columns arranged in orthogonal queues (with not very different spans and uniformly) can be done through the Equivalent Frame Method. This consists of dividing the slab into two orthogonal series of strips, following the line of columns. The total load should be considered in each frame formed and the internal force resulting from this method are the bending moments in the bars representing the slabs strips.

In this work, the block strips more requested by horizontal load (berthing load) were taken into account. These ones comprise the strips parallel to the direction of the berthing load. In total are four lines of piles (strips) that generate two pairs of plane frames. Each frame was modeled and solutioned by finite element software SAP2000. For the application of the berthing load, a process was used in which employed the Ftool program as a solution tool for the model.

3.3.1 Loads on the grid model

The four block strips with their respective widths are displayed in Fig. 7-a, limited by dashed lines. Due to the symmetry of the dolphin, it is possible to note that: F1 = F4 (Frame 01) and F2 = F3 (Frame 02). Thus, the four strips generate two equivalent frames, according to the Fig. 7-b. In these frames, the horizontal bars represent the block strips and the inclined bars with length of 17.7 m and vertical with length of 17.2 m represent the piles. The vertical bars of the frames (Fig. 7-b) are the piles with slope out of the plane that contains the frame (see Fig. 1 or Fig. 7-a). It is emphasized that the intersection of the inclined bars with the vertical bars (Fig. 7-b) does not generate a node in the location. Therefore, the program (SAP2000) resolves the structure considering that there is no interaction between these bars.

The cross sections of the bars representing the strips are rectangular, with base equal to the width of the strip (Fig. 7-a) and height equal to h=1.50 m. The bars representing the piles have their cross-sectional according to Fig. 4-a.

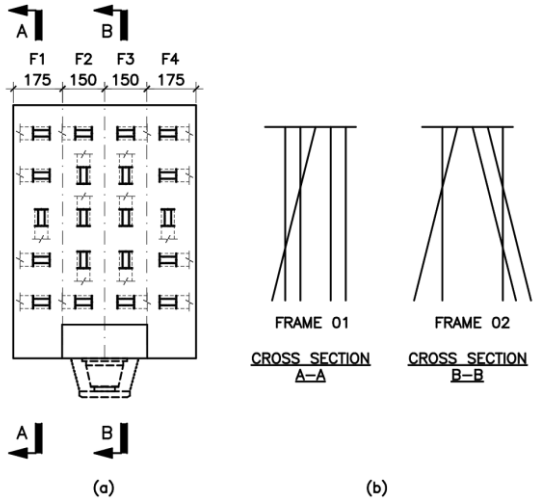

Fig. 7 (a) Block strips. (b) Equivalent frames. Measures in centimeters (cm)

3.3.2 Loads on the grid model

The deadweight (Q_{PP}) and live load (Q_{SC}) were applied as uniformly distributed load along the length of the strips: $\boldsymbol{Q_{PP} = \gamma_c \cdot h \cdot l_f}$ and $\boldsymbol{Q_{sc} = sc \cdot l_f}$, respectively, where lf is the width of each strip.

For the application of the horizontal load (berthing load), the stiffness method was employed considering the block as a rigid diaphragm. Thereat, each frame receives a portion of the horizontal load proportional to its stiffness to the horizontal translation.

This process was done as follows: (a) an arbitrary horizontal load of 1000 kN was applied at the left end of each horizontal bar (block strip) of the equivalent frames 01 and 02 (Fig. 7-b); (b) the horizontal displacement of the upper knots of each frame was obtained, through the SAP2000; (c) the stiffness of each frame was calculated by the ratio between the force value (1000 kN) and the value of the corresponding displacement, as is exposed in Table 3; (d) a rigid beam (rigid member) was modeled in Ftool to represent the rigid diaphragm (dolphin block), supported on elastic translational supports, as presented in Fig. 8.

These support represent the strips (frames) and their stiffness coefficients are equal to the stiffness determined as per the item (c); (e) the berthing load (901 kN) was applied in the central position of the beam; (f) the reaction of each translational elastic support was obtained in the Ftool program and is displayed in Table 4, where these reactions are the portion of the horizontal load (berthing load) that each frame receives.

Horizontal loads (reactions) shown in Table 4 (obtained by the process described above) and its moments (with lever arm equal to 1.20 m), were applied in each equivalent frame, at the left end of each horizontal bar.

Table 3. Stiffness coefficients of the equivalent frames

Equivalent frame	Matching strips	Horizontal force applied (kN)	Displacement (m)	Spring constant (kN/m)
1	1 and 4	1000	0.0488	20491.8
2	2 and 3	1000	0.0163	61349.7

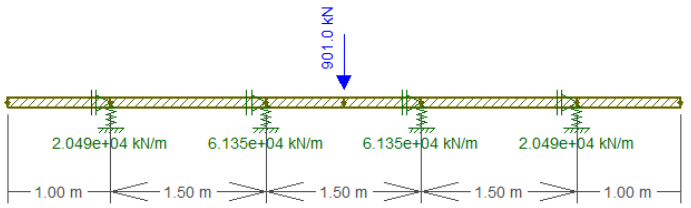

Fig. 8 Rigid beam (Rigid Member) in the Ftool program

Table 4. Rigid beam reactions

Equivalent frame	Matching strips	Support Reaction (kN)
1	1 and 4	112.8
2	2 and 3	337.7

3.4 Loads Combination

According to NBR-6118[2], the last normal combinations of this work, shown in Table 5, can be expressed, both for vertical and horizontal loads, by:

$$F_d = \gamma_g \cdot F_{g,k} + \gamma_q \left(F_{q1,k} + \psi_0 F_{q2,k} \right) \quad (1)$$

The weighting coefficients of the actions in the Ultimate Limit State and the reduction coefficients of the variable loads adopted were, respectively: γg=1.4; γq=1.4 and ψ0=0.6.

Table 5. Loads combinations

Combination	Permanent load	Main variable load	Secondary variable load
1	Deadweight	Berthing load	Live load
2	Deadweight	Live load	Berthing load

4. Results and Discussions

In relative terms, the finite element model with the use of plate elements is closest to the actual structure, followed by the grid model and finally, the equivalent frame models. The values of the normal compression forces and bending moments along the lines of piles tend to be smaller in the first method and grow as the structure is simplified. It is possible to observe in Fig. 9 for the normal compression force and Fig. 10 for the bending moment.

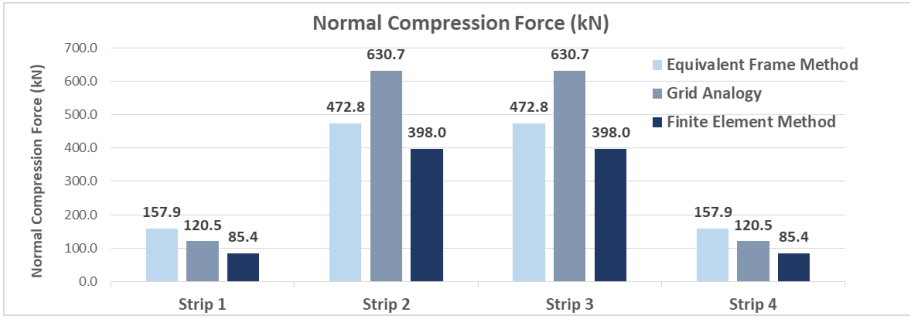

Fig. 9 Normal compression force in the dolphin block

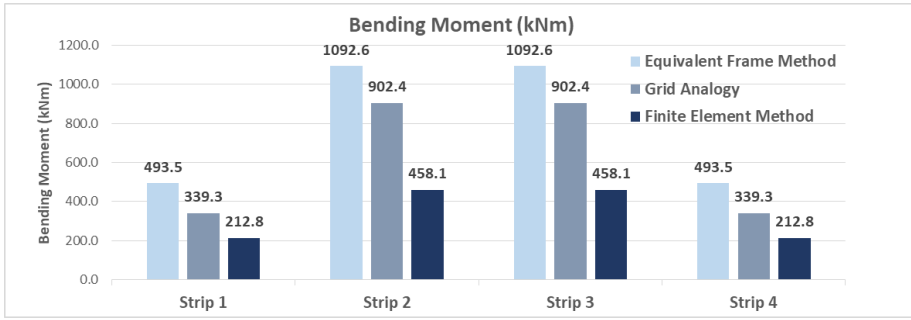

Fig. 10 Bending moment in the dolphin block

Observing Fig. 9 and Fig. 10, it is noted that the finite element model offered the lowest values for both internal forces: normal compression force and bending moment, along the

lines of piles. This occurs due to the presence of the plate element that gives a greater absorption and, simultaneously, the distribution of these internal forces.

The normal compression force is mostly resulting from the horizontal berthing load. It is noted in Fig. 9 that for strips 2 and 3 the grid model exceeded the normal compression force values of the equivalent frame models. This is due to the application of the berthing load, in the grid model, directly at the ends of the bars, which represent strips 2 and 3, thus generating a normal force of $\mathbf{1.4 \times 450.5 = 630.7}\ \boldsymbol{kN}$ in these strips. On the other hand, the equivalent frames received a portion of the berthing load proportional to its stiffness. Therefore, the force is distributed between the four block's strips, which results in a normal compression force value less than the resulting from the grid model. Still, the two simplified models overestimated the values resulting from the finite element model, going according to the trend.

The bending moments resulting from the three methods followed the expected: higher bending moment values for the simplest model – equivalent frame models, decreasing to the grid model and containing the smallest values for the most robust model– finite element model.

5. Conclusion

It is notorious that the design of a breasting dolphin through the Equivalent Frame Method or even through of the Grid Analogy is a conservative one. However, using a program that solves structures by the stiffness method it is possible to design the structure with greater speed, simplicity and satisfying the security levels. In particular, the Equivalent Frame Method showed up be suitable for this type of structure, because it follows the tendency to overestimate the values of the grid model, except for the central strips, which still overestimates the values given by the Finite Element Method. Therefore, it is possible to conclude that this method can be employed for a pre-design of a breasting dolphin block or a conservative design that satisfies the security levels.

References

[1] Araújo JM. Curso de concreto armado (4 ed., Vol. 3). Rio Grande: Dunas, 2014.
[2] Associação Brasileira de Normas Técnicas. NBR 6118: Projeto de estruturas de concreto - procedimento. Rio de Janeiro: ABNT, 2014.
[3] Computers and Structures, Inc. CSI Analysis Reference Manual - SAP2000 Advanced 14.2.2. University Avenue: Berkeley, 2010.
[4] Fentek. Marine Fendering Systems. Hamburg: Fentek, 2008.
[5] Martha LF. Ftool - Um programa gráfico-interativo para ensino de comportamento de estruturas. Rio de Janeiro: Tecgraf/PUC- Rio, 2018.
[6] Mason J. Obras portuárias. Rio de Janeiro: Campus, 1981.
[7] PIANC (International Navigation Association). Guidelines for the Design of Fender System. Report of Working Group 33. Bruxelas: PIANC, 2014.
[8] Tsinker GP. Port Engineering - Planning, Construction, Maintenance, and Security. Hoboken: John Wiley & Sons, Inc, Michigan, 2004.
[9] Vaz LE. Método dos Elementos Finitos em análise de estruturas. Rio de Janeiro: Elsevier, 2011.

Research on Engineering Structures & Materials
journal homepage: http://jresm.org
MIM Research Group

Research Article

Verification of a genetic algorithm for the optimization of stiffened plates through the constructal design method

Marcelo Langhinrichs Cunha[a,1], Emanuel da Silva Diaz Estrada[b,1], Grégori da Silva Troina[c,1], Elizaldo Domingues dos Santos[d,1], Luiz Alberto Oliveira Rocha[e,2], Liércio André Isoldi[*,f,1]

[1] *Federal University of Rio Grande - FURG, Rio Grande, RS, Brazil*
[2] *University of Vale do Rio dos Sinos - UNISINOS, São Leopoldo, RS, Brazil*

Article Info

Article history:
Received 07 Mar 2019
Revised 22 Apr 2019
Accepted 15 May 2019

Keywords:

Genetic Algorithm;
Ribbed plates;
Constructal Design;
Finite Elements;
Optimization

Abstract

This work is a feasibility study of a Genetic Algorithm (GA) based geometric optimization of stiffened plates subjected to transverse loads. For that, the Constructal Design method was used in order to define the search space, aiming to minimize the stiffened plate's central deflection, while keeping the total volume of material constant. The number of longitudinal Nls and transverse Nts stiffeners and the relation hs/ts, the ratio between the height and the thickness of the ribs, were considered as degrees of freedom of the studied optimization problem. In order to estimate the displacement field of the plate reinforced with stiffeners, the Finite Element Method (FEM) was used through the ANSYS® Mechanical APDL software. For the verification, the results obtained in the present study were compared with those obtained by Troina (2017), which used Exhaustive Search (ES) as optimization technique. The results indicated that is more efficient using GA than ES since the former requires the analysis of a lesser amount of cases in order to determine the optimal geometric configuration; there being reductions of up to 47,09% on the number of simulations.

© 2019 MIM Research Group. All rights reserved.

1. Introduction

Thin plates reinforced with stiffeners are broadly employed to resist transverse distributed and/or concentrated loads in a wide gamma of structures such as bridges, ship hulls, vehicles and ships [1]. According to [2], the foremost advantage of using stiffened plates is on the structural efficiency because these structures allow to reduce the total weight without compromising on its rigidity.

Stiffened plates were the subject of study of many researches, among them we can highlight: Bedair [3] studied these structural elements, idealizing them as plate-beam system, through the Sequential Quadratic Programming (SQP) method; Kallassy and Marcelin [4] investigated the feasibility of applying Genetic Algorithms (GA) on the topological optimization of the reinforcements in stiffened plates; the Boundary Element Method (BEM) was used by Tanaka and Bercin [5] to evaluate the influence of stiffeners with various cross-sections on the mechanical behavior of plates under bending; Sapountzakis and Katsikadelis [6] employed the Analogous Equation method to analyze beam-reinforced plates in order to estimate the shear stress on the interface between plate and stiffeners. For that, simply supported rectangular plates with one longitudinal reinforcement with different heights were considered: Hasan [7] investigated the optimal positioning of rectangular beam-type reinforcements on stiffened plates subjected to a

[*]Corresponding author: liercioisoldi@furg.br
[a] orcid.org/0000-0003-1083-7341; [b] orcid.org/0000-0003-4088-5002; [c] orcid.org/0000-0002-4408-562X; [d] orcid.org/0000-0003-4566-2350; [e] orcid.org/0000-0003-2409-3152; [f] orcid.org/0000-0002-9337-3169
DOI: http://dx.doi.org/10.17515/resm2019.123ms0307

static and uniform load by using the *NASTRAN*® software to determine the displacements and maximum stresses acting on the plate; Troina [8], through the Constructal Design method associated with Exhaustive Search (ES), performed a study with respect to the central deflection of rectangular stiffened thin plates minimization.

Although it enables the individual evaluation of each degree of freedom involved in the studied optimization problem, the usage of ES in the search space defined by the application of the Constructal Design method is computationally expensive when a broad number of degrees of freedom are studied. Therefore, GA becomes an interesting alternative for the proposed geometrical optimization process.

Thus, this study seeks to evaluate the feasibility of applying GA, associated with computational modeling and the Constructal Design method, to determine the optimal geometric configuration that minimizes the central deflection of stiffened plates. For that, the verification was performed through a comparison between the obtained results and those presented by Troina [8].

2. Constructal Design Method

The Constructal Theory presumes that geometrical configuration of a flow system is not result of chance, but actually it is the result of a physical principle called Constructal Law, being, thus, a physics phenomenon. These systems evolve in such a way that it better distributes the flaws, easing the flow. More specifically, when it comes to Solid Mechanics problems, the flow is related to the flow of stresses acting on the structural component [9].

According to Bejan [10], the Constructal law is employed through the Constructal Design method, which enables determining the best configuration of a given system. For that, the flow should be malleable and the geometry should be subjected to global restrictions, besides varying the degrees of freedom.

In the present work, the Constructal Design method was employed seeking to define the search space for the GA-based optimization. For that, a plate with length a = 2 m, width b = 1 m and thickness t = 0.02 m was picked as reference. Then, a volume fraction ϕ (as Eq. (1)) of the reference plate was transformed into transverse and longitudinal stiffeners.

$$\phi = \frac{V_s}{V_r} = \frac{N_{ls}(ah_st_s) + N_{ts}[(b - N_{ls}t_s)h_st_s]}{abt} \quad (1)$$

being, V_r the volume of the reference plate and V_s the volume of the plate that was transformed into longitudinal and transverse reinforcements, i.e., the stiffeners volume. Moreover, N_{ls} and N_{ts} stand for, respectively, the number of stiffeners in the longitudinal and transverse directions. Lastly, h_s and t_s are the height and thickness of the stiffeners, respectively. Figure 1 shows schematically a plate with 2 longitudinal reinforcements and 3 in the transverse direction. It is worth highlighting that the dimensions a and b were kept constant in relation to the reference plate in the stiffened plates, thus the volume converted into stiffeners was taken from the reference plate by reducing its thickness.

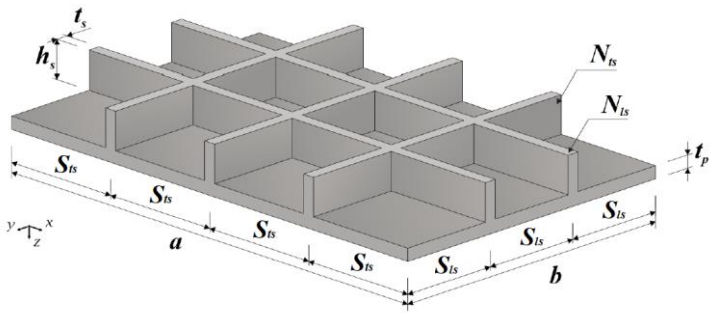

Fig. 1 Stiffened plate with 2 longitudinal and 3 transverse stiffeners

Aiming to determine the geometric configuration that optimizes the mechanical behavior of stiffened plates with respect to the central deflection, the following degrees of freedom were considered: N_{ls}, N_{ts} and h_s/t_s (ratio between the stiffeners' height and thickness). As in [8], 25 different combinations of transverse and longitudinal stiffeners, varying N_{ls} and N_{ts} from 2 to 6, were analyzed. Furthermore, t_s values were adopted based on standard thickness of steel plates between 3.75 mm and 76.6 mm. In addition, h_s should not be higher than 0.3 m in order to avoid a disproportionality between the height of the longitudinal and transverse directions reinforcements and the planar dimensions of the plate. It is important to highlight that the stiffeners have a rectangular cross section and are evenly spaced as shown, respectively, in Eq. 2 and 3:

$$S_{ls} = \frac{b}{(N_{ls}+1)} \tag{2}$$

$$S_{ts} = \frac{a}{(N_{ts}+1)} \tag{3}$$

Lastly, as in [8], 5 volume fractions ø: 0.1, 0.2, 0.3, 0.4 and 0.5 were studied. Regarding the material of the simulated plates, structural steel A-36 with Poisson coefficient and Young's modulus of, respectively, 0.3 and 200 GPa was considered. All the numerically simulated stiffened plates were considered as simply supported and subjected to a uniform transverse load of 10 kPa.

3. Genetic Algorithm

Darwin, on his theory of evolution by natural selection, explained how biological organisms evolve through generations based on the principle of survival of the fittest. Since such a mechanism works in nature, simulating the natural evolution through a method that deals with optimization problems becomes an interesting alternative [11]. Thus, GA is a meta heuristic optimization method based on nature, using natural evolution and genetics concepts, where operators such as selection, reproduction and mutation are applied [12].

The GA was implemented in JAVA and integrated with ANSYS® by utilizing scripts in APDL (Ansys Parametric Design Language). The implemented algorithm can be visualized, schematically, in Fig. 2. The process starts with a population constituted of random individuals and then, through ANSYS® *Mechanical* APDL software, the mechanical behavior of each individual is estimated. Thereafter, based on the obtained deflection results, each individual is availed and ranked. Then, a new population is created by combining desirable characteristics from the current generation through the selection, reproduction and mutation genetic operators. Lastly, the current population of individuals is replaced by the newly generated offspring, excepting the fittest individuals, which are preserved

unchanged through the elitism strategy. This process is repeated until the stop criteria is satisfied.

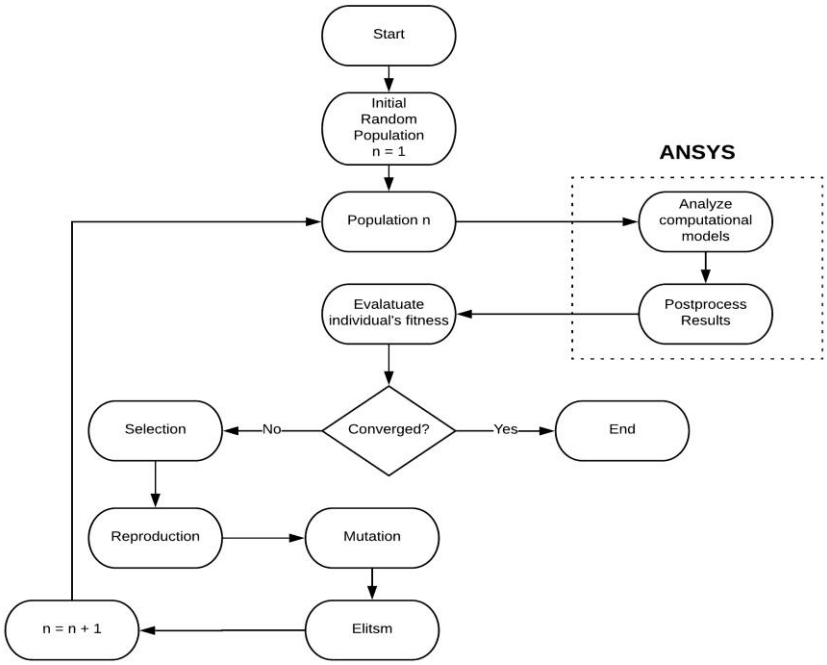

Fig. 2 Flowchart of the implemented Genetic Algorithm.

To represent the chromosomes, it was decided to use a real coding, where each gene associated with the chromosome is directly defined by the value of a degree of freedom of the problem. Figure 3 shows the general representation of a chromosome used in the present work.

As aforementioned, through Genetic Algorithms it is possible to determine which are the fittest individuals to a given problem. In order to do so, the parameter *fitness*, which is inversely proportional to the plate's central deflection, was defined as in Eq. 4. In other words, the smaller the central displacement of the plate, the greater its *fitness* and, hence, the capability of passing on its genes to the upcoming offspring.

$$fitness = \left(\frac{1- P}{U_z}\right) \quad (4)$$

being, U_z the central deflection of the stiffened plate and P a penalty imposed to individuals that violate the constraint regarding the maximum allowed height of transverse and longitudinal reinforcements.

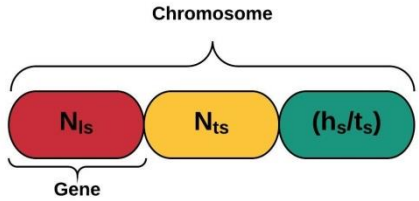

Fig. 3 Representation of a chromosome.

According to [13], the application of penalties is a widespread technique when dealing with restrictions in optimization problems. In order to deal with the restriction imposed on the stiffeners height, the penalty P was defined as:

$$a = \left(\frac{h_s - h_{s,lim}}{h_{s,lim}}\right) + 0.10 \tag{5}$$

$$P = (a, 0.95) \tag{6}$$

being $h_{s,lim}$ the maximum allowed height, which, in the present study, was defined as 0.3 m.

Through Eqs. (5) and (6), one can observe that the penalty P lies on the interval [0.10; 0.95]. These values were determined after successive test during the algorithm implementation.

In the selection genetic operator, a portion of the population (parents) is selected to generate new individuals (offspring) through the reproduction. The tournament technique was used because it offers numerous advantages over equally popular methods, as being more efficiently implementable and enabling to easily adjust the selection pressure [14]. In this selection method, a given number of individuals t_{size} is randomly selected from the population then the individual with the greatest *fitness* is used on the reproduction operator. In this work, the tournament size was defined as 5.

The reproduction genetic operator allows the exchange of desired characteristics between individuals. Since the analyzed degrees of freedom are discrete, a discrete reproduction was used as in [15]: being $x = \{x_1, \ldots, x_n\}$ and $y = \{y_1, \ldots, y_n\}$ the parents selected through the tournament. Then, the offspring $z = \{z_1, \ldots, z_n\}$ is given by:

$$z_i = \{x_i\}\ ou\ \{y_i\} \tag{7}$$

where, x_i or y_i are selected with a probability of 50%.

Moreover, mutation is responsible for performing minor alterations in the individuals generated on the reproduction. For that, uniform mutation was adopted, where the operator changes the value of a selected gene to a random value located between the upper and lower limits of that gene [11]. The mutation rate was considered as 0.10.

The elitism strategy was applied seeking to assure that the best individuals remained on the population of possible solutions. This strategy was employed analogously to Deb et al. [16] on their work about multi objective problems optimization using genetic algorithms: being P_t the population of N parents and Q_t their N offspring, both populations are combined in such a way that we obtain $R_t = P_t \cup Q_t$ with size $2N$. Then, elitism is applied to R_t and the N most fitted individuals are selected to the next generation. It is important to highlight that in all performed simulations a population with N = 20 individuals was adopted.

4. Computational Modeling

The computational modeling of the analyzed stiffened plates, as aforementioned, was performed on ANSYS® *Mechanical* APDL, through the Finite Element Method (FEM). For the numerical simulations, the finite element SHELL281, which is a shell element that has 6 degrees of freedom on each of its 8 nodes. In Troina et al. [17] and Cunha et al. [18], it was shown that discretizing stiffened plates using this element leads to satisfactory results regarding the deflection on the analyzed structural component.

Regarding the mesh refinement utilized in the simulations, four different meshes densities were considered: M1, M2, M3 and M4; where the finite element size of each mesh was a fraction of the plate's width (M1: $b/20$, M2: $b/40$, M3: $b/60$, M4: $b/80$). The mesh considered as independent was the mesh M3 and therefore quadrilateral shell elements measuring 16,67 mm were used in the simulations.

For brevity's sake, more information about the computational model of the stiffened plates numerical simulations, its verification as well as the mesh convergence test can be obtained in [8,17,18].

5. Results and Discussion

As aforementioned, the verification of the GA was performed considering 5 different values for the volume fraction $\varnothing$: 0.1, 0.2, 0.3, 0.4, and 0.5. Since GA is a stochastic method, the experiment using the implemented algorithm was executed five times for each analyzed case. Figs. 4, 5, 6, 7, and 8 show the convergence through the generations to the optimal value obtained by Troina [8] where the *fitness* values of the most fitted individuals are a average of the 5 runs.

As one can notice in the presented graphs, through the genetic algorithm, it was possible to determine the optimal geometric configuration for each analyzed case. The best result was obtained for $\varnothing = 0.1$, where the convergence was reached on the fifth generation of individuals, while $\varnothing = 0.5$ presented the slowest convergence, on the tenth generation.

Based on the data obtained through the performed optimization processes, Tab. 1 shows a comparison between Exhaustive Search, performed by Troina [8], and Genetic Algorithm with respect to the amount of required numerical simulations to determine the geometric configuration that minimizes the central deflection of the stiffened plates.

It can be observed, in all studied cases, that the optimization using GA demanded the analysis of a smaller amount of geometries in comparison with ES. It was observed reductions on the number of required simulations varying from 24.24%, for $\varnothing = 0.5$, and 47.09%, for $\varnothing = 0.1$. Thus, the geometric optimization technique that utilizes an evolutive strategy proves itself to be more efficient than ES on the central deflection minimization of plates reinforced by stiffeners.

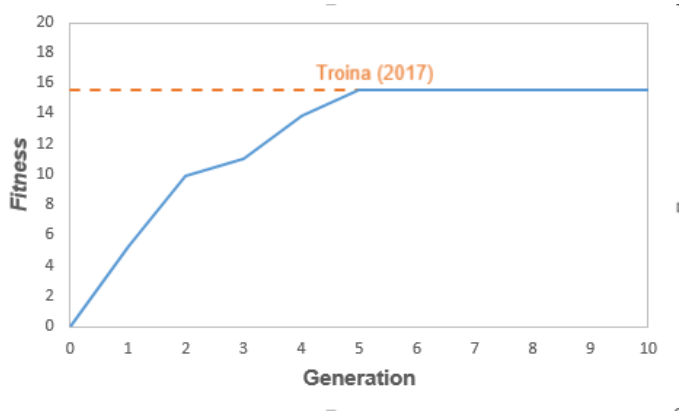

Fig. 4 Convergence for ø = 0.1

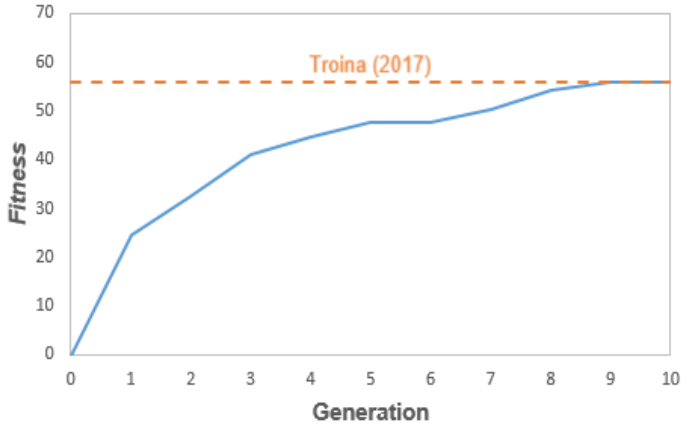

Fig. 5 Convergence for ø = 0.2.

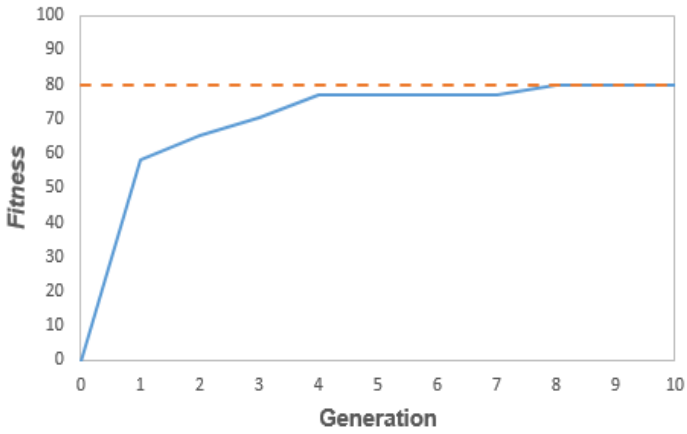

Fig. 6 Convergence for ø = 0.3.

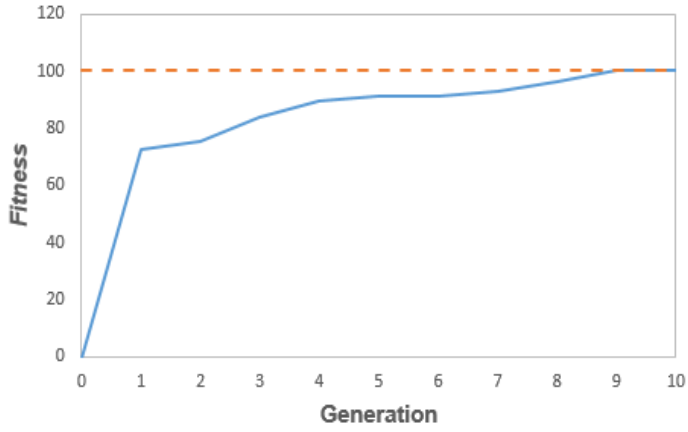

Fig. 7 Convergence for ø = 0.4.

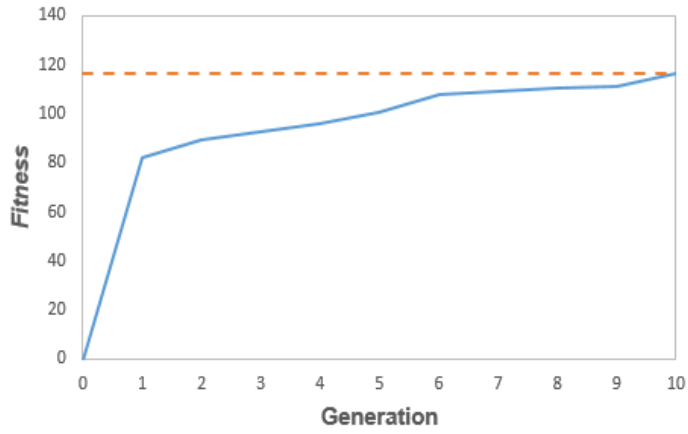

Fig. 8 Convergence for ø = 0.5.

Table 1. Comparison between ES and GA

ø	Exhaustive Search				Genetic Algorithm			
	Optimal configuration			Nº of performed simulations	Optimal configuration			Nº of analyzed individuals (average)
	N_{ls}	N_{ts}	(h_s/t_s)		N_{ls}	N_{ts}	(h_s/t_s)	
0,1	2	3	56,66	189	2	3	56,66	100
0,2	2	5	88,21	237	2	5	88,21	180
0,3	2	5	59,41	252	2	5	59,41	160
0,4	2	5	44,40	256	2	5	44,40	180
0,5	2	5	35,03	264	2	5	35,03	200

6. Conclusion

The viability of applying GA, allied with the Constructal Design Method and computational modeling, on the geometric optimization of stiffened plates with respect to the central deflection was ascertained.

Moreover, it was noticed that, for all analyzed cases, the genetic algorithm was more efficient than the exhaustive search since the former requires a smaller amount of simulations to determine the optimal geometry, being possible to reach a reduction of up to 47.09% on the number of analyses and hence there is a significant reduction of the demanded processing time of the optimization.

Another advantage of GA over ES is that the former, when the stop criterion is reached, provides a family of feasible designs. Since it is not always possible to manufacture the best individual, for practical reasons, the designer can choose any solution of the last generation of individuals without significantly affecting the solution quality. On the other hand, when using ES, this is not possible due to the wide dispersion of possible solutions.

On future works, it is intended to extend the performed analysis and evaluate the influence not only of the number of stiffeners and the ratio h_s/t_s but also other degrees of freedom. Moreover, through the application of Genetic Algorithms it is possible to execute multi objective optimizations, considering the deflections as well as the stresses that act upon the stiffened plate.

7. Acknowledgments

The authors thank FAPERGS (Research Support Foundation of Rio Grande do Sul), CNPq (Brazilian National Council for Scientific and Technological Development) and CAPES (Brazilian Coordination for Improvement of Higher Education Personnel) for the financial support.

References

[1] Shanmugan NE, Liew JYR, Thevendran V. Thin-walled Structures – Research and Development, Elsevier, Singapore, 1998.
[2] Bedair OK. Analysis and limit state design of stiffened plates and shelss: a world view. Applied Mechanics Reviews, 2009; 62(2): 020801. https://doi.org/10.1115/1.3077137
[3] Bedair OK. Analysis of stiffened plates under lateral loading using sequential quadratic programming (SQP). Computer and Structures, 1997; 62(1): 63 – 80. https://doi.org/10.1016/S0045-7949(96)00281-7
[4] Kalassy A, Marcelin JL. Optimization of stiffened plates by genetic search. Structural Optimization, 1997; 13: 134-141. https://doi.org/10.1007/BF01199232
[5] Tanaka M, Bercin AN. Static bending analysis of stiffened plates using the boundary element method. Engineering Analysis with Boundary Elements, 1998; 21-147. https://doi.org/10.1016/S0955-7997(98)00002-2
[6] Sapountzakis EJ, Katsikadelis JT. Analysis of plates reinforced with beams. Computational Mechanics, 2000; 26: 66-74. https://doi.org/10.1007/s004660000156
[7] Hasan MM. Optimum design of stiffened square plates for longitudinal and square ribs. Al-khwarizmi Engineering Journal, 2007; 3(3): 13-30.
[8] Troina GS (2017). Modelagem computacional e método design construtal aplicados à otimização geométrica de placas finas de aço com enrijecedores submetidas a carregamento transversal uniforme. Master Thesis, Federal University of Rio Grande, Rio Grande, Brazil.
[9] Bejan A, Lorente S. Design with Constructal Theory, John Wiley Sons, Hoboken, NJ, USA, 2008. https://doi.org/10.1002/9780470432709
[10] Bejan A. Shape and Structure, from Engineering to Nature, Cambrigde University Press, Cambridge, England, 2000.

[11] Sivanandam SN, Deepa SN. Introduction to genetic Algorithms, Springer-Verlag, Berlin, 2008.
[12] Mitchel M. An introduction to genetic algorithms. MIT Press, Cambridge, 1996.
[13] Chehouri A, Younes R, Perron J, Illinca A. A constraint handling technique for genetic algorithms using a violation factor. Journal of Computer Sciences, 2016; 12(7): 350-362. https://doi.org/10.3844/jcssp.2016.350.362
[14] Miller B, Goldenberg D. Genetic algorithms, tournament selection and the effects of noise. Complex Systems, 1995; 9(2): 193-212.
[15] Mühlenbein H, Schlierkamp-Voosen D. Predictive models for the breeder genetic algorithm. Evolutionary Computation, 1993; 1(1): 25-49. https://doi.org/10.1162/evco.1993.1.1.25
[16] Deb K, Prapat A, Agarwal S, Meyarivan T. A fast and elitist multiobjective genetic algorithm: NSGA-II. IEEE Transactions on Evolutionary Computation, 2002; 6(2): 182-197. https://doi.org/10.1109/4235.996017
[17] Troina GS, de Queiroz JPTP, Cunha ML, Rocha LAO, dos Santos ED, Isoldi LA. Verificação de modelos computacionais para placas com enrijecedores submetidas a carregamento transversal uniforme. Revista Cereus, 2018; 10(2): 285-298., Schlierkamp-Voosen D. Predictive models for the breeder genetic algorithm. Evolutionary Computation, 1993; 1(1): 25-49. https://doi.org/10.1162/evco.1993.1.1.25
[18] Cunha ML, de Queiroz JPTP, Troina GS, Rocha LAO, dos Santos ED, Isoldi LA. Modelagem computacional e método design construtal aplicados à otimização geométrica de placas finas de aço com enrijecedores submetidas a carregamento transversal. Proceedings of *XXIV Congresso Nacional dos Estudantes de Engenharia Mecânica – CREEM*, 2018.

Research on
Engineering Structures & Materials

CONTENT

Research on
Engineering
Structures & Materials

Research Group